

AD-A017 611

THE ACTIVITY OF TRACE METALS IN AQUEOUS SYSTEMS AND  
THE EFFECT OF CORROSION CONTROL INHIBITORS

Rosalie Urzendowski, et al

Albuquerque University

Prepared for:

Air Force Weapons Laboratory

October 1975

DISTRIBUTED BY:

**NTIS**

National Technical Information Service  
U. S. DEPARTMENT OF COMMERCE

332068

AFWL-TR-75-203

AFWL-TR-  
75-203

AD A U I 7 6 1 1

# THE ACTIVITY OF TRACE METALS IN AQUEOUS SYSTEMS AND THE EFFECT OF CORROSION CONTROL INHIBITORS

Sister Rosalie Urzendowski, Ph.D  
Arthur H. Guenther, Ph.D

University of Albuquerque  
Albuquerque, New Mexico 87140

October 1975

Final Report



Approved for public release; distribution unlimited.

Reproduced by  
NATIONAL TECHNICAL  
INFORMATION SERVICE  
U.S. Department of Commerce  
Springfield, VA 22151

**AIR FORCE WEAPONS LABORATORY**  
**Air Force Systems Command**  
**Kirtland Air Force Base, NM 87117**

This final report was prepared by the University of Albuquerque, New Mexico under Contract F29601-73-C-0110, Job Order 62601F8809, with the Air Force Weapons Laboratory, Kirtland Air Force Base, New Mexico. Mr. Wayne Wasson (DYX) was the Laboratory Project Officer-in-Charge.

When US Government drawings, specifications, or other data are used for any purpose other than a definitely related Government procurement operation, the Government thereby incurs no responsibility nor any obligation whatsoever, and the fact that the Government may have formulated, furnished, or in any way supplied the said drawings, specifications, or other data is not to be regarded by implication or otherwise as in any manner licensing the holder or any other person or corporation or conveying any rights or permission to manufacture, use, or sell any patented invention that may in any way be related thereto.

This report has been reviewed by the Information Office (OI) and is releasable to the National Technical Information Service (NTIS). At NTIS, it will be available to the general public, including foreign nations.

This technical report has been reviewed and is approved for publication.

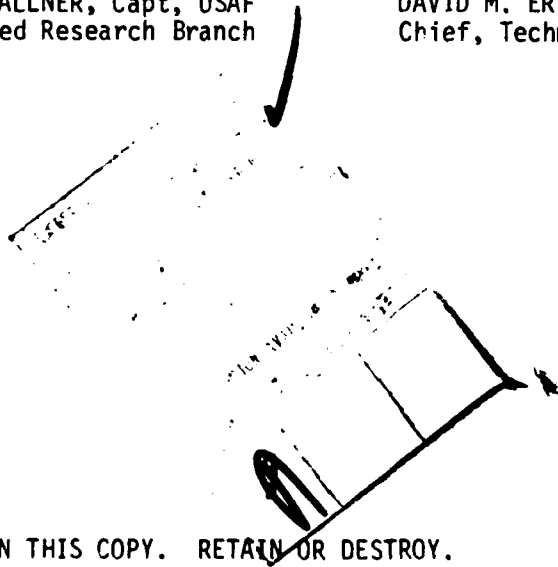
*Wayne Wasson*

WAYNE WASSON  
Project Officer

FOR THE COMMANDER

*Richard A. Wallner*  
RICHARD A. WALLNER, Capt, USAF  
Chief, Applied Research Branch

*David M. Ericson, Jr.*  
DAVID M. ERICSON, JR, LTC, USAF  
Chief, Technology Division



DO NOT RETURN THIS COPY. RETAIN OR DESTROY.



UNCLASSIFIED

SECURITY CLASSIFICATION OF THIS PAGE(When Data Entered)

its use as a dielectric medium for capacitors. The specific conductance, pH, and the analysis of ionic impurities were used as the basis for evaluating the water purity. From source to use, the water was studied to determine contamination, either ionic or with atmospheric gases such as nitrogen and carbon dioxide. The effect of metallic corrosion in water was studied kinetically in conjunction with equilibrium precipitation of solid phases, chemical implications of impurity removal processes together with various analytical techniques. The principles of metallic corrosion were broadly surveyed with special reference to the controlling factors of immersion and atmospheric corrosion, as well as their application to the prevention of corrosion under service conditions. Extensive measurements were made on various inorganic, polymeric, and organic additives employed in metallic water systems to study their effectiveness in preventing corrosion. For capacitor dielectric systems for which a low conducting dielectric is needed, organic mixtures proved to be the most satisfactory.

ii  
UNCLASSIFIED

SECURITY CLASSIFICATION OF THIS PAGE(When Data Entered)

## PREFACE

The authors wish to express their gratitude to Mr. V. E. Kunzler and Mr. E. W. Wasson for their assistance in obtaining the necessary supplies and equipment and to Leonie Boehmer for computational assistance. Appreciation is also extended to Jo Ann Sedall, Jean Barrera and Al White for performing many of the experimental measurements.

Appendix A and Appendix B of this report contain reprints of articles on thermal studies performed under this contract. Appendix A: "The Combination of Thermal and Ultrasonic Data to Calculate Gruneisen Ratios and Various Thermodynamic Functions", by Sr. Rosalie Urzendowski, Ph.D., and Arthur H. Guenther, Ph.D., was presented at the 1973 International Symposium on Thermal Expansion of Solids, held at Lake of the Ozarks, Missouri, November 7-9, 1973. The paper was published in the American Institute of Physics Conference Proceedings Volume, No. 17, entitled Thermal Expansion-1973, edited by R. E. Taylor and G. L. Denman.

Appendix B: "The Use of Thermal and Ultrasonic Data to Calculate The Pressure Dependence of the Gruneisen Parameter," by S. R. Urzendowski, and A. H. Guenther, was presented at the American Chemical Society Symposium on Analytical Calorimetry held at Los Angeles, April 1974. The paper was published in the symposium volume entitled: Analytical Calorimetry, Volume 3, edited by R. S. Porter and J. F. Johnson.

## CONTENTS

<u>Section</u>		<u>Page</u>
I	INTRODUCTION	6
II	EXPERIMENTAL APPARATUS AND METHOD	8
	Hydrogen Ion (pH) Measurements	8
	Constant Temperature Regulation	8
	Conductivity Measurements	9
	Electrogravimetry	9
	Polarography	10
	Absorption Spectrophotometric Methods	15
	Flame Photometer	16
III	MATERIALS STUDIED	18
	Ultrapure Water	18
	Metals Studied	25
	The Corrosion Resistance Inhibitors Tested	25
IV	THEORY	33
	Properties of Pure Water	33
	Effect of Atmospheric Gases on Water Purity	36
	Water Correction	42
	Regeneration of Contaminated Water	42
	The Corrosive Properties of Water	45
	The Use of Inhibitors To Prevent Corrosion	52
V	EXPERIMENTAL RESULTS AND DISCUSSION	56
	Analysis of Water Samples	56
	The Selection of Proper Metals to Be Used as Electrodes	74
	The Effect of Additives in Preventing Corrosion	80
VI	CONCLUSIONS	98
	APPENDIX	
	A    THE COMBINATION OF THERMAL AND ULTRASONIC DATA TO CALCULATE GRUNEISEN RATIOS AND VARIOUS THERMODYNAMIC FUNCTIONS	103
	B    THE USE OF THERMAL AND ULTRASONIC DATA TO CALCULATE THE PRESSURE DEPENDENCE OF THE GRUNEISEN PARAMETER	125

SECTION I  
INTRODUCTION

Water as a dielectric in capacitive storage elements, transmission lines, voltage generators and voltage grading situations are of extreme interest in the development of high energy density storage systems. This interest stems from the extremely high dielectric constant of water compared to other common solid and liquid dielectrics such as various plastics and transformer oil. The interest is not only in the possibility of developing compact light weight storage systems but to afford short transmission lengths from energy stores to various transducers in numerous nuclear weapon detonation simulators. In many cases the water is pressurized to decrease the hydrodynamic phase of bubble breakdown when the water is stressed by high electric fields. Obviously any consideration of water as a dielectric medium will require an understanding of the attack of high resistivity water on conducting elements in high voltage electrical components. For this reason it was deemed advisable to investigate the corrosive action of high purity water on metals and to determine the degradation of the water dielectric with time. That portion of the program concerning the corrosion aspects of the above general subject is the main theme of this report.

The activity of trace metals in aqueous systems and their impact on the use of water as a tool in research and/or industry is well known. Detailed water characterization defines the degree of water purity and/or contamination and its application in atomic absorption, flame photometry, enzymology, conductance measurements, and in the production of standard reference solutions. The ability of modern steam generating equipment to

economically produce electric power or process steam is directly dependent on proper water treatment.

Several authors (ref. 1 to 6) define the limits in parts per billion (ppb) for boiler water as: total solids 50, oxygen 5, silica <0, copper 10,  $\text{CaCO}_3$  hardness 0,  $\text{CO}_2$ , and pH 8.8 to 9.1 in copper alloy condenser tubes or pH 9.5 to 9.7 in copper free systems. The total solids and alkalinity are set to minimize any tendency toward foaming in the boiler drum. Alkalinity limits minimize the danger of caustic attack and silica levels are defined to prevent turbine deposits.

The use of water as a dielectric medium between metallic capacitor plates, as a primary coolant for nuclear reactors, with klystron tubes for generating microwave energy, and for crystal growing in the semiconductor industry depends on the absence of minute quantities of metallic oxides or other contaminants.

- 
1. D'Elia, R.A., Howard, D.L., and Cameron, D.K., "Want Better Feed Water". Water and Wastes Engineering, July, 1972.
  2. Cootner, P.H., and Lof, G.O.G., Water Demand for Steam Electric Generation: An Economic Projection Model, Washington, D.C., resources for the Future, Inc., 1965.
  3. American Water Works Association, Water Quality and Treatment. A Handbook, of Public Water Supplies, 34d ed., New York: McGraw-Hill Book Co., 1971.
  4. Besselievre, E.B., The Treatment of Industrial Waters. New York: McGraw-hill Book Co., 1969.
  5. Babcock, J., and Wilcox, H., "Water Treatment for Industrial Boilers," BR-884, August, 1968.
  6. Lux, J.A., "Boiler Water Quality Control in High Pressure Steam Power Plants," Water and Waste Treatment Journal, September, 1962.

Lux et al., (ref. 6) define typical feedwater quality requirements for nuclear steam generators as: resistivity 1 to 5 megohm-cm, total solids 80 to 400 ppb, copper and iron 2 ppb, chloride 5 to 10 ppb, and silica 10 ppb. Deposition on steam generating surfaces must be avoided to prevent loss of efficiency and costly shutdowns for cleaning operations. Boiling water reactor systems are even more critical, since any deposit can result in overheating and failure of the reactor core itself.

Water used in crystal growing, in the coating industry, in the manufacture of microwave tubes and semiconductor elements, or as a dielectric medium must be of the highest purity. Minute amounts of dissolved contaminants can interfere with chemical or biological test procedures and may even dissolve the interim parts of a capacitor system by picking up a contaminant load and thus decreasing the dielectric or solvent properties.

The College of American Pathologists (ref. 7) classify "Type I Reagent Grade Water" as having a minimum resistivity of 10 megohm-cm. For comparison, the classical laboratory distillation method of purification has a resistivity of 0.5 megohm-cm (single distillation) and does not meet the minimum specifications of the Type I Reagent Grade Water. Totally pure water contains no contaminants and has a theoretical resistivity of 18.3 megohm-cm at 25°C.

Ultra pure water approaches totally pure water in contaminant concentration (less than 0.01 ppm and electrical resistance more than 18 megohm/cm). For all practical purposes, ultrapure water and Type I Reagent Grade Water are identical. Ordinary tap water carries up to 1000

---

7. The Barnstead Basic Book on Water, Barnstead Company, Boston, Mass., 1971.

ppm of dissolved minerals, ionic salts, live bacteria, viruses, and dead organic matter. Because of these contaminants, tap water has a relatively low resistivity of roughly 50,000 ohm-cm.

The purpose of this study is to obtain an accurate, representative analysis of the quality of the water obtained from the Kirtland AFB water purification system (ref. 8) and to evaluate its use as a dielectric medium between metallic capacitor plates.

Specifically, the present work is an electrochemical treatise on water to (1) evaluate the initial suitability of the water for use as a dielectric medium in capacitance measurements (ref. 9), (2) determine which metallic components are best suited as materials for capacitor plates, and (3) evaluate any necessary treatment requirements which could be applied to prevent and/or subdue corrosion of metallic elements submerged in high purity water.

The physical integrity of the water dielectric was determined by observing physico-chemical properties such as temperature, hydrogen ion concentration, and the conductivity of the solvent, before the system was subjected to an electric current. The effect of chloride ion contamination of the water from the pH electrode used for the analytical measurements was also noted and appropriate corrections applied.

The suitability of metallic components was studied by submerging various metals or alloys in high purity water and observing the concentration of metallic contaminants present as a function of time, as well as changes in hydrogen ion concentration and specific conductivity. Sensitive

- 
8. Illinois Water Treatment Company, 840 Cedar St., Rockford, Illinois.
  9. Urzendowski, Rosalie and Guenther, Arthur H., The Study of Corrosive Contaminants Present in Water Capacitors, AFWL-TR-73-179, Air Force Weapons Laboratory, Kirtland Air Force Base, New Mexico, 1973.

instrumental methods of analysis such as spectrophotometry, colorimetry, conductivity, quantitative electrogravimetric analysis, and polarography, were used for the water analysis. The metallic stability order toward corrosion previously proposed (ref. 9) was expanded to include aluminum 2024 alloy, aluminum, cadmium, cooper, lead, molybdenum, nickel, tin, tungsten, and zinc rods, and magnesium-thorium HM-21 A alloy. The metals or alloys used simulate capacitor components before the system was subjected to an electric current.

Organic and inorganic additives, as well as water soluble polymeric materials, were added to the systems containing metals or alloys submerged in known concentrations of ultrapure water in order to study the effect of additives in preventing corrosion or in regenerating water systems which show signs of corrosion. In this way the purity of the water was maintained, and the danger from corrosion of capacitor electrodes was diminished.

## SECTION II

### EXPERIMENTAL APPARATUS AND METHOD

#### 1. HYDROGEN ION (pH) MEASUREMENTS

The Fisher Acumet\* Model 420 Digital pH/Ion Meter affords precise and accurate pH or millivolt measurements. A Markful II\* unbreakable, no refill, combination (glass-reference) electrode of high electrical stability was used for the pH measurements. The contamination of the test solutions by the salt solution of the reference electrode was essentially eliminated because the unit has no external openings and is filled with a low viscosity gel which evaporates at an extremely slow rate. However, in some extreme cases, proper corrections were made for solutions contaminated by the salt solution of the reference electrode. After standardization with three buffer solutions of pH 5, 7, and 10, the pH data were accurate to  $\pm 0.01$  pH unit. Data obtained using the expanded scale provided for 0.001 pH resolution and 0.1 millivolt when used as a millivoltmeter.

Specific ion electrodes for nitrate and divalent cations, were used with the pH meter and read on the millivolt scale. Readings were accurate to  $\pm 0.1$  millivolt.

#### 2. CONSTANT TEMPERATURE REGULATION

All measurements were made by placing the respective solutions in a constant temperature bath regulated by a K-2/R Lauda/Brinkmann Circulator. The recorded temperatures were accurate to  $\pm 0.02^{\circ}\text{C}$ . A Freon

---

\* Acumet is the registered trademark for Fisher Scientific.

\*\* Markful II is the registered trademark for Markson Scientific, Inc.,  
Box NPR, Del Mar, California 92014.

12 refrigerant with distilled water as the circulating liquid made operation possible over the temperature range  $\pm 1^{\circ}\text{C}$  to  $\pm 40^{\circ}\text{C}$ .

### 3. CONDUCTIVITY MEASUREMENTS

A standard conductivity meter<sup>(\*)</sup> was used to obtain all conductance measurements. The instrument operates over five ranges selectable with a front panel range switch. Temperature variations of the sample solution are compensated for automatically and continuously by a thermistor network within the probe. The five ranges in  $\mu\text{mhos/cm}$  are, respectively: Range 1: 0 to 2; Range 2: 0 to 20; Range 3: 0 to 200; Range 4: 0 to 2000; and Range 5: 0 to 20,000.

The same conductivity probe (cell constant 1.0) was used for all five ranges of the meter. It contains tungsten electrodes and two thermistors which are enclosed in a stainless steel tube in the center of the cell end of the probe. The probe housing is constructed of Noryl<sup>(\*\*)</sup> thermoplastic. The thermistors compensate for sample temperature variations between 0 and  $100^{\circ}\text{C}$ .

### 4. ELECTROGRAVIMETRY

A Fisher Electroanalyzer was used to determine cupric ions generated from copper and brass samples. The analysis involved the deposition of the desired metallic element upon a previously weighed cathode, followed by the subsequent reweighing of the electrode plus deposit to obtain, by difference, the quantity of that substance.

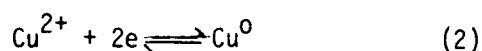
The experimental apparatus consisted of a large platinum gauze cathode and a smaller platinum anode incorporated in the instrument.

---

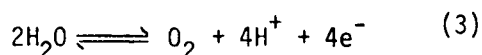
\* Hach Model 2511. Conductivity Meter, Hach Chemical Company, Ames, Iowa, 50010

\*\* Noryl is the General Electric Trade Name.

Both electrodes were immersed in the solution to be analyzed and the applied voltage and current were monitored continuously. The solution was continuously stirred by the anode which was rotated by a synchronous motor. For deposition of metallic copper from its ionic solution, a constant voltage of 1.5 volts was applied so that rapid and quantitative deposition of copper occurred. The reduction of cupric ions at the cathode resulted in a copper-plated platinum electrode as follows:



whereas at the anode, the oxidation of water was virtually the sole reaction:



For additional theory see references 10, 11, and 12. The results of the experiments performed on pure copper and the brass samples are given in Table 1.

## 5. POLAROGRAPHY

The polarographic method was used to analyze ionic solutions of several of the remaining metallic ions such as cadmium, zinc, tin, lead, nickel, and tungsten. The method is based on the interpretation of current voltage curves obtained by the electrolysis of a metal ion solution in a cell consisting of a dropping mercury (micro) electrode and a large, nonpolarizable reference electrode. The genius of the method is that it yields a diffusion current,  $i_d$ , which is directly proportional to the concentration of the electrolyzed species and a half-wave potential,  $E_{1/2}$ , which is characteristic of each species. The potential of the cathode

10. Willard, H.H., Merritt, L.L., and Dean, J.A., Instrumental Methods of Analysis, D. Van Nostrand Company, Inc., New York, N.Y., 1960.
11. Ayres, G.H., Quantitative Analysis, Harper and Row Publishers, New York, 1968, p. 525.
12. Urzendowski, Sr. Rosalie, Polarographic, Potentiometric, and Calorimetric Studies in Aqueous Dioxane Media, Dissertation, Notre Dame University, 1964.

Table 1  
ELECTRODEPOSITION OF COPPER

1. Electroanalysis of copper in brass <sup>(1)</sup>		
Additive in H <sub>2</sub> O <sup>(2)</sup>	No. 10	No. 5
Wt. of metal in solution, mg <sup>(3)</sup>	1.66	1.48
Vol. of solution used, ml	175	175
Wt. of Cu found, mg	0.97	0.86
2. Electroanalysis of Copper <sup>(4,5)</sup>		
Additive in H <sub>2</sub> O <sup>(2)</sup>	None	No. 7
Wt. of metal in solution, mg <sup>(3)</sup>	0.27	1.22
Vol. of solution used, ml	170	50
Wt. of Cu found, mg	0.25	1.99

---

<sup>1</sup> Table 6, No. 4.

<sup>2</sup> Table 7

<sup>3</sup> Determined from weight loss of metal

<sup>4</sup> Table 6, no. 6

<sup>5</sup> Table 6, no. 7

was calculated by means of the Nernst equation. Hence,

$$E_{\text{cathode}} = E_{\text{Ox-Red}}^0 - \frac{0.059}{n} \log \left( \frac{[\text{Red}]_o}{[\text{Ox}]_o} \right) \quad (4)$$

where the zero subscripts signify that the indicated activities apply only to the film immediately adjacent to the cathode and  $n$  refers to the number of moles of electrons involved in the reduction. The applied potential was expressed as

$$E_{\text{applied}} = E_{\text{cathode}} + E_{\text{anode}} \quad (5)$$

It was assumed that the junction potential in the cell is negligibly small, and currents, on the order of  $10^{-6}$  ampere (microampere), are minute. The anode of the cell was a saturated calomel electrode  $E_{\text{SCE}} = -0.242$  V, are therefore

$$E_{\text{applied}} = E_{\text{Ox-Red}}^0 - \frac{0.059}{n} \log \left( \frac{[\text{Ox}]_o}{[\text{Red}]_o} \right) + E_{\text{SCE}} \quad (6)$$

which in turn, can be arranged to give

$$\frac{n(E_{\text{applied}} - E_{\text{SCE}} - E_{\text{Ox-Red}}^0)}{0.059} = \log \left( \frac{[\text{Red}]_o}{[\text{Ox}]_o} \right) \quad (7)$$

This process allows the calculation of the ratio of the reactant to the product activities at the electrode surface. As the applied potential becomes more negative this ratio becomes smaller. At a given applied potential ( $\text{Cd}^{2+} \sim -0.6\text{v}$ ), sufficient reduction of the oxidant  $[\text{Ox}]$  will occur instantaneously to establish a concentration ratio in the surface film of the solution. The momentary current required for this would diminish rapidly to zero were it not for the fact that more Ox ions or molecules migrate into the surface film from the bulk of the solution. Since the electrochemical reaction is instantaneous and since the movement of ions is controlled by diffusion alone (thermal or mechanical convection and electrostatic attraction of ions has been eliminated), the diffusion

current,  $i_d$ , is proportional to the concentration of Ox at the surface.

Thus, the equation

$$i_d = k [Ox] \quad (8)$$

is the basis of quantitative polarography (ref. 13 through 20).

The polarographic instrument used\* was calibrated with a series of standard solutions. From such data the concentration of the metal ion in the unknown solutions were determined. The sensitivity and accuracy compare favorably with colorimetric and spectrophotometric methods. The lower concentration limit for some of the metals was  $10^{-7}M$  and as little as 0.001 percent could be determined in 50 mg samples, (See Table 2).

- 
13. Milner, O.H., The Polarographic Method of Analysis, Chem. Ed., Pub. Co., Easton, Pa., 1951.
  14. Kolthoff, I.M. and Lengane, J.J., Polarography, Vol. I and II, Interscience Publishers, New York, 1959.
  15. Meites, L., Polarographic Techniques, Interscience Publishers, Inc., New York, 1959.
  16. Kanning, C.W., Quantitative Analysis, Prentice Hall, Inc., New York, 1949, p. 389.
  17. Skoog, D.A. and West, D.M., Analytical Chemistry, Holt, Rinehart and Winston, New York, 1963, p. 541.
  18. Sandell, E.B., Colorimetric Determination of Traces of Metals, Interscience Publishers, New York, 1959.

\* Sargent Model XV Polarograph.

Table 2

IDENTIFICATION OF CORROSION PRODUCTS  
BY POLAROGRAPHY

Metal ion measured <sup>(1)</sup>	W(III)	Sn (II)	Pb (II)
Volume of solution analyzed, ml	10	10	10
Supporting electrolyte	1N KNO <sub>3</sub>	1N HCl	1M HCl
Voltage range, volts	0+ -2	0 + -2	0 - -1
Additive added to H <sub>2</sub> O <sup>(2)</sup>	No. 11	None	None
Conc. of metal ion obtained, moles/liter x 10 <sup>4</sup>	0.30	0.00	10.90

---

 1 Table 6,

2 Table 7, No. 11

## 6. ABSORPTION SPECTROPHOTOMETRIC METHODS

The spectrophotometric studies were restricted to color sensitive substances which absorb in the visible range of the spectrum. The metal ions were complexed to form colored solutions and the quantitative concentration of the ions was determined with a spectrometer\*. The unknown substance concentration was estimated by noting its light absorption within a narrow wavelength range. In practice, the absorption of the solution was measured at a particular wavelength by noting the photocell response with the absorption cell filled with solution, compared to the response when the absorption cell contained a nonabsorbing solution. The method was ideal to determine solution concentrations of  $10^{-6}$  or even  $10^{-7}$  M with an accuracy of 1 to 2 percent of the total amount of constituent present.

The method is based upon the observation of the amount of light which is absorbed by a solution (ref. 14 to 21). The light absorbed is proportional to the concentration of the substance and also the thickness of the layer of solution through which the light passes. Mathematically this is expressed by the Beer - Lambert Law which states

$$\log \frac{I_t}{I_0} = -abc \text{ or } \frac{I_t}{I_0} = 10^{-abc} \quad (9)$$

in which  $I_t$  and  $I_0$  are the intensities of the transmitted and incident light, respectively;  $c$  is the concentration of the constituent in the solution;  $b$  is the thickness of the layer of solution; and  $a$  is a proportionality constant (absorption coefficient) which depends on the specific nature of the

---

\* Bausch and Lomb Spectronic 20

19. Spectronic 20 Instruction Manual, Bausch and Lomb, Rochester, New York.

20. Industrial Methods Manual - Aluminum Alloys Section, Bausch and Lomb, No. 33-29-03.

21. Kolthoff, I.M., Sandell, E.B., Meehan, E.J., and Brukenstein, S., Quantitative Chemical Analysis, 4th Edition, The Macmillan Co., Toronto, Canada, 1969.

colored constituent. The equation may be written as

$$I_t = I_0 \cdot 10^{-abc} \quad (10)$$

where the intensity of transmitted light in terms of the incident light can be utilized to compare the absorption developed in the unknown solution to that in a series of standards. By controlling the volume and solvent, the terms a and b are eliminated so that plots of percent transmittance versus concentration (g/l) are obtained for the standard solutions, and from these plots the concentration of the unknown can be read directly. An additional instrument\* that utilizes a circular variable interference filter with a wavelength range of 400 to 700 nanometers (nm), was used. Special wavelength dial positions are marked for suspended solids testing (infrared light range) and for the measurement of water color.

#### 7. FLAME PHOTOMETER.

The flame photometer\*\* which was used to analyze sodium and potassium ions (Na+ and K+) consisted essentially of six parts: (1) a pressure regulator or flowmeter for the fuel gas (propane), (2) an atomizer (sample consumption 3.5 ml/min), (3) a burner, (4) an optical system, (5) a photo-sensitive detector, and (6) a digital readout for indicating the output of the detector.

The sample to be analyzed was diluted at 100:1 ratio with standard lithium solution and sprayed under controlled conditions into the flame. The instrument automatically compensates for variations in air or propane fuel, and the flame ignites as soon as the proper air/fuel ratio is present. The light from the flame enters a monochromator to isolate the desired

---

\* Hach Direct Reading DR/2 Spectrophotometer

\*\* Corning Model 450 Flame Photometer

region of the spectrum. A photocell and an electronic amplifier measure the intensity of this isolated radiation. After the photometer was carefully calibrated with solutions of known concentration, the instrument was able to correlate the intensity of a given spectral line of the unknown with the concentration of an element present which emits the appropriate radiation. The sodium and potassium ion values were simultaneously displayed on electronic digital readout in meq/l and are accurate to  $\pm 0.05$  meq/l  $\text{Na}^+$  and  $\pm 0.02$  meq/l  $\text{K}^+$ .

## SECTION III

### MATERIALS STUDIED

#### 1. ULTRAPURE WATER.

Ultrapure water was obtained from the ion-exchange demineralization system located at the Air Force Weapons Laboratory.\* Figure 1 illustrates the schematic of the Model MB-595 Mixed Bed Deionizer where (1) is a 24 x 96 inch Kero seal-lined mixed bed exchanger tank with removable head for ready access to internal distribution; (2) is the 18 by 37 inch polyethylene (37 gal) caustic regenerant tank; (3) is a VY00IT conductivity cell which leads to (4) the conductivity bridge that continually monitors the resistivity of the pure water; (5) is the sight flow strainer for protection against resin entering the treated water line; (6) is a 3 by 12 inch plexiglas observation window for visual monitoring of resins during regeneration cycles; (7) is a 16 by 21 inch polyethylene acid regenerant vessel (15 gal) which is permanently piped; (8) is a totalizing straight reading water meter; (9) is a 1 1/4 inch backwash sight glass; and (10) is a 0 to 100 psig water pressure gauge.

The anion and cation exchange resins used in the system were obtained from the Illinois Water Treatment Company. The Illco C-361 W resin consists of sulfonated polystyrene cation exchange bead in the hydrogen form ( $H-R_C$ ). The Illco A-244 resin is the quaternary ammonium anion exchange resin in the hydroxyl form ( $R_a - OH$ ). Figure 2 illustrates the chemical changes which take place when the combined resins retain the dissolved ions in water and in turn chemically replace them with ion-free water.

---

\* Kirtland Air Force Weapons Laboratory, Kirtland, New Mexico

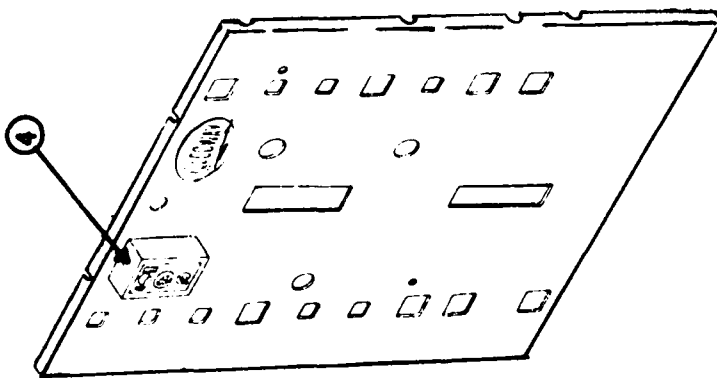
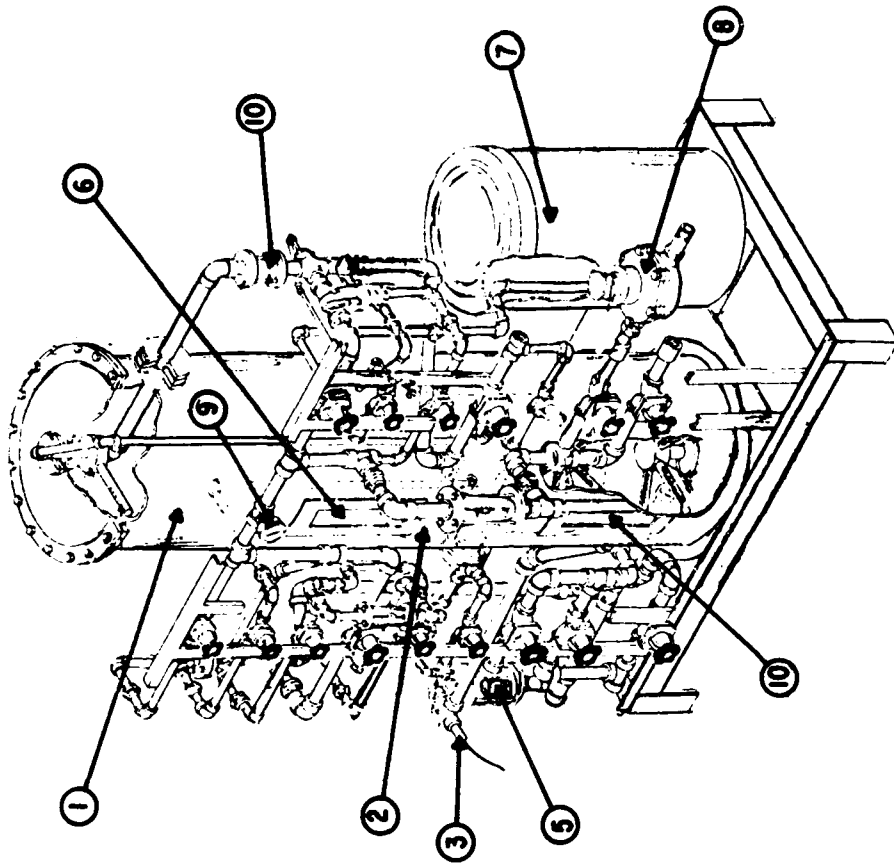


FIGURE 1  
SCHEMATIC OF THE MODEL MB-595 MIXED BED DEIONIZER

$\text{Ca}^{++}$ $\text{Mg}^{++}$ $\text{Na}^+$ (etc)	$\text{SO}_4^-$ $\text{HCO}_3^-$ $\text{Cl}^-$ (etc)	$\text{H-R}_c$ $\text{R}_o\text{-OH}$	$\text{Ca}^{++}$ $\text{Mg}^{++}(\text{R}_e)$ $\text{Na}^+$ (etc)	$\text{SO}_4^-$ $(\text{R}_o) \text{HCO}_3^-$ $\text{Cl}^-$ (etc)	$\text{H}_2\text{O}$
CATION IMPURITIES WATER PHASE	CATION ANION RESIN SOLID PHASE	RESIN SOLID PHASE	RESIN SOLID PHASE	RESIN PHASE	PURE WATER

FIGURE 2  
THE QUALITY OF TREATED WATER

The resins are regenerated by being backwashed to separate anion and cation resins so that regenerating chemicals are introduced separately into each type of resin. The chemicals used to reconvert the resins into the hydrogen and hydroxyl cycles were hydrochloric acid and sodium hydroxide, respectively. After regeneration, the resins are air mixed and drained into a settled resin bed in the mixed bed exchanger tank. The unit is service rinsed to drain until the desired water purity is reached, as monitored on the resistivity bridge.

The system is designed to deliver a chemically pure effluent which contains less than 1 part per million total ionizable solids. Resistances can be as high as 18 megohms under ideal conditions and routine operation produced 15 megohm since the resins must be separated prior to regeneration, the system is not as efficient as when the resins are contained in individual columns. The unit generally produces water having a resistance between 0.5 and 10 megohms; the latter is obtained after multiple rinsings of the regenerated resin. The system also provides for carbon dioxide and silica absorption so that the effluent is free of  $\text{SiO}_2$  and  $\text{CO}_2$ .

The ultrapure water used for sampling was collected under an atmosphere of argon and transferred to a 20 gallon plastic container\* and then transferred to the analytical test station\*\*.

At the testing laboratory, 175 ml of the ultrapure water was transferred (under an atmosphere of nitrogen) into individual glass or plastic

---

\* Nalgene 2211, Rectangular Polyethylene 15 liter Container. Fisher Scientific, 4102 Greenbriar Drive, Houston, Texas.

\*\* Analytical Laboratory, University of Albuquerque, St. Joseph Place, NW, Albuquerque, New Mexico 87140.

bottles (approximately 225 ml total volume). The stoppered bottles were then placed in the precision constant temperature bath\* which was maintained by a constant temperature regulator. Duplex pumps are connected to separate pressure and suction sections on the regulator which permit circulation through the enclosed water bath.

The precision utility bath (27 inches long by 10 1/2 inches wide by 7 inches deep) was placed in a wooden box with the dimensions and appropriate outlet attachments illustrated in figure 3. Eight inches of the front panel and 12 inches of the top panel of the box were removed and sealed with clear plastic to permit access to the work area in the bath. Outlets for the conductivity probe and pH electrodes were provided in the plastic covering. Nitrogen gas entered from one of two outlets located on the top of the box. An inert atmosphere was simulated by flushing nitrogen gas through the system. Since some air may have entered the system when the various sample containers were introduced into the bath, the inert atmosphere may have been contaminated with a minimal amount of air.

The initial measurements of  $k$  and pH, as well as measurements made on solutions saturated with  $\text{CO}_2$  and  $\text{N}_2$ , were made in air free plastic glove bags\*\*\* The plastic bags were not selfsupporting, therefore, a wooden frame was inserted into the bag to hold it upright (figure 4). After the sample solutions were introduced into the bag, it was sealed with a bulkhead which contained two double ended hose fittings for semi permanent connection to

---

\* Thelco-Model 13470-062, Van Waters and Rogers Scientific.

\*\* Lauda/Brinkman K-2/R, Lauda Brinkman Div., Westbury, N.Y., 11590.

\*\*\* Instruments for Research and Industry, 108 Franklin Avenue, Cheltenham, Pa., 19012.

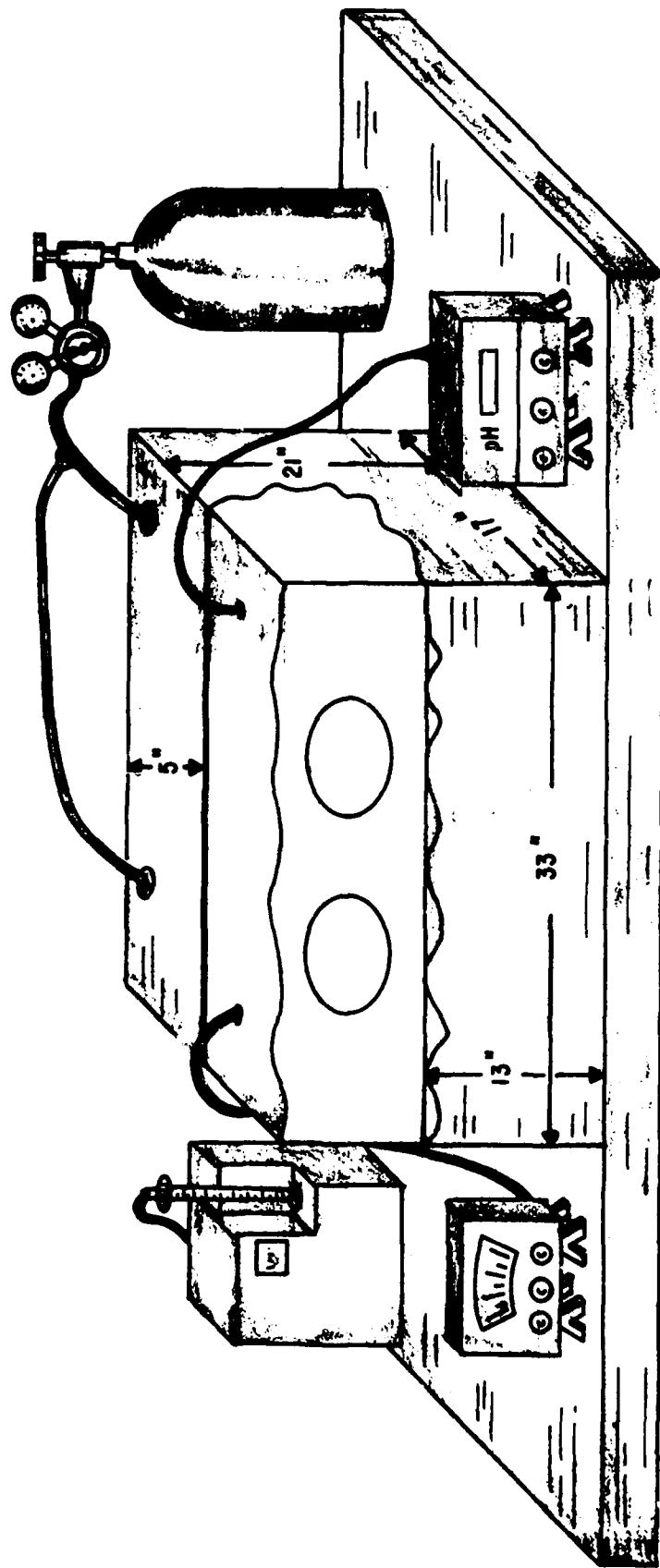


FIGURE 3  
LAB APPARATUS

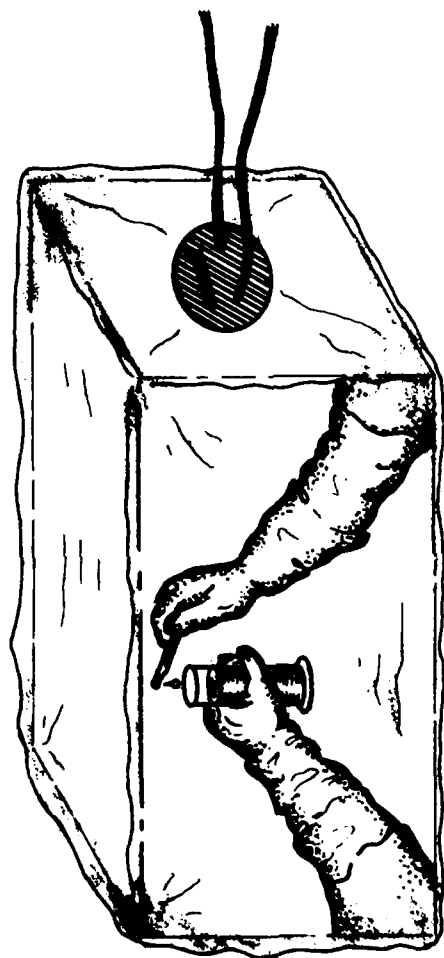


FIGURE 4

GLOVE BAG TO PERFORM STUDIES UNDER VACUUM

nitrogen feed or a vacuum line. The glove bags were not available for all measurements. Values listed in tables 3, 4, and 5 are considered to be obtained in the absence of air and were used to make the appropriate corrections.

## 2. METALS STUDIED.

Several metals and/or alloys were polished, weighed accurately, and submerged in 175 ml of ultrapure water to note corrosive effects as a function of time. Pertinent data on the materials regarding purity, concentration, description, etc., are listed in Table 6.

## 3. THE CORROSION RESISTANCE INHIBITORS TESTED.

Several types of inorganic and organic chemical and polymeric corrosion inhibitors were studied in order to determine their effectiveness with various metallic systems. The description of these materials is given in Table 7.

Table 3  
 THE EFFECT OF CARBON DIOXIDE  
 ON THE pH AND k OF ULTRA  
 PURE WATER AT 25°C

<u>Time, min.</u>	<u>pH</u>	<u>k, <math>\mu</math>mhos/cm</u>	<u>CO<sub>2</sub>mg/l</u>
0.0	6.82	0.96	0.8
0.5	5.40	1.15	84.0
1.0	4.60	1.30	168.0
1.5	4.40	1.35	293.0
2.0	4.24	1.40	423.0
2.5	4.23	1.42	432.0
3.0	4.24	1.45	440.0
3.5	4.23	1.48	443.0
4.0	4.22	1.50	446.0
4.5	4.21	1.52	511.0
5.0	4.20	1.54	576.0
10.0	4.20	1.75	640.0

Table 4  
 VARIATION OF pH AND k AFTER  
 SATURATION WITH NITROGEN

<u>Time, Min.</u>	<u>pH</u>	<u>k, <math>\mu</math>hos/cm</u>	<u>CO<sub>2</sub>, mg/l</u>
0	6.82	0.96	0.80
2	6.94	1.05	0.60
4	6.97	1.18	0.59
6	7.00	1.21	0.58
3	7.01	1.22	0.57
10	7.03	1.23	0.55
15	7.04	1.24	0.53
20	7.05	1.25	0.54
25	7.06	1.27	0.52
30	7.08	1.31	0.50
35	7.09	1.33	0.51
40	7.10	1.35	0.51

Table 5  
 VARIATION OF pH AND k  
 WITH ADDITION OF SILICA

<u>SiO<sub>2</sub>, ml</u>	<u>pH</u>	<u>k, <math>\mu</math> mhos/cm</u>	<u>CO<sub>2</sub>, mg/l</u>
0.0	6.82	0.96	0.80
0.1	6.30	2.70	0.83
0.2	6.22	2.63	0.82
0.4	6.21	2.85	0.82
0.5	6.20	2.92	0.83
1.0	6.18	3.30	0.82
1.5	6.00	3.34	0.83
2.0	5.98	3.38	0.82
3.0	5.99	3.40	0.83
4.0	6.04	3.45	0.83
5.0	6.08	3.50	0.83
6.0	6.13	3.55	0.83
10.0	6.18	3.60	0.83
10.0*	6.24	22.50	0.83

---

\* After standing 50 days.

Table 6

## DESCRIPTION OF METALLIC SYSTEMS STUDIED

<u>Metal</u>	<u>Weight,<sub>2</sub></u>	<u>Additive in 175 ml H<sub>2</sub>O</u>	<u>Source and Purity</u>
1. Aluminum 2024	0.7237	(1)	AFWL, 93.4%, Cu 4.5, Mg 1.5, Mn 0.6, den. 2.70,
	0.5466	(2)	
	0.5527	(3)	
	0.7198	(4)	
	0.7198	(5)	
	2.7624	(6)	
2. Aluminum	2.2170	(7)	ALFA, <sup>9</sup> 99.999%, Si 3, Fe 2, Cu 1, others <1
3. Aluminum	4.1619	(7)	AFWL, 99.9%
4. Brass, No. 356 extra high leaded	2.1772	(1)	AFWL, Cu 58.7, Pb 2.4, Zn 38.5, den. 0.307 lbs/ins <sup>3</sup> , sp. heat 0.03 btu/lb <sup>0</sup> F.
	3.6152	(7)	
	3.6546	(2)	
	4.1425	(3)	
	4.1397	(4)	
	3.6104	(6)	
5. Cadmium	1.7999	(4)	ALFA, <sup>9</sup> 99.99% den. 8.64, melting point 320.9 <sup>0</sup> C
6. Copper Rod	1.7969	(1)	ESPI, <sup>10</sup> 99.99%, Fe 0.1, Ca 0.1, Bi 0.2.
	1.9693	(8)	
7. Copper Wire	1.2478	(2)	J.T. Baker, 99.9% Sb, Sn, Fe, and Pb each 0.005%, Mn and P each 0.001%, Ag 0.002%
	1.2209	(3)	
8. Lead	2.3020	(1)	ESPI, <sup>10</sup> 99.9999% Fe <.1, Ca 0.1, Mg 0.1, Ag <.1
	2.2852	(8)	
	2.4438	(7)	
9. Magnesium - Thorium HM 21A	0.2593	(8)	AFWL, Mg 97.2% Th 2%, Mn 0.8%, nonferrous alloy
	0.2538	(1)	
	0.2540	(7)	
	0.2612	(4)	
	0.2626	(5)	

Table 6 cont'd

10. Molybdenum Rod	2.0751	(1)	ALFA <sup>9</sup> , #201, 99.97% den. 10.2, Ni 30, Fe 30, W 100, Si 50
	2.0904	(8)	
	2.0818	(4)	
	2.0848	(5)	
	2.0909	(5)	
11. Nickel Rod	1.2192	(1)	ESPI <sup>10</sup> , K 3602 D 99.995%, Cu 10, Co 10, Fe 10, S 10, C 10
	1.2047	(8)	
	0.9034	(7)	
	0.8935	(6)	
		(6)	
12. Steel, Maraging	1.5866	(1)	AFWL, Ni 17.8, Mn 0.18, Mo 4.56, Co 9.14, Si 0.12
	1.5166	(8)	
	1.5022	(7)	
13. Steel, Cold Rolled	1.7875	(1)	AFWL, C 0.28-0.34, Mn 0.60-0.90, P 0.04 max., S 0.05, den. 0.283 lb/in <sup>3</sup> , sp. heat 0.10-0.11 btu/lb/ °F
	4.5952	(7)	
	5.6571	(2)	
	5.4214	(3)	
	4.9905	(5)	
14. Steel, Stainless	1.8837	(1)	AFWL, C 0.25 max, Mn 2 max, P 0.45 max, S 0.03 max., Si 1.5- 3.0, Cr 23-26, Ni 19-22, den. 0.22 lb/in <sup>3</sup>
	3.5065	(7)	
	1.6251	(2)	
	1.1256	(3)	
	1.6103	(4)	
15. Tin	1.3651	(1)	ESPI <sup>10</sup> , K5182, 99.999% Cu 0.2, Fe 0.5, In 0.2, Mg 0.5, Pb 1.0, Sb 2
	1.3816	(8)	
	4.4893	(7)	
	4.4914	(4)	
		(4)	
16. Tungsten Rod	2.0524	(1)	ALFA <sup>9</sup> , #341, 99.98%, den. 19.35, Ni 15, Fe 30, Mo 10, Cr 20, Ca 20
	2.0485	(8)	
17. Tungsten Mallory 2000	4.5987	(7)	AFWL, 95%, Ni 3.5%, Cu 1.5%
18. Zinc Rod	1.4297	(1)	ESPI <sup>10</sup> , K 5611 D, Cu <2, Pb <3, Cd, Fe, Mg each <1.
	1.4191	(7)	
	1.4113	(4)	

1. 0.42 g CS
2. 0.95 g Jaguar J2S-1
3. 20 ppm RoVer
4. 1 ml Kerosene plus 1 ml Hydrazine
5. 5 ml LC15
6. 0.05 g Polymer 1212A
7. 0.1 g Jaguar Plus
8. No additives added
9. ALFA Inorganics, Ventron, Beverly, Mass., Purity data in ppm.
10. Electronics Space Products, Inc., 854 So. Robertson Blvd., Los Angeles, Calif. 90035.

Table 7  
ADDATIVES USED TO PREVENT OR SUPPRESS CORROSION

Additive	Source, Description	Amount Used per 175ml vol.	Solution pH	Solution k, umhos/cm
1. Calgon CS	*Calgon Corporation: Combination of Sodium Nitrate-borax and organic inhibitors which prevents corro- sion of ferrous and non ferrous metal and alloy surfaces; light tan granular material.	0.419 g	9.09	3100
2. Hydrazine	Eastman Organic Chemicals; 95+%	2 ml	11.45	192
3. LC-15	*Calgon Corporation: alkaline material which eliminates corrosive attack by hydrogen re- duction mechanisms: liquid formulation of corrosion inhibiting chemicals and dispersant polymer.	25 ml	9.04	1710
4. Jaguar Plus	**Stein, Hall and Co., Inc.; high molecular weight cationic guar derivative; viscosity 1% solution is 800- 1600cps; coagulant aid for potable and industrial water treatment.	0.1 g	7.30	125
5. Polymer 1212A	**Stein, Hall and Co., Inc.; high molecular weight non-ionic guar derivative; viscosity 1% solution is 2500- 3000cps; high degree of compatibility with polyvalent salts.	0.05 g	7.44	18.6
6. $\text{CHCl}_3$	Baker Chemical Co.	1.05 ml	5.26	17.3
7. RoVer	Hach Chemical Co.	3.5 mg	4.98	22.0

Table 7 Continued

Additive	Source, Description	Amount Used per 175ml vol.	Solution pH	Solution K, umhos/cm
8. Polymer JB	**Stein, Hall, and Co., Inc; 3-D gel formation which plugs or diverts addatives.	0.05 g	6.83	12.3
9. Polymer F-3	**Stein, Hall and Co., Inc.; anionic poly- electrolyte; viscosity of 4% solution is 400-800cps.	0.1 g	8.26	330
10. Polymer J2S1	**Stein, Hall and Co., Inc.; nonionic alkali and salt compatible thickener; viscosity of 1% solution is 4000-5000cps.	0.1 g	6.45	20
11. Kerosene- Hydrazine	Eastman Kodak Co.	2 ml	10.47	125
12. LC-15	*Calgon Corporation. see No. 3	5 ml	10.36	410

\* Calgon Center, Pitts, Pa. 15230

\*\* 605 Third Avenue, New York, NY. 10016

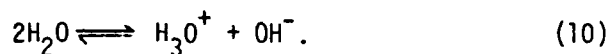
## SECTION IV

### THEORY

#### 1. Properties of Pure Water.

Although water is generally regarded as a non-conductor of electricity, sensitive instruments show that it does conduct to a very small extent.

This conductance results from the dissociation of a very small fraction of the water molecules into hydrogen and into hydroxyl ions as illustrated by



By definition, in totally pure water, the concentrations of these two ions must be identical and a calculated specific conductance of  $0.055 \mu\text{mhos/cm}$  is observed.

The equilibrium expression for the ionization of water is

$$\frac{[\text{H}^+][\text{OH}^-]}{[\text{H}_2\text{O}]} = K_{\text{ion}} = 1.81 \times 10^{-16} \text{ at } 25^\circ\text{C.} \quad (11)$$

where  $K_{\text{ion}}$  represents the ionization constant of pure water and the brackets represent concentration. In all dilute aqueous solutions the concentration of undissociated water,  $[\text{H}_2\text{O}]$ , may be considered constant. At room temperature, a liter of pure water weighs 997 grams or  $997/18 = 55.4$  moles per liter, therefore,

$$[\text{H}^+][\text{OH}^-] = K_{\text{ion}} [\text{H}_2\text{O}] = (1.81 \times 10^{-16})(55.4) = 1 \times 10^{-14} = K_{\text{w}} \quad (12)$$

where  $K_{\text{w}}$  is the ion product constant of water. Dissociation (and  $K_{\text{w}}$ ) increase with temperature; therefore, since  $\text{pH} = -\log [\text{H}^+]$ , the pH should decrease with temperature.

When  $[H^+] = [OH^-] = 1 \times 10^{-7}$ , the solution is neutral. When  $[H^+] > [OH^-]$ , the solution is acidic, and when  $[H^+] < [OH^-]$  the solution is alkaline or basic. The measurement of pH will therefore be a measure of the change of  $[H^+]$  due to corrosion.

The problem of definitions and standards of pure water has been approached by several organizations which have attempted to set standards for determination of water quality and to define specifications for pure water. The United States Pharmacopoeia (U.S.P.) has set specifications for Purified Water, U.S.P. which certifies water produced by either distillation or ion exchange to be pure enough for use in medicines provided it passes certain tests described for evaluating the contaminant levels. It further qualifies other kinds of water purity, notably Water for Injection, U.S.P., which must meet the double requirements of sterility and freedom from pyrogenicity in addition to chemical purity. The American Chemical Society (ACS), the College of American Pathologists (CAP), and the American Society for Testing and Materials (ASTM) have also established specifications for "reagent grade" water. The various specifications are given in Table 8 which was compiled from data presented in references 22 to 25.

- 
22. Wickett, J.A., Chemical Processing, 25, No. 15, 20, 1962
  23. Phillips, S.L., Mack, D.A. and MacLeod, W.D., "Instrumentation for Water Quality Monitoring," Anal. Chem., 46, 345A, 1974.
  24. Instrumentation for Environmental Monitoring: Water, LBL-1, Vol. 2, Technical Information Division, Lawrence Berkeley Laboratory, Berkeley, California 94720.
  25. Brown, E, Skougstad, M.W., and Fishman, M.J., "Methods for Collection and Analysis of Water Samples for Dissolved Minerals and Gases," Book 5, Chap. AI, U.S. Geological Survey, 1970. Available from: Superintendent of Documents, U.S. Government Printing Office, Washington, D.C. 20402.

Table 8  
STANDARD SPECIFICATIONS FOR REAGENT GRADE WATER

ASTM Specifications	Type I	Type II	Type III	Type IV
Total matter, max. mg/l	0.1	0.1	1.0	2.0
Specific conductance, umho/cm (25°C)	0.06	1.0	1.0	5.0
pH at 25°C	6.8-7.2	6.6-7.2	6.5-7.5	5.0-8.0

CAP Specifications	Type I	Type II	Type III
Heavy metals, mg/l maximum	0.01	0.01	0.01
Specific conductance, umho/cm (25°C)	0.10	2.00	5.00
Silicate, mg/l, maximum	10.0	0.5	0.2

ACS Specification	Reagent Grade Water
Specific conductance, umhos/cm at 25°C:	Not more than 2.0
Silicate (as SiO <sub>2</sub> ):	Not more than 0.01 ppm
Heavy metals (as Pb):	Not more than 0.01 ppm

The purity, quality, or degree of deionization of water is usually determined by measuring the specific resistance of the water. Since ionizable solids in water will conduct an electrical current and decrease the specific resistance of water, the greater the ionizable solid content, the lower the resistance of the water.

The specific conductance,  $k_{sp}$ , of water is defined as the reciprocal of the resistance in ohms, measured between opposite faces of a centimeter cube of an aqueous solution at a specified temperature (see ref. 9).

The  $k_{sp}$  of pure water can be calculated from the equivalent conductances of the hydrogen and hydroxyl ions by

$$k_{sp} = (\Lambda_{H^+} + \Lambda_{OH^-}) \cdot d \cdot K_w^{1/2} \quad (13)$$

where  $\Lambda_{H^+}$  is the equivalent conductance of  $H^+$ ,  $\Lambda_{OH^-}$  is the equivalent conductance of the  $OH^-$ , and  $d$  is the density of water. The  $k_{sp}$  of ultra pure water at  $25^\circ C$  is  $0.055 \mu\text{mhos/cm}$  or  $R = 18.24 \text{ Meg ohms-cm}$ .

A change in specific conductance would indicate the presence of other electrolytes. As ionizable substances are added, the conductance would increase, thus providing a measure of the total ion concentration of the water sample. Conductivity measurements can therefore be related to dissolved solid concentrations, and conductivity is a useful guide to the purity of distilled or demineralized water. Table 9 (taken from ref. 26) illustrates the change in conductivity as a function of concentration of many common electrolytes.

## 2. Effect of Atmospheric Gases on Water Purity.

Dissolved gases may have a pronounced effect on the conductivity of

- 
26. Reagent Grade Water Purification For the Laboratory, Tech. Bulletin 22, Ion Exchange Products, Inc., 4500 N. Clark St., Chicago, Illinois, 60640.

Table 9

SPECIFIC CONDUCTANCE, RESISTANCE, APPROXIMATE ELECTROLYTE CONTENT  
DEIONIZED WATER AT 25°C

Sp. Cond. In μmhos	Sp. Resis. in Ohms	APPROXIMATE ELECTROLYTE CONTENT, ppm			
		NaCl	HCl	NaOH	CO <sub>2</sub>
0.1	10,000,000	0.04	0.01		
0.2	5,000,000	0.08	0.02	0.03	
1	1,000,000	0.4	0.13	0.2	0.8
2	500,000	0.8	0.26	0.4	2.5
4	250,000	1.6	0.55	0.8	9.5
6	166,000	2.5	0.9	1	20
8	125,000	3.2	1.2	1.5	40
10	100,000	4	1.5	2	70
20	50,000	8	2	4	320
30	33,333	14	3	5	730
40	25,000	19	4	6	1,400
50	20,000	24	4.5	7	2,200
60	16,666	28	5.5		
70	14,286	33	6.5		
80	12,500	38	7.5	11	
90	11,111	43	8		
100	10,000	50	9	14	
200	5,000	100	18	27	

the solution. It is generally necessary to reduce the concentration of these gases and/or to correct for those present. Electrical conductivity cannot be precisely related to all dissolved solids because some dissolved solids, such as silica and certain types of organic matter, contribute little or nothing to the conductivity.

When atmospheric gases are brought into contact with air, a certain amount will dissolve. The maximum solubility depends on temperature, pressure, and the relative strength of the bonds formed between the water and the gas molecules. At low pressures solubility usually decreases with temperature, whereas, at high pressures it may increase with temperature.

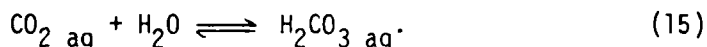
In dilute solutions gas solubility follows Henry's Law

$$X = p / H \quad (14)$$

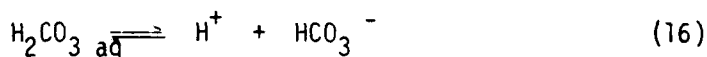
where X is the liquid mole fraction, p is the partial pressure of the gas, and H is Henry's constant. The measured value of H depends on the temperature and strength of intermolecular bonding.

The gases that make appreciable contribution to atmospheric contamination of water are nitrogen, oxygen, and carbon dioxide.

Carbon dioxide dissolved in water produces considerable electrical conductivity due to the fact that the gas combines with water to form carbonic acid



The acid then dissociates stepwise to form bicarbonate ion



which has a dissociation constant defined by

$$K_1 = \frac{[\text{H}_3\text{O}^+][\text{HCO}_3^-]}{[\text{H}_2\text{CO}_3]} = 1.72 \times 10^{-4} \quad (17)$$

The bicarbonate ion can further dissociate into carbonate and hydrogen ions by



and this second dissociation constant,  $K_2$ , is

$$K_2 = \frac{[\text{H}_3\text{O}^+][\text{CO}_3^{=}]}{[\text{HCO}_3^-]} = 4.68 \times 10^{-11} \quad (19)$$

can be expressed by the equilibrium between carbon dioxide and carbonic acid (Eq. 15) by

$$K_{\text{eq}} = \frac{[\text{H}_2\text{CO}_3]}{[\text{CO}_{2\text{aq}}]} = 2.6 \times 10^{-3} \quad (20)$$

As a result, the often quoted value for  $K_1$  of  $4.4 \times 10^{-7}$  corresponds to

$$\frac{[\text{H}^+][\text{HCO}_3^-]}{[\text{CO}_{2\text{aq}}] + [\text{H}_2\text{CO}_3]} = 4.47 \times 10^{-7} \quad (21)$$

It is immaterial which value of  $K_1$  is used, provided it is specified whether  $\text{H}_2\text{CO}_3$  or the sum of  $\text{CO}_{2\text{aq}}$  and  $\text{H}_2\text{CO}_3$  is being considered. For practical purposes, the total concentration of carbon dioxide will be used (Eq. 21) but for simplicity of writing, the equilibrium reactions, will be represented by the designate  $[\text{H}_2\text{CO}_3]$ , to represent the total concentration of carbon dioxide.

Since there are five species in solution, five equations relating the ionic concentrations are necessary. These five equations include:  $K_w$  (Eq. 12),  $K_1$  (Eq. 21),  $K_2$  (Eq. 19), the initial concentration of the acid,  $C_A$ , and the charge balance equation.

Since the material balance depends on the initial concentration of the acid  $C_A$  (moles/liter), the concentration of those species containing the carbonate component must add up to the amount initially present:

$$C_A = [\text{H}_2\text{CO}_3] + [\text{HCO}_3^-] + [\text{CO}_3^{=}] \quad (22)$$

The charge balance is represented by the following equation

$$[\text{H}_3\text{O}^+] = [\text{OH}^-] + [\text{HCO}_3^-] + 2 [\text{CO}_3^{=}] \quad (23)$$

since the sum of the moles of the species carrying a positive charge must equal that for the negative charge. The factor 2 before  $[\text{CO}_3^{=}]$  is necessary because it takes two moles of  $\text{H}_3\text{O}^+$  to neutralize the two equivalents of charge of the carbonate ion.

To arrive at the final equation, equation (23) is solved for  $[\text{HCO}_3^-]$  and substituted into equation (17) which becomes

$$K_1 = \frac{[\text{H}_3\text{O}^+]( [\text{H}_3\text{O}^+] - [\text{OH}^-] - 2 [\text{CO}_3^{=}] )}{[\text{H}_2\text{CO}_3]} \quad (24)$$

Equation (23) is then solved for  $[\text{HCO}_3^-]$  and substituted in equation (19) to give

$$K_2 = \frac{[\text{H}_3\text{O}^+] [\text{CO}_3^{=}]}{[\text{H}_3\text{O}^+] - [\text{OH}^-] - 2 [\text{CO}_3^{=}]} \quad (25)$$

Equation (22) is solved for  $[\text{H}_2\text{CO}_3]$  and substituted in equation (24) giving

$$K_1 = \frac{[\text{H}_3\text{O}^+]( [\text{H}_3\text{O}^+] - [\text{OH}^-] - 2 [\text{CO}_3^{=}] )}{C_A - [\text{HCO}_3^-] - [\text{CO}_3^{=}]} \quad (26)$$

Equation (23) is solved for  $[\text{HCO}_3^-]$  and substituted in equation (26) to yield

$$K_1 = \frac{[\text{H}_3\text{O}^+]( [\text{H}_3\text{O}^+] - [\text{OH}^-] - 2 [\text{CO}_3^{=}] )}{C_A - [\text{H}_3\text{O}^+] + [\text{OH}^-] + 2 [\text{CO}_3^{=}] - [\text{CO}_3^{=}]} \quad (27)$$

Equation (25) is solved for  $[\text{CO}_3^{=}]$

$$[\text{CO}_3^{=}] = \frac{K_2 ( [\text{H}_3\text{O}^+] - [\text{OH}^-] )}{([\text{H}_3\text{O}^+] + 2 K_2)}$$

and equation (28) is substituted in equation (27) to yield

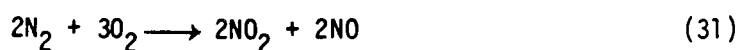
$$K_1 = \frac{H_3O^+ \left( [H_3O^+] - [OH^-] - \frac{2K_2([H_3O^+] - [OH^-])}{[H_3O^+] + 2K_2} \right)}{C_A \left( [H_3O^+] - [OH^-] - \frac{K_2([H_3O^+] - [OH^-])}{[H_3O^+] + 2K_2} \right)} = \frac{[H_3O^+][A]}{C_A - [B]} \quad (29)$$

The concentration of the acid is then obtained by rearrangement of equation (29).

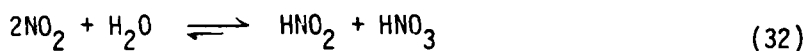
$$C_A = [B] + \frac{[H_3O^+][A]}{K_1} \quad (30)$$

The evaluation of the specific conductivity and pH of pure water in equilibrium with the carbon dioxide of the atmosphere is of great importance in obtaining proper water corrections. Whatever the method of preparation of pure water and how small the initial specific conductivity of the newly prepared water, its value rises rapidly on standing to certain limits of CO<sub>2</sub> absorption and then remains practically constant. The conducting impurities in such waters consist almost entirely of carbonic acid (refs. 26 to 29).

Nitrogen gas may react with dissolved oxygen in water to form oxides of nitrogen by



The nitrogen oxides in turn may react with water to form nitric acid by



(for this last equation the equilibrium is shifted only slightly to the

27. Fricke, G.H., Carpenter, R.L., and Battino, R., "Effect of Various Gases on the pH of Water," Jour. Phys. Chem., 77, 826, 1973.

28. Jencks, W.P., "General Acid - Base Catalysis of Complex Reactions in Water," Chem. Reviews, 72, 705, 1973.

29. 1955 Book of ASTM Standards, Part 7, American Society for Testing Materials, Phil., Pa., 1956.

right). The presence of oxygen is therefore undesirable because it aids in the formation of acids (Eq. 31) or it may oxidize any metallic material present in solution.

### 3. Water Correction.

The proper method of applying a water correction is not immediately obvious because of the uncertainty as to the exact nature and amount of impurities present in the contaminated water. If it is assumed that the conductivity and pH changes are due solely to absorbed carbon dioxide, then the total concentration of carbonic acid,  $C_A$ , can be calculated from equation (30) and thus the difference between the conductivity and pH of pure and contaminated water would be due to the carbonic acid contamination. After this water correction, the amount of corrosion of metallic ions could be determined.

On the other hand, if it is assumed that a minute concentration of ions are present because of improper techniques used in ion exchange regeneration of resins, the concentration of these ions must be known so that their effect on the conductivity of the water can be determined.

### 4. Regeneration of Contaminated Water.

The water purification system which results in reagent grade water exceeding the highest ASTM and CAP specifications is obtained by assembling various purification elements and components. Generally, an activated carbon purifying cell followed by a mixed bed ion exchange purifying cell and a submicron filter is an acceptable system of purification. The cation and anion exchange resins in the mixed bed system have the capacity to remove a specific amount of ionizable solid from the water, after which the resins become exhausted and are unable to further remove additional

ions. When the resins do become exhausted, they can be regenerated so that their ion exchange capacity is restored. The cation resin is regenerated with acid, usually hydrochloric or sulfuric; the anion resins are regenerated with alkali, usually caustic soda.

Ion exchange resins are solid, insoluble beads capable of removing dissolved ions. Cation exchangers will remove cations while the anion exchangers will pick up anions including silica and other weak acids. The choice of the ion exchanger to be used for water treatment depends on the composition of the raw water, the intended water use and the degree of ionic impurity removal required. Softening of hard water by cation exchange is generally understood. However, this form of treatment only changes the nature of the cationic impurities but does not decrease the total dissolved solids. Where deionization is required, a combination of cation and anion exchangers is necessary. The most satisfactory method for obtaining ultra-high purity water is the use of these two general types of ion exchangers in a single unit containing the proper mixture of these materials.

The quality of the treated water will be reflected by the raw water composition. Ultra-high purity water of greater than 10 megohms-cm and less than 0.1 ppm silica is generally possible.

Mixed bed demineralization is the most efficient method known for producing low conductivity water. Distillation, deionization, reverse osmosis and filtration are methods commonly used to produce reagent grade water. Each has limitations and none alone can meet most of the purity standards. For example, water produced by distillation - the classical laboratory method of purification - has a resistivity approaching 0.5 Megohm-cm and does not meet the minimum specifications for Type 1 reagent grade water.

Table 10  
 A COMPARISON OF WATER QUALITIES OBTAINED BY  
 VARIOUS PURIFICATION METHODS

	Resistance ohm/cm	Specific Conductance umho/cm
Theoretical	26,000,000	.0385
Water after 28 distillations in quartz	23,000,000	.0435
Mixed bed demineralization no pretreatment	18,000,000	.0555
Four bed demineralization	1,000,000- 4,000,000	1-.25
Three distillations in quartz	2,000,000	.5
Three distillations in glass	1,000,000	1
Two bed demineralizer	500,000- 1,000,000	2-1
Water in equilibrium with CO <sub>2</sub> in air	700,000	1.4
Single distillation in glass	500,000	2
USP distilled water	100,000- 500,000	10-2

Table 10 shows a comparison of the quality of water obtained by various purification methods.

5. The Corrosive Properties of Water.

Corrosion, in the broad sense, connotes the whole range of reactions between metals and their nonmetallic environments. Corrosion is referred to as a reversion, or partial reversion, from the metastable condition of the metal to the stable condition of the mineral. The processes involved are complex, and the many factors which enter into the process may be distinguished between those associated with the metal and those associated with the environment.

Most of the corrosion that is of industrial importance takes place in solutions which are feebly acid from the  $\text{CO}_2$  of the atmosphere with oxygen as a cooperating agent. The hydrogen ion from carbonic acid gives up its electrical charge at the surface of the metal to become hydrogen gas, and the metal goes into solution as metallic ions. If a small amount of oxygen is present with the  $\text{CO}_2$ , the oxygen will oxidize the film of gaseous hydrogen so that more hydrogen ion is released and corrosion continues. McKay and Worthingham (ref. 30) have shown the interdependence of acidity and oxygen concentration on corrosion. If the concentration of hydrogen ion is low, pH 6 to pH 9, and very little oxygen is present, the driving force of the ions in solution will continue until free hydrogen gas collects on the metal but further corrosion ceases because of the absence of oxygen.

It is generally agreed that the mechanism of underwater corrosion is electrochemical in nature in which hydrogen evolution or oxygen absorption occurs. Even though separate electrodes cannot always be distinguished

---

30. McKay, H. and Worthington, W., Corrosion Resistance of Metals and Alloys, Reinhold Publishing Co., New York, 1936.

spatially, the basic features of an electrochemical cell made up of anodic and cathodic components are present.

The corrosion of metals by liquids is known to involve two distinct processes. First, the metal ions, which are normally fixed in a regular sequence in the solid metal, leave their positions and begin a free existence in the solution. This loss of metal results in corrosion damage. The second phase of the reaction is concerned with a reductive process. The departure of the positive ions leave the metal with an excess of negative electrons; these negative charges at once enter into some form of reductive process at the metal surface which may include one of the following reactions:

a. Conversion of dissolved oxygen to  $\text{OH}^-$  so that  $\frac{1}{2} \text{O}_2 + \text{H}_2\text{O} + 2e \rightleftharpoons 2\text{OH}^-$  (in neutral solution)

b. Discharge of hydrogen ions to give hydrogen gas:  $2\text{H}^+ + 2e \rightleftharpoons \text{H}_2$  (in strong acid solution)

c. Reduction of other ions in the electrolyte

To conform with the similar process occurring during the electrolysis of solutions, the loss of metal and the reductive process are termed anodic and cathodic reactions, respectively. (Anodic = loss of metal; cathodic = reductive process.) Since the electricity produced when the metal dissolves is utilized in the reductive process, it is clear that the anodic and cathodic reactions are tied together and proceed at exactly the same rate.

The corrosivity of water (refs. 3 to 9) is measured by the chemical action of the water on a standard sample of a given material sensitive to the corrosive substances of interest. Pure water in an uncorrodible vessel should never leave a deposit. Although this ideal case has been very nearly reached in some instances, deposits are still formed in most water or steam systems.

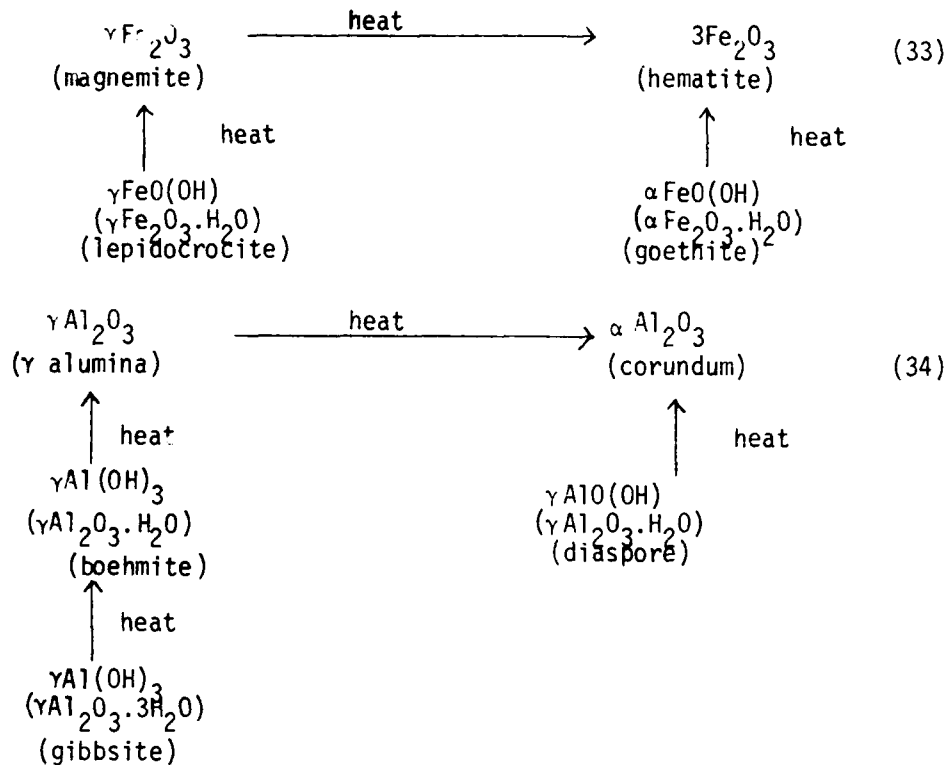
Inorganic deposits result from corrosion of containing surfaces; from precipitation by chemical reaction between two or more constituents of the water; or precipitation from physical causes, such as change in solubility with pressure or temperature, by evaporation to dryness, or by relief of supersaturation.

Corrosion in boilers can be caused by oxygen, which usually produces a characteristic pitting at the water line; by galvanic attack resulting from the presence of scales or deposits; and by direct attack of iron by water at very high temperatures.

The deposits or scales formed generally result from elements such as calcium, magnesium, iron, silicon, and aluminum. The relatively soluble metallic salts which form in solution may combine with the hydroxide of the same metal and form insoluble basic double salts. These are often found on metallic surfaces as corrosion products where water contains a considerable amount of oxygen. An alkaline condition is not always required and the compounds may be formed at pH values below 7.0. Copper can form basic carbonates, chlorides, and sulfates. Atacamite ( $\text{CuCl}_2 \cdot 3\text{Cu}(\text{OH})_2$ ) is frequently found as a hard, very adherent corrosion deposit in condenser tubes. Zinc forms a basic carbonate as  $2\text{ZnCO}_3 \cdot 3\text{Zn}(\text{OH})_2$  and a basic magnesium chloride,  $\text{MgCl}_2 \cdot 5\text{Mg}(\text{OH})_2 \cdot 8\text{H}_2\text{O}$ , may be formed in sea water.

Carbonates of most of the alkaline earth and heavy metal elements are insoluble while the respective bicarbonates are much more soluble; heat and an increase of pH value shift the bicarbonate to the normal carbonate form to produce the respective insoluble compounds.

The class of hydrated oxides contains principally the trivalent corrosion and precipitation products of iron and aluminum. The "hydrated oxides" of iron and aluminum are interrelated in that temperature and time cause the more highly hydrated forms to lose water and undergo alterations of crystal structure. This relationship is shown in the following scheme.:



It is believed that the  $\gamma$  monohydrates (lepidocrocite and boehmite) in industrial deposits are more likely formed by recrystallization from rapidly precipitated amorphous gels. The  $\alpha$  monohydrates (goethite and diasporé) are more likely to have formed without the gel precursor. The  $\gamma$  forms are usually formed at lower temperatures than are the  $\alpha$  forms. There is also a series of hydrated oxides of zinc, but the composition of this series is indefinite.

Simple hydroxides precipitate from solutions of high pH values, or under special conditions, hydrolyze in corrosion reactions. Calcium hydroxide may scale out in lines carrying lime slurries or in super heaters and steam lines by thermal hydrolysis of a previously deposited calcium carbonate. Ferrous hydroxide  $\text{Fe}(\text{OH})_2$  has been identified in corrosion pits and nickel hydroxide  $\text{Ni}(\text{OH})_2$  in exfoliated flakes from cupro-nickel stage heaters.

Metal oxides are invariably the products of corrosion reactions, the dehydration of hydrated oxides, or the decomposition of carbonates. The oxides may be loose and porous or compact and adherent according to the conditions of formation. Oxygen for the formation of the oxide can be provided by dissolved oxygen in water or by bound oxygen from molecular  $\text{H}_2\text{O}$ . In the latter instance, hydrogen is also produced.

Magnetite ( $\text{Fe}_3\text{O}_4$ ) is formed under the greatest variety of conditions.  $\text{FeO}$ ,  $\text{Fe}_3\text{O}_4$ , and  $\text{Fe}_2\text{O}_3$  can all be found in aqueous corrosion products of iron according to the amount of oxygen present.  $\text{Fe}_3\text{O}_4$  and occasionally  $\text{FeO}$  are the principal impurities in steam.

The two copper oxides, cuprite ( $\text{Cu}_2\text{O}$ ) and tenorite ( $\text{CuO}$ ) may both be components of boiler sludge or corrosion films on copper, brass, or bronze. High oxygen concentrations and high pH values are favorable conditions for the formation of tenorite, whereas cuprite is more likely the solid phase of a lower pH and lower dissolved oxygen concentrations.

Corundum ( $\text{Al}_2\text{O}_3$ ) has been found in high-pressure boilers and turbines as an alteration of precipitated alumina. Zincite ( $\text{ZnO}$ ) is a hot water corrosion product on metallic zinc

Uncombined silica as quartz or cristobalite forms by the hydrothermal alteration of solid silicates or by direct crystallization from dissolved silica. Quartz ( $\text{SiO}_2$ ) is one of the hardest of the minerals, but the crystal size is small in water deposits so that the extreme hardness of the natural mineral is not imparted to the deposit. Quartz formation in steam turbines is caused by volatile transport of silica from the boiler water. Cristobalite is another form of crystalline silica in steam turbine deposits. Uncombined silica may also be a component of siliceous boiler scales.

Free silica in heat exchanger deposits results from the deposition of sand or dirt suspended in the cooling water. The principal property of such deposits depends on the substance forming the matrix of the individual grains of silica.

The silicates of single cationic elements are classified as simple silicates. The calcium and magnesium silicates have incongruent solubilities and contain water of hydration when formed hydrothermally. The composition of the solids are dependent on temperature and pressure as well as on the relative concentrations of the dissolved reacting ions.

The hydrous magnesium silicates, serpentine ( $3\text{MgO} \cdot 2\text{SiO}_2 \cdot 2\text{H}_2\text{O}$ ), talc ( $3\text{MgO} \cdot 4\text{SiO}_2 \cdot \text{H}_2\text{O}$ ) and sepiolite ( $2\text{MgO} \cdot 3\text{SiO}_2 \cdot 2\text{H}_2\text{O}$ ), are soft, rather poorly crystallized compounds. Detection by instrumental means is not always successful. The formation results from the alteration and crystallization of an absorption complex of dissolved silica on magnesium hydroxide. Serpentine forms under the most varied conditions and for this reason is the most common of the three forms.

The hydrous calcium silicates, gyrolite ( $2\text{CaO} \cdot 3\text{SiO}_2 \cdot \text{H}_2\text{O}$ ), xonotlite ( $5\text{CaO} \cdot 5\text{SiO}_2 \cdot \text{H}_2\text{O}$ ), and foshagite ( $5\text{CaO} \cdot 3\text{SiO}_2 \cdot 3\text{H}_2\text{O}$ ), like the hydrous magnesium silicates, crystallize poorly but unlike them may be hard, tough, and highly insulating. The common form is xonotlite, with gyrolite and foshagite being somewhat rare.

The anhydrous simple silicates, fayalite ( $2\text{FeO} \cdot \text{SiO}_2$ ), mullite ( $3\text{Al}_2\text{O}_3 \cdot 2\text{SiO}_2$ ), olivine ( $2(\text{Mg},\text{Fe})\text{O} \cdot \text{SiO}_2$ ), and forsterite ( $2\text{MgO} \cdot \text{SiO}_2$ ), are common high temperature dehydration products of related hydrous forms. Willemite ( $2\text{ZnO} \cdot \text{SiO}_2$ ) is one of the few anhydrous simple silicates formed hydrothermally.

The sodium silicates,  $\text{Na}_2\text{SiO}_3$  and  $\beta\text{Na}_2\text{Si}_2\text{O}_5$ , are somewhat soluble in high temperature steam and therefore are components of turbine blade deposits. Their water solubility is appreciable so that they may be removed by washing the turbine internally with wet steam.

Silicate compounds of more than one cationic element are classified as complex silicates. These hydrothermally formed compounds are often crystallized from environments of very high heat input and are usually hydrous. Regions of high heat input become highly concentrated in boiler water salts that contain sodium silicate. In these regions conditions exist which are favorable to reactions with oxides of aluminum, iron, and calcium to form the respective sodium silicate complexes. The sodium silicate complexes are not easily corrected by treatment of the water since they may form in water with no hardness present. All are very hard and adherent and resist dissolution by ordinary acid cleaning procedures. They may form in place on the steam-generating surface or by reaction with acmite ( $\text{Na}_2\text{O} \cdot \text{Fe}_2\text{O}_3 \cdot 4\text{SiO}_2$ ). Analcite ( $\text{Na}_2\text{O} \cdot \text{Al}_2\text{O}_3 \cdot 4\text{SiO}_2 \cdot 2\text{H}_2\text{O}$ ) is the most common aluminum analog and may be present in sludge form as well as scale.

Natrolite ( $\text{Na}_2\text{O} \cdot \text{Al}_2\text{O}_3 \cdot 3\text{SiO}_2 \cdot 2\text{H}_2\text{O}$ ) and noselite ( $5\text{Na}_2\text{O} \cdot 3\text{Al}_2\text{O}_3 \cdot 6\text{SiO}_2 \cdot 2\text{SO}_3$ ) occur much less frequently than analcite. Acmite has also been found in turbine blade deposits suggesting that the components of the reaction may be steam soluble.

#### 6. The Use of Inhibitors To Prevent Corrosion.

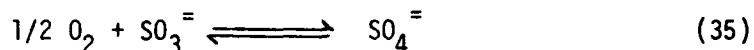
A variety of chemical compounds when present in water in which a metal is immersed, have the property of retarding or sometimes completely inhibiting corrosion. Sodium benzoate is an example of a safe inhibitor, and at a concentration of 1 percent or more, it will protect steel (but not cast iron) immersed in aqueous solutions. If chlorides are present in the water, the concentration of sodium benzoate should be increased to give adequate protection.

Sodium nitrite added to water gives protection both to cast iron and steel, but attacks soldered joints. However, a mixture of sodium nitrite and sodium benzoate may be used to protect both cast iron and steel, and suitable mixtures do not attack soldered joints (refs. 31 and 32).

In systems where corrosion by oxygen is a factor, protection can be obtained by adding a long chain aliphatic amine, such as octadecylamine, which forms a polarized film over the surface of the metal and serves as a physical barrier against attack to both carbon dioxide and oxygen. Maguire (ref. 33) discusses both filming and neutralizing amines; the latter are generally favored because of the lower cost.

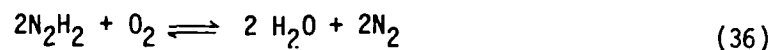
- 
31. Vernon, W.H.J., "Sodium Benzoate as a Safe Inhibitor of Prevent Corrosion," Research Jour., 5, 54 (1952).
  32. Thornhill, R.S., "Corrosion Inhibitors", Research Jour., 5, 324 (1952).
  33. Maguire, J.J. "After Boiler Corrosion", Ind. Eng. Chem. 46, 994 (1954).

Dissolved oxygen may be removed from water by a vacuum deaeration process or by addition of a reducing agent such as sodium sulfite to serve as an oxygen scavenger. Sulfite reacts with oxygen as indicated



where the sulfite is converted to sulfate. While the reaction is rapid at high temperatures but slow at ordinary temperatures, small concentrations of copper or cobalt may be used to catalyze the reaction (ref. 34).

At very high pressures hydrazine is often used as an oxygen scavenger, the reaction being



The advantage of this treatment is that no solids are introduced; however, the nitrogen formed may be converted to ammonia.

Carbonic acid may be partially removed by boiling; however, the dissociation of carbonic acid produces a small concentration of hydrogen ions which cause a typical grooved type of corrosion that is especially severe at stressed points such as bands or threads. Carbonic acid may be neutralized by adding amines or ammonia to the water. The function of the additives is to maintain the pH above 7.4. In low pressure systems (less than 15 psi) cyclohexylamine is often used, whereas, at high pressures morpholine (diphenyleneimide oxide) is effective. The amines react with carbon dioxide to form very weak carbamic acids thus:



Ammonia itself is infrequently employed as a neutralizing agent because the corrosive effect of oxygen on copper is greatly intensified in the presence of ammonia.

---

34. Pye, D.J., "Chemical Fixation of Oxygen", J. Am. Water Works Assoc., 39, 1121 (1947).

Hydroxyl ion in contact with metal under stress leads to deterioration and eventual failure of the metal. High sulfate alkalinity ratios are recommended along with the addition of sodium nitrate, sulfonates, and the like, as preventive treatment in riveted boilers.

Anodic inhibitors may be used to form protective films over the anodic areas. Very strong oxidizing agents such as dichromate ion, render iron impassive by forming a film of oxides on the surface of the metal. The metal is thus, in effect, made more electronegative. Under this condition it is not oxidized by hydrogen ion, nor does it reduce cupric ion. Darrin (ref. 35) describes the use of chromate as an anodic inhibitor while Hatch (ref. 36) shows the effectiveness of small concentrations of polyphosphates in producing cathodic polarization on copper surfaces.

When instruments are to be used in contact with corrosive liquids, it is imperative that suitable materials should be used. Generally, organic plastic materials are resistant to an atmosphere contaminated by inorganic vapors. The use of polyethylene powder for producing a tough protective coating on metals is known; the name Telcothene\* being given to the powder.

Metals differ greatly in their resistance to corrosion, and the behavior of a given metal varies considerably with circumstances. Stainless steels owe their inertness to an oxide layer on the surface. Zinc, cadmium, nickel, and chromium are widely used as plating metals for the protection of iron, steel and brass (ref. 37).

A method of polishing steel by chemical attack has recently been described (ref. 38). The steel is degreased by immersion in a hot alka-

- 
35. Darrin, M., "Chromate Corrosion Inhibitors in Bi-metallic Systems", Ind. Eng. Chem., 33, 755 (1941).
  36. Hatch, G.B., "Inhibition of Galvanic Attack of Steel with Phosphate Glasses," Ibid., 44, 1780 (1952).

line metal cleaner, followed by a short dip in dilute sulfuric acid and then suspended in an oxalic acid- sulfuric acid- hydrogen peroxide bath which acts as a polishing fluid. The polished surface has an increased degree of resistance to mild corrosive conditions, ascribed to the formation of a smooth dense oxide film ( $60\text{\AA}$  thick).

---

\*Tradename of the Telegraph Construction and Maintenance Company, Ltd.

37. Evans. U.R., "Metallic Corrosion, Passivity and Protection", Research Journal, 5, 220 (1952).
38. Marshall, W.A., "Chemical Polishing of Steel", Research 7, 89 (1954).

## SECTION V

### EXPERIMENTAL RESULTS AND DISCUSSION

#### 1. ANALYSIS OF WATER SAMPLES

##### a. Impurities Present in Water

Slight deviations in the original pH and specific conductivity values for ultra pure water suggested possible contamination by: (1) solid impurities associated with improper rinsing techniques after regeneration of the resin (See Section III: MATERIALS STUDIED) or (2) water contamination resulting from dissolved atmospheric gases, especially nitrogen, oxygen, and carbon dioxide.

In order to determine the effect of improper rinsing techniques a detailed analysis of the water was made to determine the concentration of possible ionic impurities such as chloride ion,  $\text{Cl}^-$ , sodium ion,  $\text{Na}^+$ , potassium ion,  $\text{K}^+$ , and solid silicate impurities of silica,  $\text{SiO}_2$ . Table 11 illustrates the result of an analysis of several 500 ml water samples. The sodium and potassium ions were determined by flame photometry (See Section II).

Chloride ion was determined by the formation of a mercury-diphenylcarbazone coordination compound (ref. 39). Chloride ions react with mercury (II) ions, and the excess mercury ions react with diphenylcarbazone to give a colored complex. The intensity of the color depends on the concentration of mercury ion and thus is inversely proportional to the concentration of chloride ion. The coordination compound has an absorption maximum at 520 nm. The concentration was determined from spectrophotometer readings.

---

39. Shales, O., and Shales, S.S., "Chloride Ion Determination by the Formation of a Mercury Diphenylcarbazone Complex", J. Biol. Chem., 140, 879 (1941).

TABLE 11

COMPOSITION OF ULTRA PURE WATER AND WATER  
SATURATED WITH CO<sub>2</sub>, N<sub>2</sub>, AND SiO<sub>2</sub> AT 25°C

Parameters	H <sub>2</sub> O <sup>(1)</sup>	H <sub>2</sub> O <sub>air</sub> <sup>(2)</sup>	H <sub>2</sub> O <sup>(3)</sup> CO <sub>2</sub>	H <sub>2</sub> O <sup>(4)</sup> N <sub>2</sub>	H <sub>2</sub> O <sup>(5)</sup> SiO <sub>2</sub>
k, umhos/cm	0.92	1.88	41.00	1.32	3.60
pH	6.82	5.82	4.20	7.10	6.18
Na <sup>+</sup> , mg/l	0.08	0.09	0.09	0.09	0.10
K <sup>+</sup> , mg/l	0.04	0.04	0.11	0.04	0.14
Cl <sup>-</sup> , mg/l	0.08	0.09	0.09	0.09	0.09
SiO <sub>2</sub> , mg/l	0.02	0.02	0.02	0.02	0.01
N <sup>6</sup> , mg/l	0.04	0.04	0.03	0.06	0.04
CO <sub>2</sub> , mg/l	0.75	1.60	640	0.62	0.78

1 Ultra pure water

4 Water saturated with N<sub>2</sub> for one hour

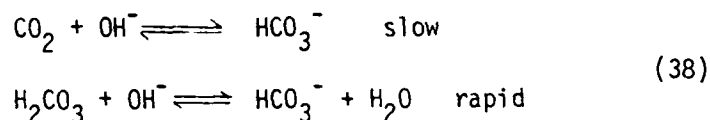
2 Water exposed to air for 3 hours

5 Water saturated with 10 ml of 1 mg/l SiO<sub>2</sub>3 Water saturated with CO<sub>2</sub> for 5 minutes

6 Nitrogen in ammonia

The soluble silicates were determined by reacting silicate with ammonium molybdate solution to form the yellow complex of silico-12-molybdate ( $\text{Si Mo}_{12}\text{O}_{40}^{-4}$ ) (ref. 40). The intensity of the color and hence the concentration in mg/l was determined spectrophotometrically.

The concentration of  $\text{CO}_2$  was determined by titrating a freshly drawn (or a freshly deaerated) sample to phenolphthalein with standard alkali. Since the reaction of  $\text{CO}_2$  and  $\text{OH}^-$  is slow (ref. 41) the former is partially lost during the titration. To correct for this situation, the titration was repeated, adding at once all the amount of alkali needed in the first titration. The chemical equations are:



The parts per million of  $\text{CO}_2$  were determined from the expression

$$\text{ppm CO}_2 = \frac{\text{titr} \times \text{N} \times 44 \times 10^6}{\text{ml of sample} \times 10^3}\tag{39}$$

where titr refers to the titer and N to the normality of the sodium hydroxide solution used.

The total nitrogen content of a water sample includes nitrate, nitrite and organic and ammonia nitrogen. Since ultrapure water is being considered here, it is assumed that only dissolved nitrogen gas and ammonia nitrogen are possible.

The nitrogen was determined by the Kjeldahl method in which the nitrogen present is converted to ammonium bisulfate by the action of sulfuric acid and a catalyst. Nitrate and nitrite are not covered by this procedure.

---

40. Bunting, W.E., "Determination of Soluble Silica in Very Low Concentrations," *Ind. Eng. Chem., Anal Ed.*, **16**, 612 (1944).

41. Kolthoff, I.M., and Belcher, R., *Volumetric Analysis Vol. III*, Interscience Pub. Co., N.Y.-London, 1957, pp. 133-166.

The impurities noted for ultra pure water (Table 11) suggest that the observed conductivity of 0.92  $\mu\text{mhos/cm}$  results mainly from the  $\text{CO}_2$  contamination. For the listed impurities a k value of 0.905  $\mu\text{mhos/cm}$  was calculated from table 9 and references 29 and 42. The value is in close agreement with the experimental value listed.

Dissolved oxygen content was not determined; however, it was assumed that up to 5.0 ppm oxygen could be present in the solution (ref. 42). A vacuum degasification stripping technique was used to obtain the pH, k, and impurity concentrations listed for ultra pure water in Table 11. Since the sample was not contaminated with air at the test station, it was assumed that any  $\text{CO}_2$  was absorbed by the water as it was drawn from the water system and transferred to the plastic storage container.

The data for column 2 were obtained by exposing a 500 ml solution of ultra pure water to the atmosphere for 3 hours. The water thus exposed absorbed an additional 0.85 mg/l of  $\text{CO}_2$  to attain a value of 1.6 mg/l. The nitrogen content as well as the concentration of  $\text{K}^+$ ,  $\text{Na}^+$ , and  $\text{Cl}^-$  remained constant; therefore the increase in  $\text{CO}_2$  (hence the increase in concentration of carbonic acid) is assumed to be responsible for the increase of k to 1.88 units and the decrease in pH to 5.82. In table 12 and figure 5 is illustrated the effect of air on the specific conductance and the pH of ultra pure water. For this study 100 ml of ultra pure water was exposed to the atmosphere for 5 1/2 hours.

Table 9 postulates a k of 1.0  $\mu\text{mhos/cm}$  for a water solution containing 0.8 part per million of carbon dioxide. Since all initial k values on ultra pure water varied from 0.81 to 1.30  $\mu\text{mhos/cm}$ , it was assumed that the

---

42. Coursey, B.M., "The Effect of Trace Additives and Impurities on Properties of High Purity Water," Engineering Division, U.S. Army Engineer Reactors Group, Ft. Belvoir, Va., 22060, AERG-ED-7109, August, 1971.

Table 12  
 THE EFFECT OF AIR ON THE  
 pH AND k OF ULTRA PURE WATER

<u>Time, min.</u>	<u>pH</u>	<u>k, <math>\mu</math>hos/cm</u>	<u>CO<sub>2</sub>, mg/l</u>
0	6.82	0.81	0.75
1	6.75	0.96	0.85
10	6.50	1.01	0.92
20	6.35	1.32	1.00
30	6.22	1.38	1.06
40	6.15	1.44	1.11
50	6.12	1.51	1.17
60	6.10	1.58	1.22
70	6.08	1.64	1.29
80	6.06	1.71	1.35
90	6.05	1.77	1.42
100	6.04	1.84	1.49
140	6.02	2.10	1.55
180	5.98	2.34	1.60

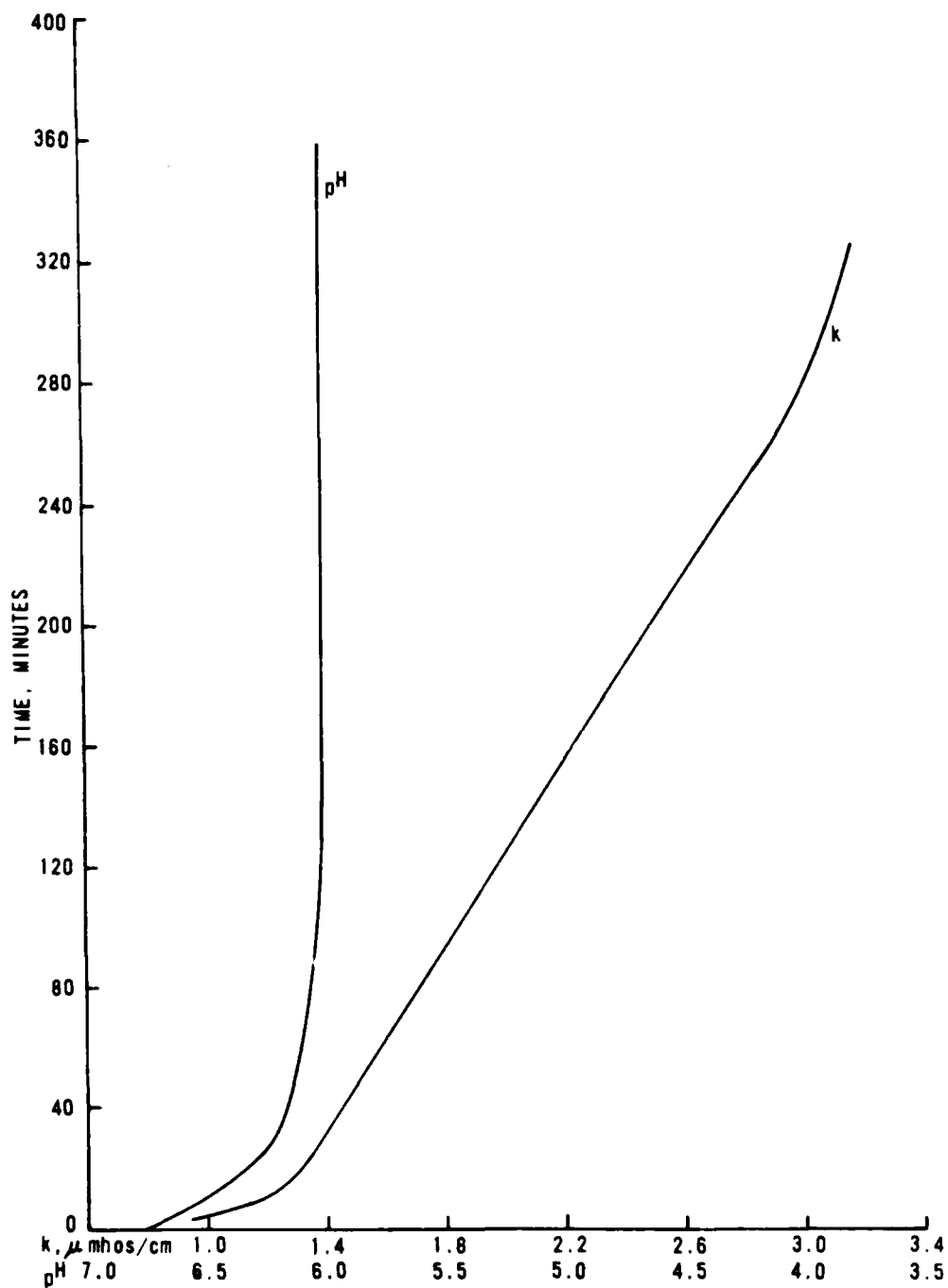


Figure 5. The Effect of Air on the pH and k of Ultrapure Water

variation was the result of atmospheric contamination.

If one assumes that variations in pH and k are associated only with carbon dioxide absorption, the concentration of carbonic acid,  $H_2CO_3$ , can be calculated from equation (30). Table 13 lists the concentrations of carbonic acid calculated by means of equation (30).

Kendall (ref. 43) and Washburn (ref. 44) found that a saturated solution of carbonic acid under atmospheric conditions at 25°C had a concentration of  $2.05 \times 10^{-6}$  moles/liter when the partial pressure of  $CO_2$  was 0.00035 atm. Coursey (ref. 42) gives a value of  $10.3 \times 10^{-6}$  as the molar concentration of the acid based on the assumption of maximum solubility of  $CO_2$  from air containing  $3 \times 10^{-4}$  mole fraction  $CO_2$  gas.

The data of table 13 indicate that the value of  $2.06 \times 10^{-6}$  moles/l for water exposed to the atmosphere is in close agreement with the value reported by Kendall and Washburn for the same type of sample. The acid concentration for the other water samples listed (table 13) varies directly with the pH of the solution.

Since an atmosphere of nitrogen gas flowed through the system when the k and pH measurements were made (Section III), studies were made on solutions saturated with nitrogen to note its effect on pH and k. The values tabulated for column five of table 11 and graphed as a function of time in figure 6 were obtained after gaseous nitrogen was bubbled directly into a 500 ml solution of ultra pure water for 1 hour. The data indicate that immediately after the nitrogen gassification, the k value rose slightly to

- 
43. Kendall, J., "The Specific Conductivity of Pure Water in Equilibrium with Atmospheric Carbon Dioxide", J. Am. Chem. Soc., 38, 1480 (1916).
  44. Washburn, E.W., "Conductance of Electrolytes in Aqueous Solution", J. Amer. Chem. Soc., 40, 106 (1918).

Table 13  
 AMOUNT OF CARBONIC ACID PRESENT  
 IN THE VARIOUS WATER SAMPLES AT 25°C

<u>Type of Water</u>	<u>[H<sup>+</sup>] x 10<sup>7</sup></u>	<u>[OH<sup>-</sup>] x 10<sup>8</sup></u>	<u>CA x 10<sup>6</sup> moles/liter</u>
H <sub>2</sub> O <sub>p</sub>	1.510	6.61	2.41
H <sub>2</sub> O <sub>air</sub>	15.14	0.66	2.06
H <sub>2</sub> O <sub>CO<sub>2</sub></sub>	631.0	0.02	1.48
H <sub>2</sub> O <sub>N<sub>2</sub></sub>	0.89	11.22	2.51
H <sub>2</sub> O <sub>SiO<sub>2</sub></sub>	5.76	1.74	2.18

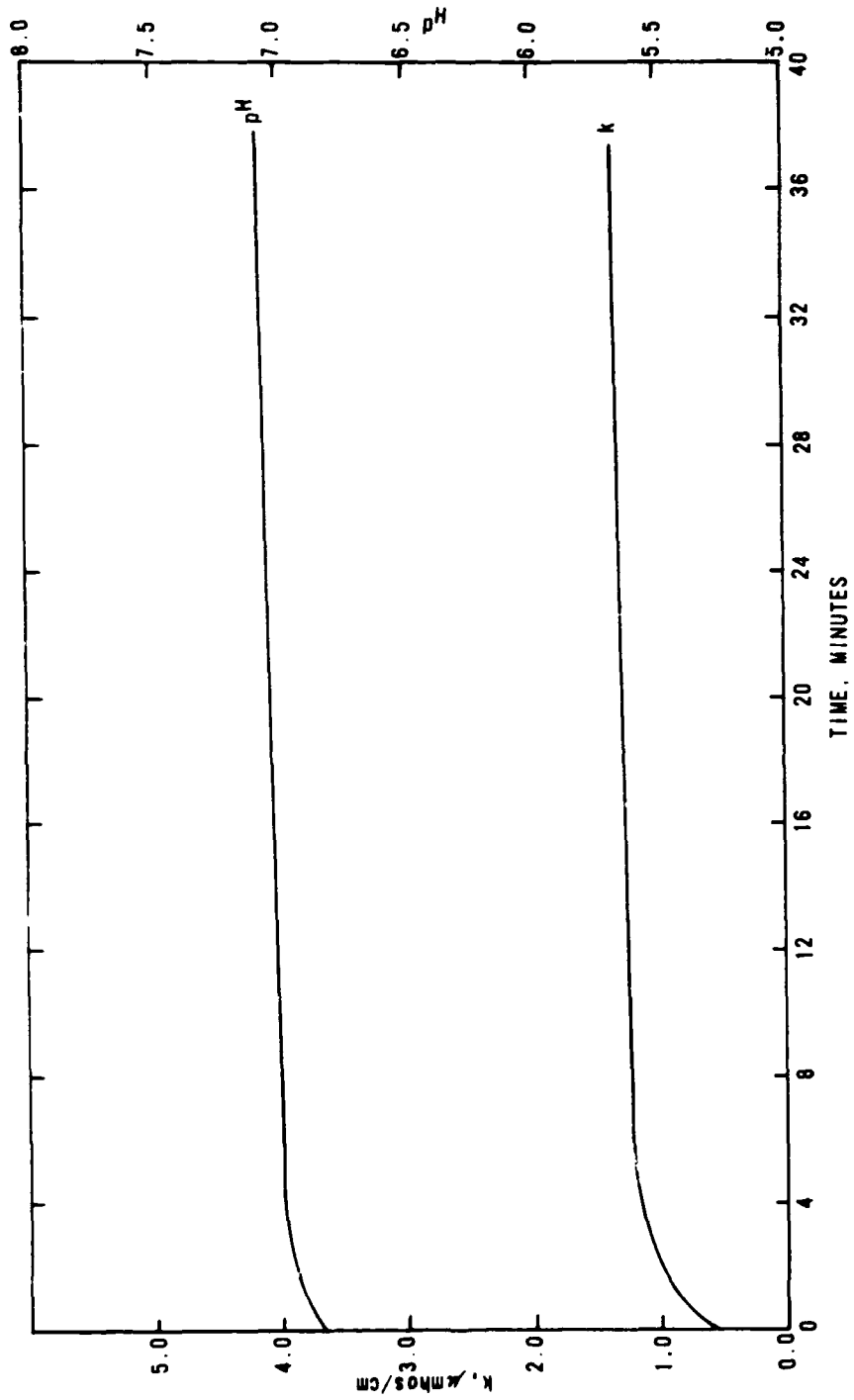


Figure 6. The Saturation of Ultrapure Water with Nitrogen

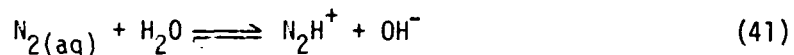
1.33  $\mu\text{mhos/cm}$ ; this was lower than the value obtained for the air study. The  $\text{CO}_2$  concentration also decreased, whereas the pH values increased (see table 4).

It appears that this inert gas does produce a definite decrease in the activity of hydrogen ions in water. One theoretical explanation is that the physical process of dissolving the gas could account for the pH rise by changing the structure of the water and so changing the activity of  $\text{H}^+$ .

A second and better possible explanation proposed by Holleran et al. (ref. 45) is that the dissolved gas acts as a Lewis base, forming weak coordinate bonds with hydrogen ions. This would result in the formation of such species as  $\text{N}_2\text{H}^+$ , nitrogenium ion. If the basicity mechanism is assumed, it can be postulated that the following will occur. First, the gaseous nitrogen is in equilibrium with dissolved nitrogen, whose concentration is proportional to the partial pressure of the gas by the following equation:

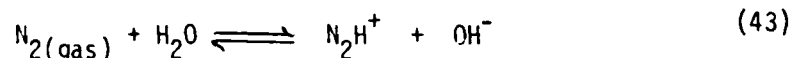


The dissolved nitrogen then acts as a Lewis base as follows



$$[\text{OH}^-][\text{N}_2\text{H}^+] = K_b [\text{N}_2(\text{aq})] = K \cdot P \quad (42)$$

where  $K_b$  is the base constant of the aqueous species and  $K$  is  $K_b K_s$ , an equilibrium constant for the overall process defined as



and it is a base constant for the gaseous species.

45. Holleran, E.M., Hennessy, J.T., and LaPietra, F.R., "Anomalous pH Changes in Solutions of Inert Gases Possibly Indicating Their Basicity," Jour. Phys. Chem., 71, 3081 (1967).

Using the expression for  $K_w$  (equation 12), where  $K_w = [H^+][OH^-]$ , and deriving an equation for the charge conservation as

$$[H^+] + [N_2H^+] = [OH^-] \quad (44)$$

gives the following relations for the saturated solution:

$$2\Delta = \log(1 + K_b \cdot K_s \cdot P / K_w) \quad (45)$$

$$K \cdot P = 10^{-14} (10^{2\Delta} - 1) \quad (46)$$

in which  $\Delta$  is the pH rise. It may be noted that  $K \cdot P$  must be at least  $10^{-14}$  if any appreciable pH change is to be found. For a pressure  $P$  of 1 atm and  $\Delta$  of 1.0 pH unit,  $K$  is about  $10^{-12}$ .

Holleran et al., (ref. 45) found that gaseous nitrogen, argon, and helium are of about equal base strength. The basic strength of the gas might be assumed to increase with the electron density in the exterior shell and the polarizability.

Significantly, the observed pH increase reported in table 11, column 5, whether explained by basicity of the gas or by changes in the structure of the water, is consistent with experimental solubility measurements. The lower the pH of the water, the greater the concentration of the nitrogen. Akerlof (ref. 46) found that the inert gases are more soluble in perchloric acid solution than in water; therefore, if the solution becomes contaminated with  $CO_2$ , it will absorb more nitrogen by this salting in effect.

Diamond (ref. 47) suggested that such salting in may be due to the association of large positive ions and nonelectrolytes caused by the enhanced water structure. It appears that the salting in of the inert gas by acid

---

46. Akerlof, G., "The Solubility of Noble Gases in Aqueous Salt Solution at 25°C," J. Amer. Chem. Soc., 57, 1196 (1935).

47. Diamond, R.M., "The Aqueous Solution Behavior of Large Univalent Ions. A New Type of Ion-Pairing," J. Phys. Chem., 67, 2513 (1963).

solutions seems to result from the association of the neutral molecules with hydrogen, however, the ability to form weak bonds with nonelectrolyte molecules by accepting a share of the exterior electrons explains both the solubility phenomenon and the pH elevation reported.

For the water saturated with  $\text{CO}_2$  for 10 minutes (column 4-table 11), the  $k$  increased to  $41.0 \mu\text{mhos/cm}$  and the pH decreased to 4.2. A corresponding increase in the carbon dioxide gas content was evident. Table 3 and figure 7 gives the change in  $k$  and pH for the solution as a function of time.

For the water saturated with 10 ml of  $\text{SiO}_2$ , the  $k$  was very difficult to obtain due to rapid conductivity fluctuations. This is evident in figure 8 for small concentrations of  $\text{SiO}_2$ . The fluctuations are probably caused by some insoluble silicates being formed in solution, and for this reason conductivity measurements are not significant for solutions contaminated with silica. The  $k$  value of  $3.5 \mu\text{mhos/cm}$  was estimated after 3 hours. A slight decrease in the pH was also observed (table 5).

The slight increase in silica content for pure water (0.02 mg/l) was probably due to the glass container in which the water was stored. Noll and Maguire (ref. 48) have published the effect of various containers on the content of silica in water. They found that in hard rubber and resin-lined cans the silica content was virtually unchanged, but with soda glass and pyrex containers the silica content increased almost 15 percent after storage for 2 weeks.

---

48. Noll, C.A. and Maguire, J.J., "Effects of Containers on Soluble Silica Content of Water Samples," Ind. Eng. Chem., Anal. Ed., (1942).

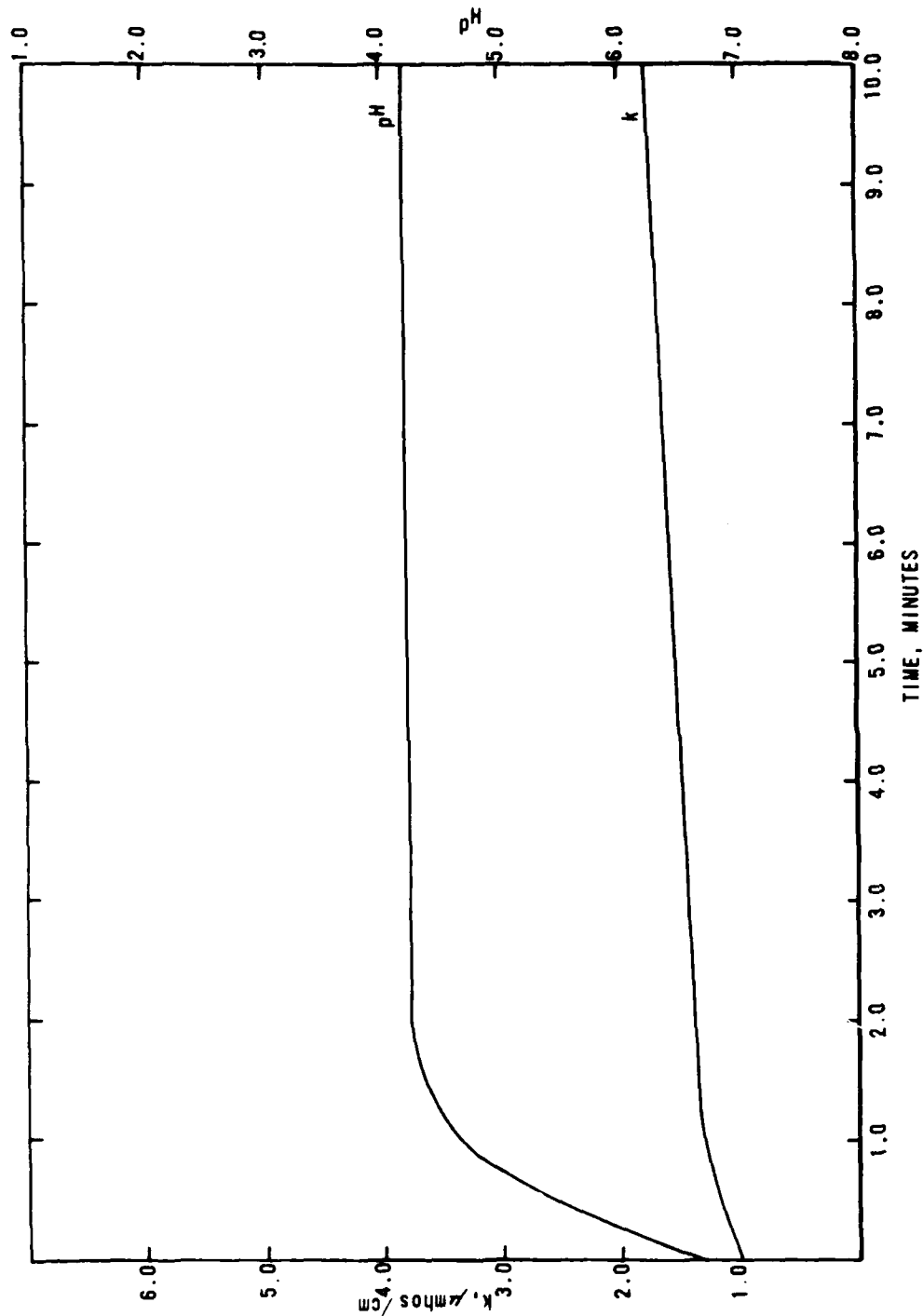


Figure 7. The Saturation of Ultrapure Water with Carbon Dioxide

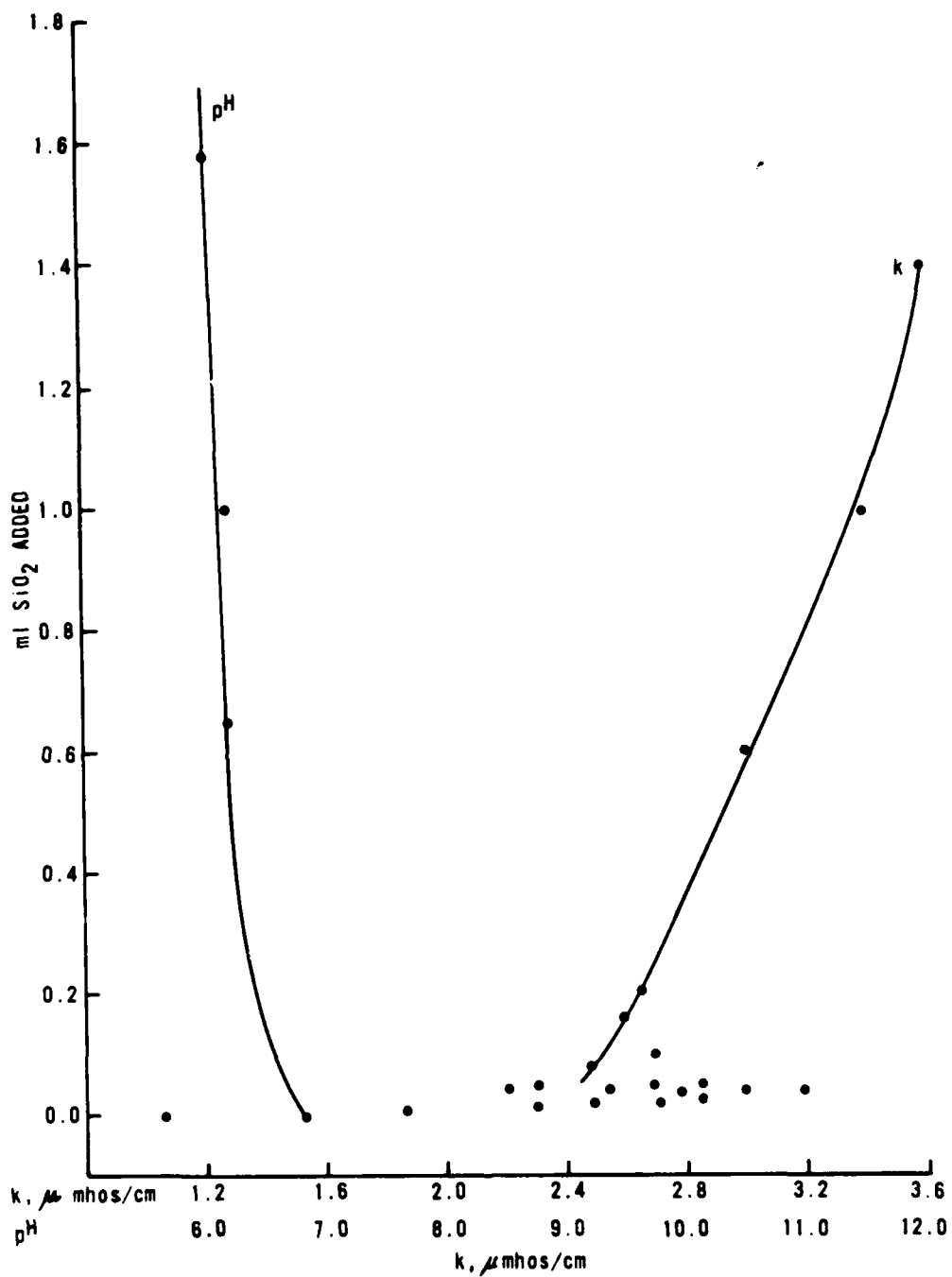


Figure 8. The Contamination of Ultrapure Water with Silica

#### b. Water Correction For Conductivity Data

Since an inert atmosphere was simulated by passing nitrogen gas through the system (see figure 3), it was necessary to observe the temporal effects of such a situation on ultrapure water.

Although pH electrodes filled with a low viscosity gel were used for all pH measurements, the ultra pure water showed some contamination from the potassium chloride reference material. Figure 9 and table 14 illustrate the effect of potassium chloride see page on the k values of ultra pure water as a function of time. Curve  $k^{(1)}$  was obtained from measurements made on water in which no pH electrodes were introduced; curve  $k^{(2)}$  is the same water in which both k and pH measurements were made.

Table 15 gives concentration data for the various gaseous and ionic impurities found in the two samples after testing for 200 days. The greater absorption of nitrogen gas by  $H_2O^{(1)}$  (no pH measurements made in this sample) is consistent with data presented by Akerlof (ref. 46). For this sample, more carbon dioxide was absorbed and hence the pH decreased; therefore, more nitrogen gas was absorbed by the salting-in effect of the acid. The decrease in absorption of carbon dioxide and nitrogen noted for sample 2 ( $H_2O^{(2)}$  - table 15) is consistent with conductivity measurements made on dilute solutions (refs. 42 through 47).

Holleran, et al., (ref. 45) have shown that dilute solutions of potassium chloride ( $10^{-3}$  to  $10^{-5}$  M) may be purged by various gases with no observable pH shift resulting. The purging gases they studied were nitrogen, oxygen, hydrogen, helium, argon, and methane, in which the absolute average deviation of pH was 0.03. This salting-out effect observed for the gases

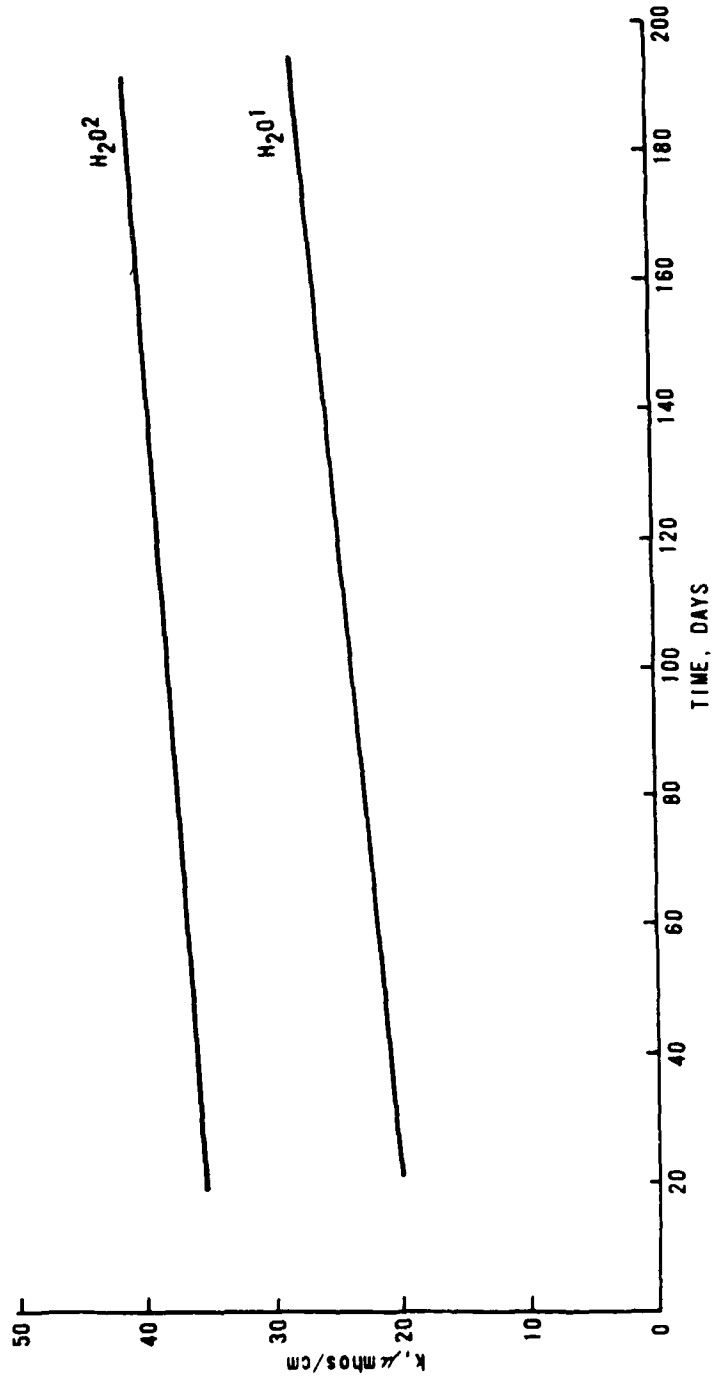


Figure 9. The Contamination of Ultrapure Water with Ions from the pH Electrodes

Table 14

WATER CORRECTION FOR CONDUCTIVITIES  
IN MICROMHOS/CM

<u>Time, days</u>	<u>H<sub>2</sub>O<sup>(1)</sup></u>	<u>H<sub>2</sub>O<sup>(2)</sup></u>	<u>k<sup>(2)</sup> - k<sup>(1)</sup></u>	<u>k<sup>(2)</sup>/k<sup>(1)</sup></u>
0	0.9	0.9	0.0	1.0
20	19.9	35.2	15.3	1.77
30	20.4	35.5	15.1	1.74
40	20.8	35.9	15.1	1.73
50	21.3	36.3	15.0	1.70
60	21.8	36.6	14.8	1.68
70	22.5	36.9	14.4	1.64
80	23.0	37.3	14.3	1.62
90	23.2	37.6	14.4	1.62
100	23.8	37.9	14.1	1.59
110	24.2	38.3	14.1	1.58
120	24.6	38.7	14.1	1.57
130	25.2	39.0	13.8	1.55
140	25.5	39.3	13.8	1.54
150	26.0	39.6	13.6	1.52

1 H<sub>2</sub>O in which only k measurements were taken.

2 H<sub>2</sub>O in which pH and k measurements were made.

Table 15

## EXPERIMENTAL DATA TO ILLUSTRATE THE EFFECT OF

## ADDITIVES ON WATER

<u>Solution (1)</u>	<u>pH<sup>(2)</sup></u>	<u>k, umhos/cm</u>	<u>CO<sub>2</sub>, mg/l</u>	<u>N<sub>2</sub>, mg/l</u>	<u>Na, mg/l</u>	<u>K, mg/l</u>
1. H <sub>2</sub> O <sup>1</sup>	--	26.0	2.08	3.05	1.45	0.16
2. H <sub>2</sub> O <sup>2</sup>	7.45	39.6	1.29	1.37	0.80	0.36
3. Calgon CS	9.08	3200	0.00	0.38	30.70	0.30
4. RoVer	4.55	56.0	5.83	4.40	0.10	0.15
5. Jaguar Plus	8.35	152	0.10	3.18	1.70	0.12
6. Polymer J2S-1	5.93	48.0	32.00	15.62	0.10	0.21
7. Polymer F-3	7.00	495	30.00	19.60	4.10	0.47
8. Polymer JB	6.84	40.0	23.00	4.40	0.30	0.15
9. Polymer 1212A	7.32	77.0	9.00	12.60	0.25	0.14
10. Chloroform	6.35	38.0	3.00	4.80	0.10	0.04
11. Hydrazine	10.50	660	0.00	(3)	0.65	0.17
12. LC-15 (5 ml)	9.14	560	53.00	8.80	5.50	0.15
13. Kerosene -Hydrazine	9.64	790	0.00	(3)	0.35	0.34

(1) Mixtures as identified in Table 7.

(2) After 150 days.

(3) The solution was too dark to take a measurement.

in electrolytic solutions is in marked contrast to the salting in effect of carbonic acid mentioned above.

Studies made under vacuum conditions for ultra pure water and water exposed to atmospheric gases (table 12) suggest a conductivity water correction of 1.38  $\mu\text{mhos/cm}$  at 25°C. This correction is attributed solely to contamination by atmospheric gases.

Figure 9 and table 14 illustrate a specific conductance deviation ( $k^{(2)}/k^{(1)}$ ) of approximately 1.6  $\mu\text{mhos/cm}$  over the entire temporal period between  $\text{H}_2\text{O}^{(1)}$  and  $\text{H}_2\text{O}^{(2)}$ . Since table 15 shows a greater absorption of carbon dioxide, nitrogen and sodium for  $\text{H}_2\text{O}^{(1)}$ , the  $k^{(2)}/k^{(1)}$  values (table 14) define all impurity differences and is associated with solubility data such as salting-in and salting-out effects plus contamination from the electrode reference materials.

## 2. THE SELECTION OF PROPER METALS TO BE USED AS ELECTRODES

Metallic container disintegration was followed by periodically measuring the conductivity and pH changes of the resulting solution. Each metal was placed in a glass container, covered with pure water, and sealed. After stated time intervals, each container was opened and the pH and the conductivity of the metallic solution was noted. The change in pH and the conductivity from that of pure water, combined with the quantitative analysis of the concentration of metallic ions present, was the direct method used to measure the amount of corrosion. Figure 10 and table 16 illustrate the change in pH and conductivity after several metals were immersed in ultra pure water for a maximum of 180 days. These changes are recorded in columns 4 and 5 of table 16 as  $\text{pH}_{\text{M}^{++}}$  and  $k_{\text{M}^{++}}$  where the subscript  $\text{M}^{++}$  defines the

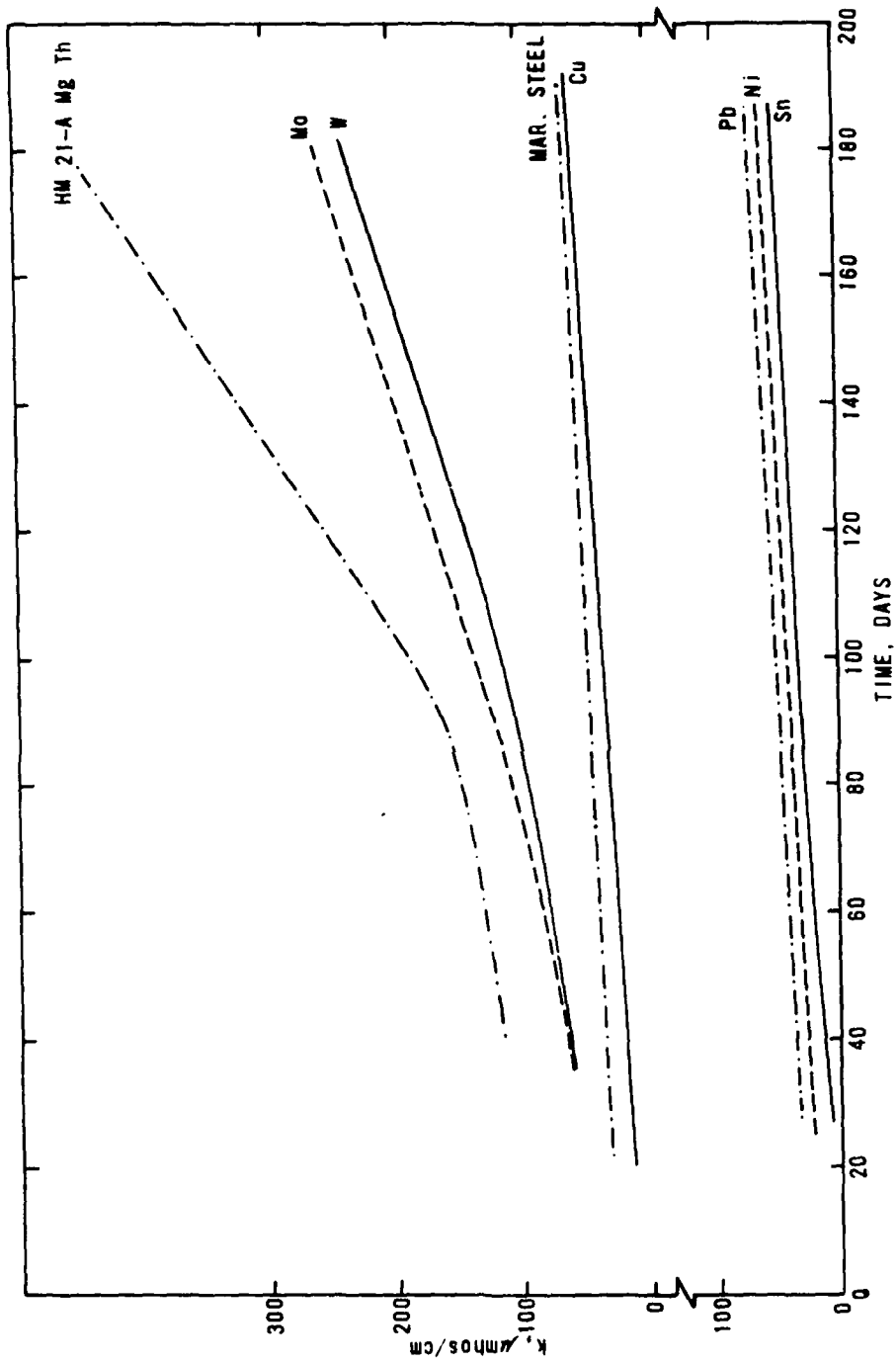


Figure 10. Conductivity Data for Metals Immersed in Ultrapure Water

Table 16

EXPERIMENTAL DATA FOR METALS  
 IMMERSED IN: ULTRA PURE WATER

AT 25°C FOR 180 DAYS

<u>Metal</u> <sup>(1)</sup>	<u>pH<sub>MS</sub></u>	<u>k<sub>MS</sub>, μmhos/cm</u>	<u>pH<sub>M++</sub></u>	<u>k<sub>M++</sub>, μmhos/cm</u>
1. Copper Rod	7.10	62.0	-0.35 <sup>(2)</sup>	11.6
2. Lead	8.19	46.0	0.75	5.4
3. Molybdenum	3.55	240.0	-3.60 <sup>(2)</sup>	199.6
4. Nickel	7.81	62.0	0.36	21.6
5. Steel, Maraging	7.86	62.0	0.41	21.6
6. Tin	7.54	37.0	0.09	-3.4 <sup>(3)</sup>
7. Tungsten	3.45	220.0	-4.00 <sup>(2)</sup>	179.6
8. HM 21 A Mg-Th	9.26	370.0	1.81	329.6

1 See description of metals in Table 6.

2 Negative value indicates  $pH_{H_2O} > pH_{MS}$

3 Negative value indicates  $k_{H_2O} > k_{MS}$

pH and conductivity attributed to the metallic ions. In equation form this becomes

$$k_{M^{2+}} = k_{MS} - k_{H_2O} \quad (47)$$

and

$$pH_{M^{2+}} = pH_{MS} - pH_{H_2O} \quad (48)$$

where  $k_{MS}$  and  $pH_{MS}$  refer to the observed specific conductance and pH of the metallic solution and  $k_{H_2O}$  and  $pH_{H_2O}$  are the values for contaminated water,  $H_2O^{(2)}$ . The negative values indicate that the pH and k of  $H_2O^{(2)}$  was higher than the values observed for the metallic solutions.

The experimental data indicated in table 16 is a measure of the chemical stability of the metals toward corrosion. The stability order previously observed (ref. 9) for metals in ultra pure water was

$$\begin{aligned} \text{St. Steel} < \text{W, Ni, Sn,} < \text{Brass} < \text{Cu} < \text{Al} < \text{Pb} < \text{Cd} \\ < \text{Fe} < \text{Zn} < \text{Mn} < \text{Carbon Steel} < \text{Mg} \end{aligned} \quad (49)$$

where the magnesium metal was the most prone to oxidation as shown by the high specific conductance value observed. The data are generally in agreement with the electrochemical series which states

$$\text{Cu} < \text{Pb} < \text{Sn} < \text{Ni} < \text{Cd} < \text{Fe} < \text{Zn} < \text{Mn} < \text{Al} < \text{Mg} \quad (50)$$

Rearrangement of the above to include the measurements made in this study result in

$$\begin{aligned} \text{stainless steel} = \text{Sn} = \underline{\text{Ni}} < \text{Cu} < \underline{\text{Pb}} < \text{Maraging steel} \quad (51) \\ < \text{Ni} < \underline{\text{W}} < \underline{\text{Mo}} < \text{Mn} < \text{W} < \text{Brass} < \text{carbon steel} < \text{Zn} < \text{Fe} < \text{Pb} < \text{HM 21 A Mg-Th} \\ < \text{Al} < \text{Cd} < \text{Mg} \end{aligned}$$

where the underlined elements represent the measurements on elements in pure water made in this study.

In general the data agree well with the series previously postulated. The small differences noted result from the variation of physical properties of the metals studied. As discussed previously, the similarity to values for the electrochemical series and to values for the heats of formation of the oxides or hydroxides, is based on the fact that the requirements for chemical stability are resistance to: (1) oxidation by acid and (2) reduction by water. The conductivity differences reported primarily result from oxidation or reduction reactions, hence the observed similarity.

The quantitative analysis of the solutions in which the metals of table 16 were immersed verified the pH and conductivity data observed. Cupric ions obtained from the corrosion of the pure metal were analyzed by electrolysis from acidic solutions according to the method of Skoog and West (ref. 17). Table 1 indicates an average of 0.3 mg of copper was plated out from a 170 ml of the copper solution, or 1.53 mg/l.

The electroanalysis of copper in brass was determined according to the procedure presented by Fischer and Peters (ref. 49). The percent of copper in the brass sample was first determined by dissolving the brass sample and then determining the copper present by electrodeposition. For 12 individual experiments performed on the brass samples, an average value of 61.5 percent copper in brass was obtained. Data for two typical analysis are listed in table 1.

The polarographic data obtained for solutions of lead ion are given in table 2. For this ion, 1.0 N  $\text{KNO}_3$  was used as the supporting electrolyte with the usual drop of 0.002 percent Triton as maximum suppressor. The polarographic curve for the contaminated solution (metal immersed for 180

---

49. Fischer, R.B. and Peters, D.G., Quantitative Chemical Analysis, W.B. Saunders, Co., Philadelphia, Pennsylvania, p. 10, 1968.

days, item no. 2 of table 16) showed  $1.09 \times 10^{-3} \text{ M Pb(II)}$  ions. The remainder of the lead ions was found in the copious white precipitate observed in the solution.

For the stannous ion,  $\text{Sn}^{2+}$ , 1.0 M HCl was used as the supporting electrolyte, plus the drop of 0.002 percent Triton per 50 ml of solution. Experimental data are listed in table 2. The analysis of the contaminated solution (item no. 6 of table 16) gave no polarographic wave at  $E_{1/2} = -0.47$  volt; therefore, it was assumed that no corrosion was present.

The  $i_d$  versus concentration data for nickel (II) standard solutions obtained in a supporting electrolyte of 0.1 N KCl plus 0.006 N HCl, gave no polarographic wave at  $E_{1/2} = -1.1$  volt. As with tin, this solution showed no metal ions in solution.

A standard solution was formed from metallic tungsten by dissolving the metal in a mixture of concentrated nitric and hydrofluoric acids. The resulting trioxide ( $\text{WO}_3$ ) was separated and dissolved in an alkaline solution. Dilute concentrations of the standard solution were studied in a polarograph at a voltage range between 0 and -2 volts with 2M HCl as a supporting electrolyte. A 10 ml sample gave a concentration of  $0.30 \times 10^{-4} \text{ M tungsten (III)}$  ions. The metal was coated with a black film which prevented any further corrosion.

For the steel sample (no. 5, table 16) a rust precipitate was observed in the solution, and the metal was covered with a black film. The sample, determined photometrically as previously described (ref. 9), showed 7.0 mg/l Ni (II).

It is known that the formation of oxide films on metals affords protection against corrosion. Nickel and tin have this tendency to form protective oxide coatings and this is probably the reason that no metallic ions were found in the solution (table 16, numbers 4 and 6). For the steel sample (no. 5), corrosion took place until the coating was formed, but once this was accomplished, no further oxidation occurred. This would also explain the low conductivity values observed in table 16.

Molybdenum (no. 3, table 16) was determined by precipitation from solution with  $\alpha$ -benzoinoxime. From 175 ml of solution, 27.6 mg of molybdenum was precipitated. This is in agreement with the weight loss of the metal, which was 27.68 mg/175 ml.

For the spectrophotometric determination of magnesium, titan yellow, the sodium salt of methylbenzothiazole-(1,3)-4,4' diazoaminobenzene-(2,2')-disulfonic acid was used (ref. 18) and gave a red color with  $Mg^{2+}$  in sodium hydroxide solution (pH 12). Data for the standard solutions developed with this dye were obtained at 525nm the concentration of magnesium ion found in the water solution (item no. 8, table 16) was 28.6 mg/l. The metal was coated with a black deposit and showed corrosion pitting.

### 3. THE EFFECT OF ADDITIVES IN PREVENTING CORROSION

The next phase of the research was to study the effect of additives in preventing corrosion or in regenerating water systems which show signs of corrosion. Several organic and inorganic additives, as well as water soluble polymeric materials (see table 7) were added to systems containing metals or alloys submerged in known concentrations of ultra pure water. The metals or alloys used simulate capacitor components before the system was subjected to an electric current.

As illustrated in table 15, the water plus additive properties were studied before metals were introduced into the solutions. In this way the values observed for the pH, the k, and the concentration of the gaseous and ionic impurities for these water solutions could be used to evaluate the metal plus solvent systems and thus make the proper corrections and conclusions.

Table 17 and figure 11 illustrate the corrosion resistant properties of Calgon CS. Of the 13 metallic systems studied, only lead, molybdenum, tungsten and HM 21-A Magnesium-Thorium alloy showed observable changes in pH and k. The combination of sodium nitrite, borax, and organic inhibitors present in the additive act as a buffering agent to automatically adjust the pH to the preferred level.

Investigations by Mansa and Szybalski (ref. 50) suggest that Calgon may be a cathodic inhibitor and that the inhibitive properties are very dependent on the movement of the solutions relative to the metal. As the velocity of flow increases, the corrosion at a particular Calgon concentration falls off to a fairly constant figure.

The optimum dose for water treatment seems to vary widely. In the large scale industrial use of Calgon, there are two methods of approach. One is to adjust the pH of the water by alkali treatment so as to bring the water on to the verge of scaling and to use 2 to 5 ppm Calgon to prevent this becoming troublesome. The other method is to maintain the pH at about 7, if necessary, by addition of acid, and to use Calgon dose of 100 ppm which can be dropped to about 20 ppm after a time. The first method is applicable to low corrosion materials; the latter method is used successfully in recirculation systems. The amount used in this study, 0.419 g

Table 17

EXPERIMENTAL DATA FOR METALS IMMERSSED IN CALGON CS  
FOR 180 DAYS (1)

<u>Metal (2)</u>	<u>pH</u>	<u>k, umhos/cm</u>	<u>Wt. loss, mg (3)</u>	<u>Ion conc. mg/l (4)</u>
1. Al 2024	9.08	3200	0.	Al, 1.90
2. Brass	9.07	3200	0.17	Cu, 0.09
3. Copper	9.07	3200	0.02	Cu, 0.05
4. Lead	8.95	3300	0.45	Pb, 2.27
5. Molybdenum	6.62	3250	42.98	Mo, 235
6. Nickel	9.08	3200	0.00	Ni, 0.00
7. Steel, Maraging	9.08	3200	0.05	Mn, 0.00
8. Steel, Cold Rolled	9.02	3200	0.00	Mn, 0.00
9. Steel, Stainless	9.07	3200	0.00	Mn, 0.00
10. Tin	9.07	3200	0.02	Sn, 0.00
11. Tungsten	5.60	3300	49.40	W, 271
12. HM 21A Mg-Thorium	10.28	3500	3.76	Mn, 0.16
13. Zinc	8.94	3200	1.78	Zn, 10.01

(1) See Table 6 and 7.

(2) See Table 6.

(3) Determined from change in weight of metal.

(4) Determined analytically.

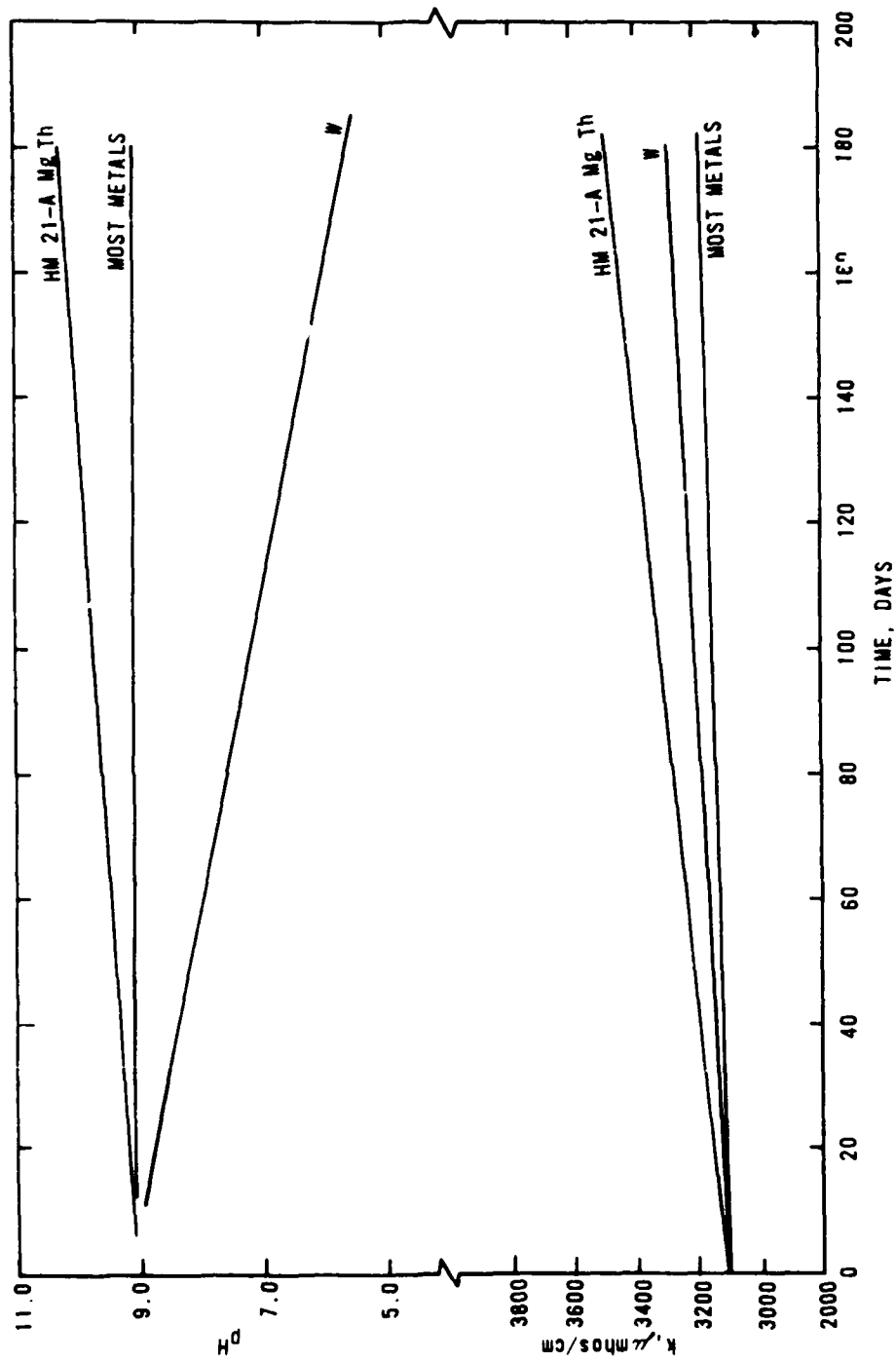


Figure 11. The Corrosion Resistant Properties of Calqon CS

per 175 ml of solution, was very effective in maintaining a pH of 9.08 and a conductivity value of 3100 to 3200  $\mu\text{mhos/cm}$ .

A comparison of the concentration of the metal ions observed in solution suggest that the addition of Calgon CS to water is more effective than pure water alone for all metals studied except molybdenum and tungsten. The HM 21-A alloy showed an increase in pH and k, however, the amount of Mo(III) ion in solution was 33% less than was found in pure water (no. 12, table 17).

Table 18 and figures 12 and 13 illustrate the corrosion inhibiting properties of Jaguar Plus (see table 7 for description of the additive). This high molecular weight cationic gum arabic derivative is used as a coagulant aid for potable and industrial water treatment. The variation of k and pH suggest that this additive is not as effective in maintaining a constant pH and k value; the original k value varied from 5 to 30  $\mu\text{mhos/cm}$  for most of the systems studied (table 18). The concentration of the ion found in solution did not always agree with the weight loss observed. The deviations were attributed to the cationic polyacrylamides present in the polymer which could couple with the available metal ions in solution.

Most of the metals were coated with a black precipitate and some as zinc, were mottled with white spots. The white spots were determined to be irregular deposits of the polymer, Jaguar Plus. These impurities would account for the discrepancies in the amount of ion observed in solution and the weight loss of the metal as listed in table 18.

Experimental data for metals immersed in Jaguar J 2S-1, RoVer, and Polymer 1212, are presented in table 19 and figures 14 and 15. The k values

---

50. Mansa, J.L. and Szybalski, W., "The Inhibitive Properties of Calgon and Micromat," *Acta Chem. Scand.*, **4**, 1275 (1950).

Table 18

EXPERIMENTAL DATA FOR METALS IMMERSSED IN  
JAGUAR PLUS<sup>(1)</sup> FOR 155 DAYS

<u>Metal</u> <sup>(2)</sup>	<u>pH</u>	<u>k, umhos/cm</u>	<u>Wt. Loss, mg</u>	<u>Ion conc. mg/l</u>
1. Al 2024	8.18	170	6.83	Cu, 19.80
2. Al (alfa)	7.97	179	0.58	Al, 2.12
3. Al (Base)	8.44	180	10.72	Al, 40.10
4. Brass	8.18	174	0.35	Cu, 0.42
5. Lead	8.34	140	4.89	Pb, 21.07
6. Molybdenum	6.90	206	8.00	Mo, 41.52
7. HM-21A Mg-Th	9.48	521	4.96	Mn, 0.04
8. Nickel	7.76	172	0.10	Ni, 0.51
9. Maraging Steel	8.29	182	9.20	Ni, 0.99
10. Steel, Cold Rolled	8.29	171	51.27	Mn, 0.01
11. Steel, Stainless	8.30	167	0.02	Mn, 0.00
12. Tin	8.34	146	0.14	Sn, 0.00
13. Tungsten	5.93	223	51.15	Ni, 0.09
14. Zinc	8.34	177	0.95	Zn, 9.52

(1) See Tables 6 and 7.

(2) See Table 5.

(3) Determined from weight loss of metal.

(4) Determined analytically.

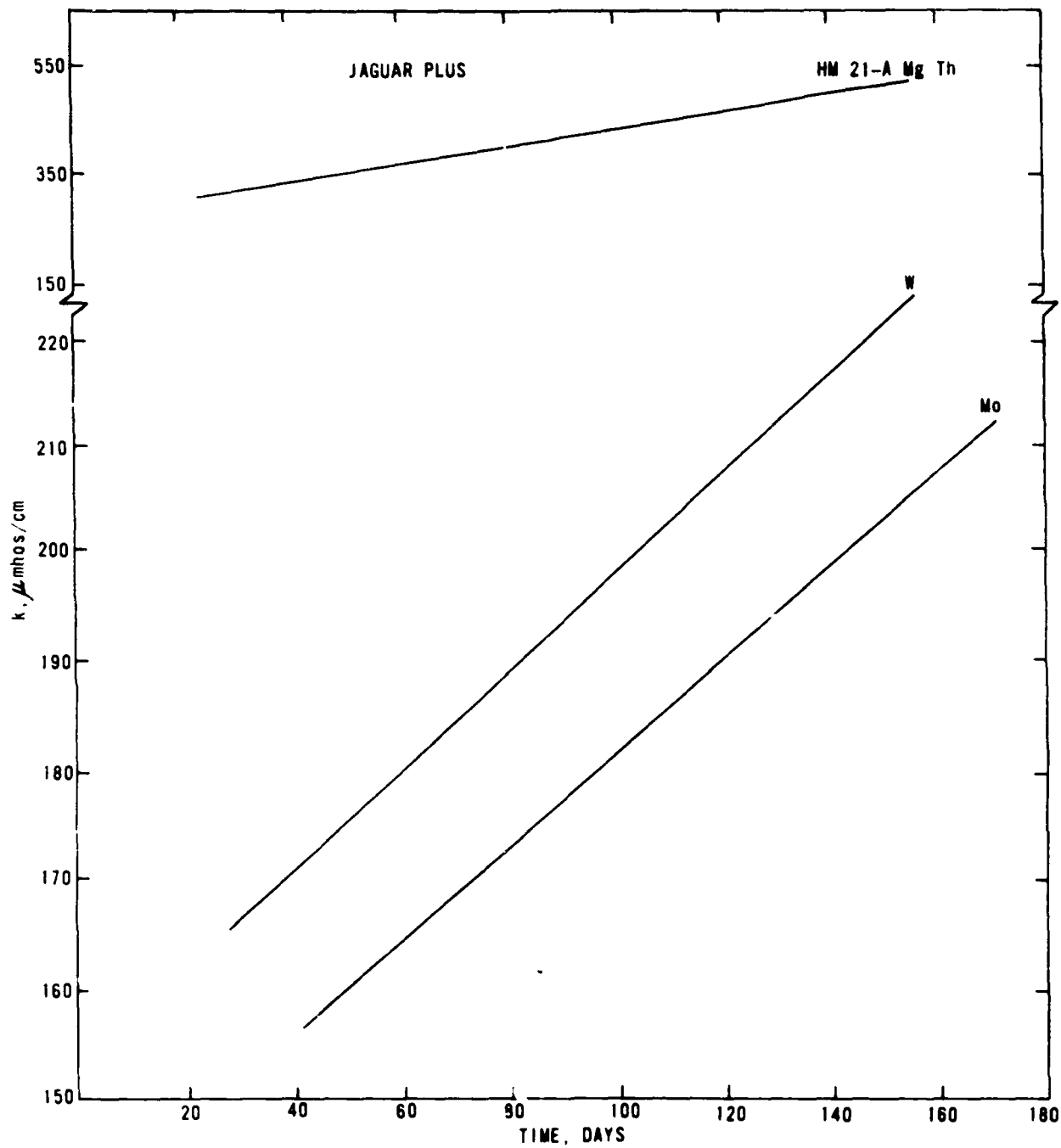


Figure 12. The Variation of pH and k of HM 21-A Magnesium Therium Alloy, Tungsten, and Molybdenum in a Jaguar Plus Solution

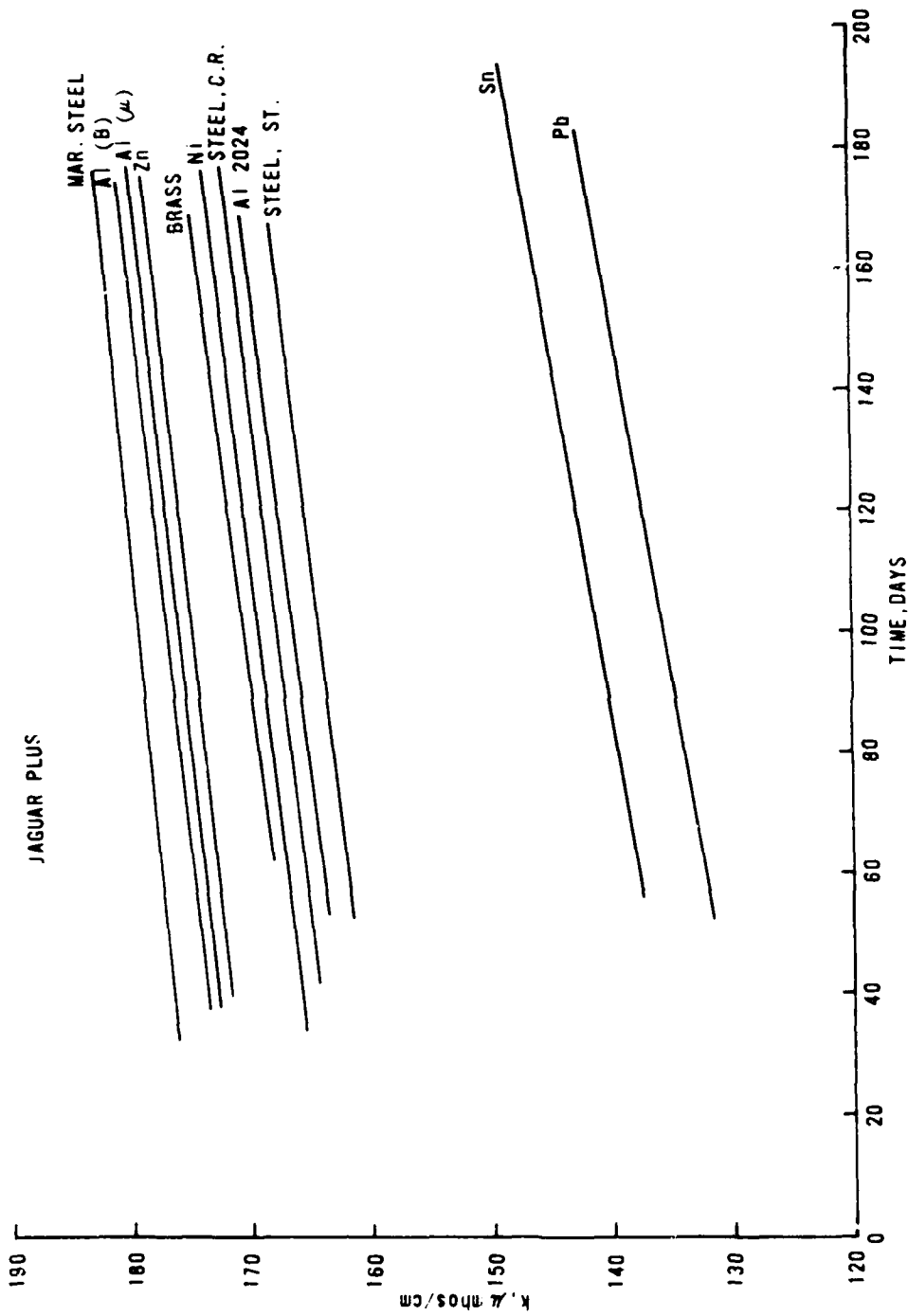


Figure 13. The Variation of pH and k for Various Metals in the Jaguar Plus Solution

Table 19

EXPERIMENTAL DATA FOR METALS IMMERSSED IN  
 JAGUAR J2S-1(1), ROVER (1) AND POLYMER 1212(1) FOR 130 DAYS

<u>Metal (2)</u>	<u>pH</u>	<u>k, umhos/cm</u>	<u>Wt. loss, mg(4)</u>	<u>Ion conc. mg/l</u>
1. Brass	5.94	24.6	1.66	Cu, 5.54
2. Steel, Stainless	5.93	25.6	0.00	Mn, 0.00
3. Al 2024	5.94	23.5	0.00	Al, 0.00
4. Copper	5.89	19.3	0.38	Cu, 0.80
5. Steel, Cold Rolled	5.98	20.6	34.06	Mn, 1.14
6. Brass	5.22	38.5	0.83	Cu, 0.69
7. Steel, Stainless	5.22	45.0	0.00	Cu, 0.00
8. Al 2024	5.22	55.0	0.37	Al, 0.25
9. Copper	5.22	52.0	1.20	Cu, 6.97
10. Steel, Cold Rolled	5.22	41.0	54.84	Mn, 2.41
11. Molybdenum	7.08	70.0	2.16	Mo, 8.32
12. Al 2024	7.20	74.5	+0.80	Al, 0.09
13. Brass	7.30	45.0	0.48	Cu, 0.69
14. Nickel	6.80	25.0	0.36	Ni, 0.96

(1) Metals 1 through 5 in Jaguar J2S-1 - See Tables 6 and 7. (3) Determined from weight loss of metal.  
 Metals 6 through 10 in Rover - See Tables 6 and 7.

Metals 11 through 14 in Polymer 1212 - see Tables 6 and 7. (4) Determined analytically.

(2) See Table 6.

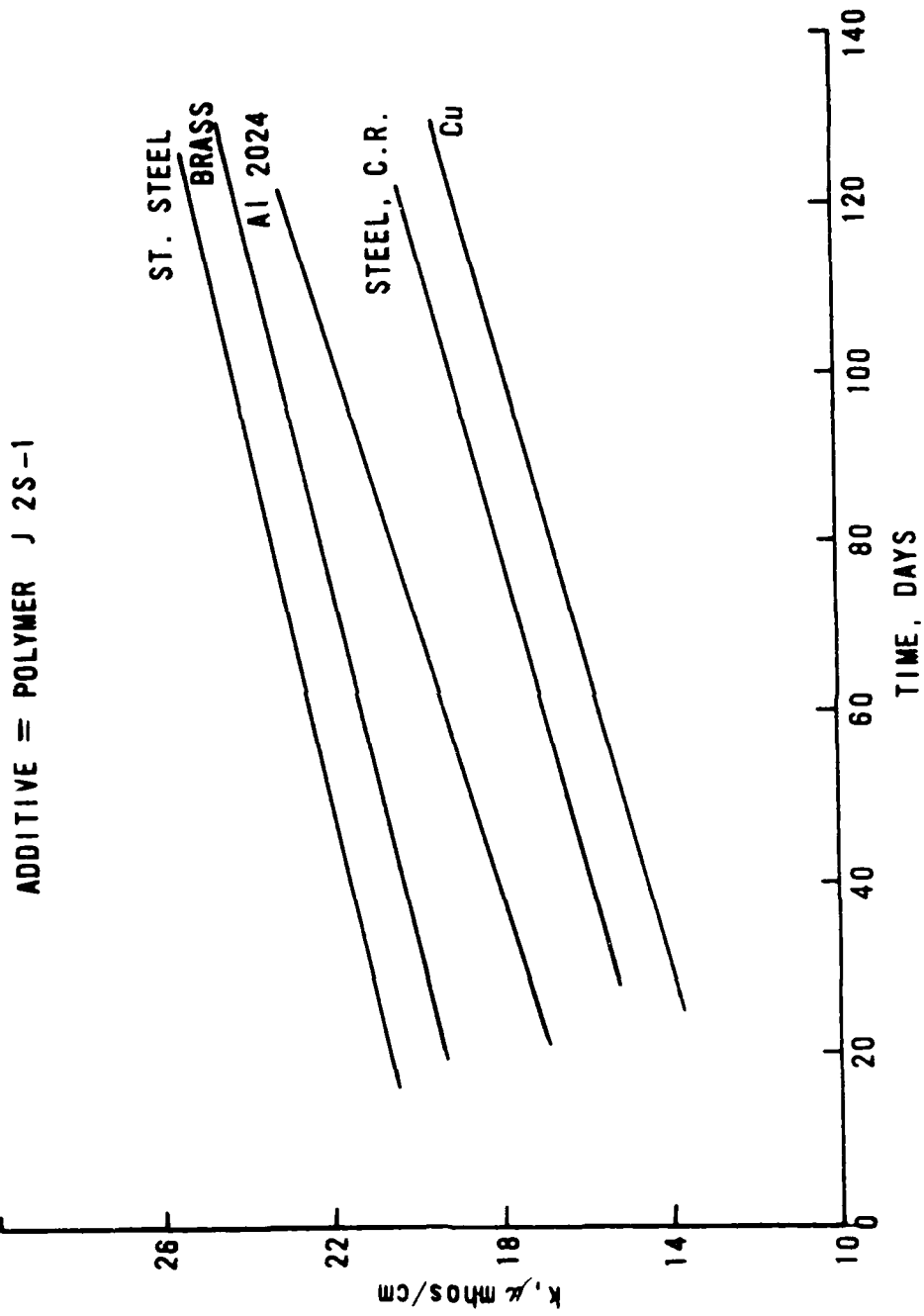


Figure 14. The Corrosion Resistant Properties of Jaguar J 2S - 1

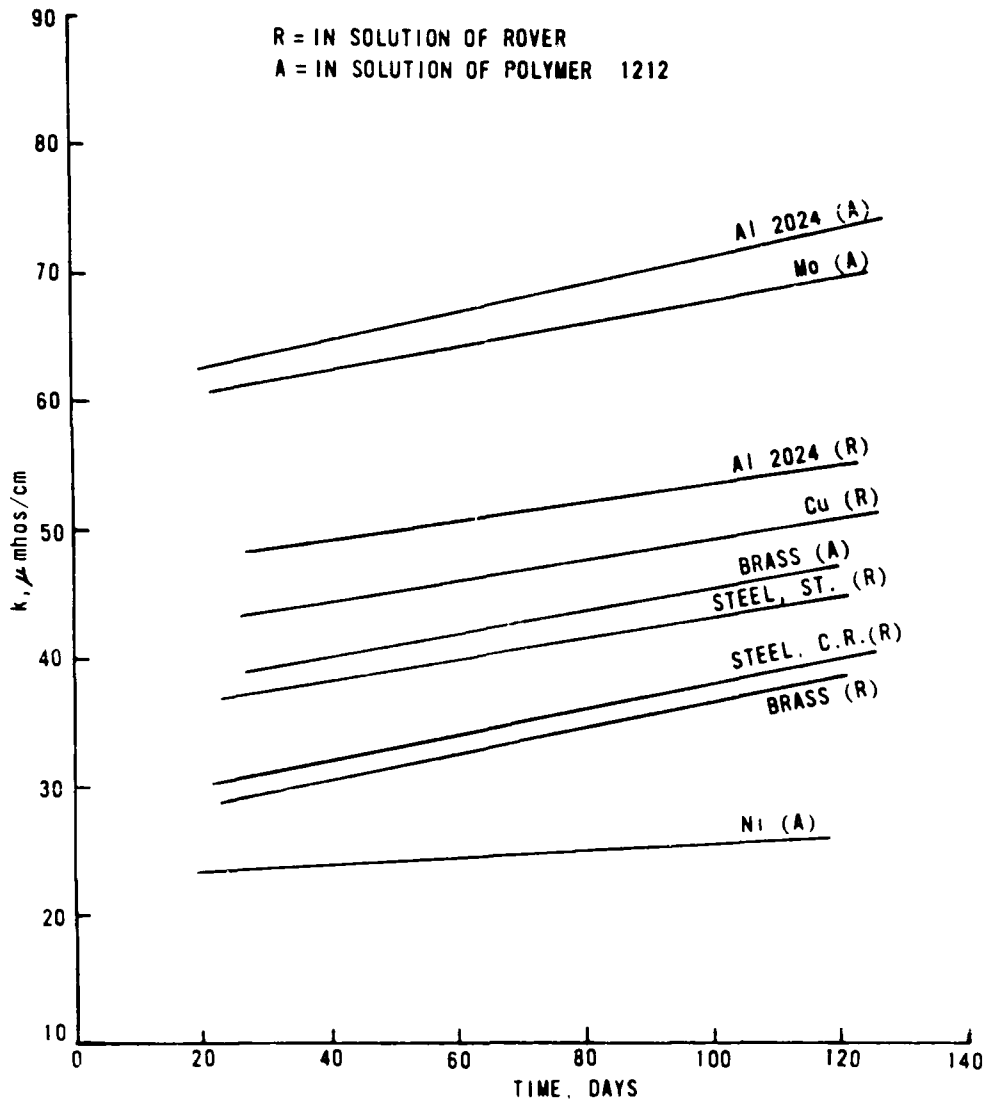


Figure 15. The Corrosion Resistant Properties of RoVer and Polymer 1212 A

observed for the metals in these solutions are much lower than the k values observed for Calgon CS and Jaguar. The maximum deviation for the k values of water solutions of RoVer, Jaguar J 2S-1, Polymer JB, and Polymer 1212 A was 37  $\mu$ mhos/cm. No metals were submerged in the Polymer JB solution, however pH and k values were followed as a function of time and are shown in figure 16.

The acid mixture of Jaguar J 2S-1 seemed to be very effective in maintaining a constant k and pH for the metals studied (table 19). No appreciable change was observed in the solution after 130 days. The analytical calculation of the ions present in the solutions containing Jaguar J 2S-1 agreed well with the values observed for the weight loss of the metals. The greatest deviation between weight loss noted and the concentration of the ion observed was for the copper sample. This solution was slightly discolored, although only 0.8 mg/l Cu(II) was evident. A greater amount of corrosion was noted for the cold rolled steel sample (no. 5, table 19) and a heavy rusty precipitate was evident; however, the analysis of the manganese ion present in steel coincided with the amount of weight loss observed.

For the metal plus RoVer mixtures, the corrosion observed was

stainless steel < Al 2024 < Brass < Cu < cold rolled steel. (52)

The Al 2024 sample was covered with a white film and the solution appeared slightly milky; the cold rolled steel sample was very dark and a great amount of a rust colored precipitate was evident. The latter was attributed to the iron present in the sample. The higher weight loss observed for brass and copper samples results from the ability of RoVer to remove copper ions from solution. It is frequently used for this purpose in determining mixtures of iron and copper spectrophotometrically.

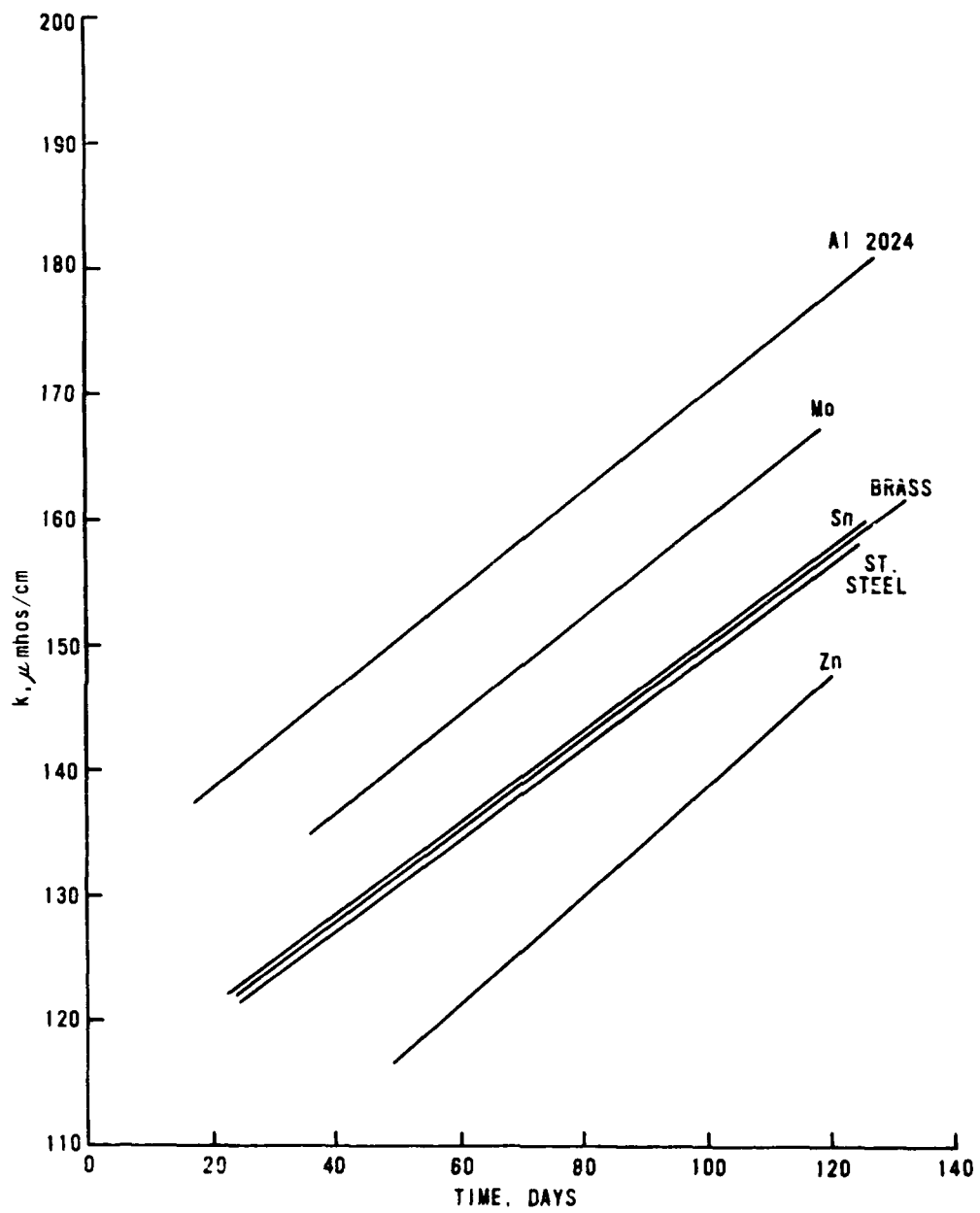


Figure 16. The Corrosion Resistant Properties of a Kerosene-Hydrazine Mixture

All the metals submerged in the solution of polymer 1212 A (numbers 11 through 14, table 19) showed signs of corrosion. Although 0.09 mg/l aluminum was noted in solution for sample 12, a weight gain was noted for the metal. The weight gain was attributed to the fine white precipitate which formed on the surface of the metal.

The brass and nickel metal samples (numbers 13 and 14 in table 19) showed no appreciable pitting or discoloration, however, the metals appeared oily on the surface. The oily coating probably hindered any further corrosion. The polymer has a high degree of compatibility with calcium and other polyvalent salts; this would account for the great amount of white precipitate observed.

Metals 1 through 8, table 20 and figure 16, show the effect of adding a mixture of 1 ml of hydrazine and 1 ml of kerosene to 175ml of ultra pure water before the metal was added. It was hoped that the oily properties of the high molecular weight hydrocarbon (kerosene) would coat the surface of the metals and that the hydrazine would raise the pH of the solution in order to eliminate the oxidizing effect of the hydrogen ion originating from the carbon dioxide and/or oxygen contamination. Because of the high k values observed for cadmium and HM 21-A magnesium throrium alloy, these metals were not included in figure 16.

Although the pH and k values fluctuated from that observed for the original solution (table 15), very few ions were observed in the solution. The fluctuation of pH and k values may be due to the errors involved in using organic materials in electrolytic measurements, as well as the insolubility of the kerosene. The greatest error was attributed to the contamination of

hydrazine by atmospheric oxygen; hydrazine readily absorbs the oxygen and becomes contaminated, resulting in a slight discoloration of the solution. The impurities caused a great fluctuation in  $k$ , but no metallic corrosion was observed. If high purity hydrazine and kerosene are both refluxed and redistilled before they are added to the ultrapure water and if a closed system is used, the mixture would be ideal as a corrosion preventative which maintains a low  $k$  value.

The pH and  $k$  values observed for the LC-15 mixture (table 15) was 9.14 and 560  $\mu\text{mhos/cm}$ , respectively. For the metal plus additive mixtures (table 20), variations in  $k$  were within 20  $\mu\text{mhos/cm}$  of the original value; however, the milligram weight loss was more dramatic. It appears that the  $k$  remained virtually constant because the metal ions precipitated out of the solution as solid contaminants. The results are graphed in figure 17. The lowest weight loss observed, 0.11 mg for molybdenum, was attributed to the dark coating observed on the metallic surface. Al 2024, cold rolled steel, and the magnesium thorium alloy all had dark coated surfaces, however, since some ions were found in the solution it was assumed that corrosion occurred before the black film was formed.

Figure 18 illustrates the change in pH and  $k$  for a chloroform mixture. No metals were studied in this mixture; however, since the  $k$  values do not exceed 40  $\mu\text{mhos/cm}$ , the hydrocarbon should be able to protect the metal from corrosion and thus maintain the low  $k$  values observed for the solution.

Table 20

## EXPERIMENTAL DATA FOR METALS IMMERSSED IN

VARIOUS ADDITIVES<sup>(1)</sup>

<u>Metals (2)</u>	<u>pH</u>	<u>k, <math>\mu</math>mhos/cm</u>	<u>Wt. loss, mg(3)</u>	<u>Ion, conc. mg/l(4)</u>
1. HM-21A Mg-Th	10.02	230	+0.01	Mg, 0.00
2. Al 2024	10.45	182	+2.59	Al, 0.00
3. Steel, Stainless	10.60	179	0.00	Mn, 0.00
4. Tin	10.55	161	4.22	
5. Molybdenum	10.45	197	0.44	Mo, 0.33
6. Cadmium	10.12	280	0.61	Cd, 1.53
7. Zinc	10.28	152	+0.30	Zn, 0.00
8. Brass	10.50	161	0.00	Cu, 0.00
9. Al 2024	8.99	585	2.05	Cu, 0.49
10. Steel, Cold Rolled	9.54	575	4.67	Mn, 0.02
11. Molybdenum	9.29	560	0.11	Mo, 0.42
12. HM-21A Mg-Th	10.12	620	2.94	Mg, 9.21

(1) Metals 1 through 8 in kerosene plus hydrazine - see table 6 and 7.  
Metals 9 through 12 in 5 ml LC 15 - see tables 6 and 7.

(2) See Table 6.

(3) Determined from weight loss of metal.

(4) Determined analytically.

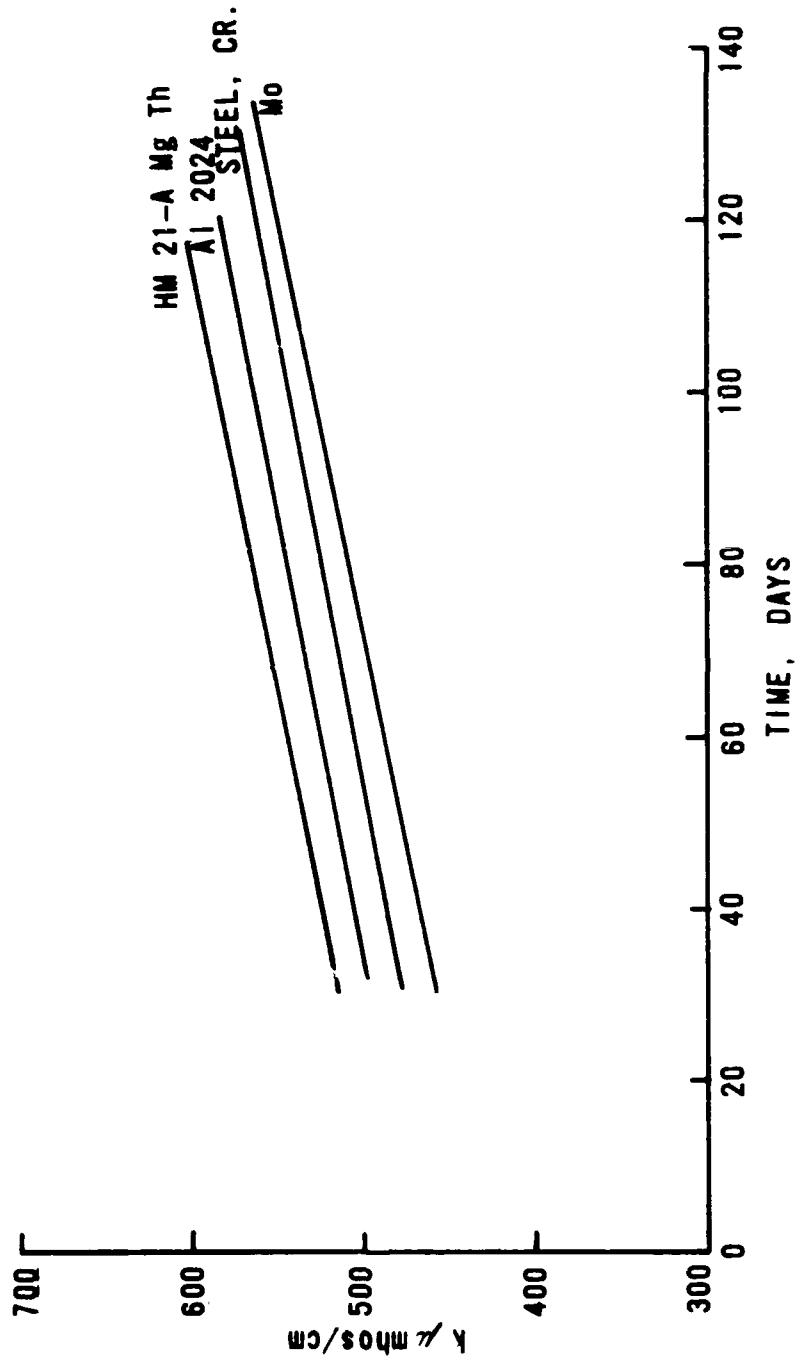


Figure 17. The Corrosion Resistant Properties of LC - 15

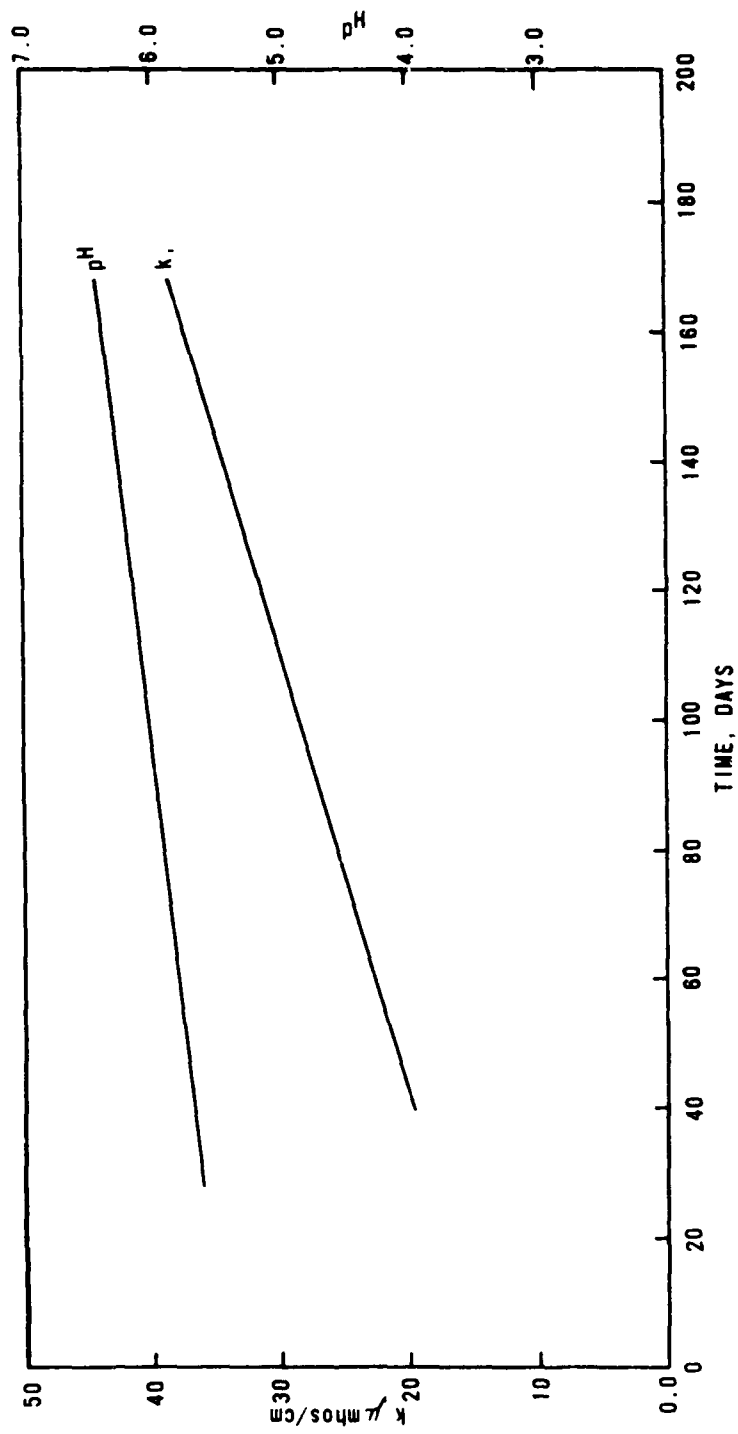


Figure 18. The Change in pH and k as a Function of Time for a Chloroform Solution

## SECTION VI

### CONCLUSIONS

This study has shown that corrosion is a complicated phenomena which depends on many factors. The slight excess of hydrogen ions in solution, resulting from the demineralization system used, as well as the minimal contact of the solution with the carbon dioxide of the atmosphere, provided the impetus for corrosion to begin. The corrosion of the metals was further accelerated by the presence of oxygen in the solutions because there is an interdependence of oxygen concentration on corrosion. Between a pH of 5 and 11 corrosion is proportional to the amount of oxygen in solution at the surface of the metal where it can act as a depolarizer.

The water purification system at the Air Force Weapons Laboratory functions well; however, proper and repeated rinsing after the purification of the resin is essential to remove all traces of ionic impurities.

When collecting water from the purification system, great care should be taken to withdraw the water under vacuum conditions. Slight contaminations from atmospheric carbon dioxide and oxygen were noted, and it was concluded that these contaminations resulted from the method of removal of water from the water purification system. The withdrawal of the water in an inert atmosphere of nitrogen and/or helium is not recommended for it was noted that the inert gases have an effect on the ultra pure water; generally they tend to make the water slightly less acidic. This is desirable as long as the level of basicity is controlled.

The traces of oxygen and carbon dioxide initially incorporated in the water caused corrosion pitting of the metals by the formation of oxides or hydroxides. The heat evolved when the metals so reacted, as well as the

electromotive force generated by the concentration cell as corrosion proceeds, was a measure of the tendency of the metals to corrode. The stability order for metals in water was determined by measuring the metallic ions in solution as well as the pH and the conductivity of the solution. The stability order proposed (equation 51) agrees well with electromotive force data and the heat of formation data for oxides and hydroxides (ref. 9). Slight deviations from the electrochemical series were attributed to galvanic corrosion or to lack of homogeneity as well as to metallic strain.

Thus, it was shown that stainless steel, tin, nickel and copper, in that order, would be the best metals to use to construct capacitor plates. Capacitor elements constructed from these metals, as well as nickel or tin coated elements, should exhibit very little corrosion in pure water, so that surface quality and capacitor size dimensions would not be affected and dielectric properties would not be modified.

The present study dealing with the effectiveness of adding inorganic, polymeric, or organic additives to prevent corrosion shows varied and complicated results. Calgon CS (at the concentrations listed) has proved to be very effective in maintaining a constant pH of 9.09 and a conductivity value of 3100 to 3200  $\mu\text{mhos/cm}$ . The high pH value suggests the presence of the normal carbonate phase; therefore, heavy metal ion precipitation with carbonate is possible.

The cationic polymer, Jaguar Plus, raised the pH value over that observed for pure water; however, excessive metallic corrosion, and hence ionic precipitation was noted. The latter was attributed to the cationic properties of the additive.

The acidic properties of RoVer proved effective in preventing the corrosion of stainless steel; however, the additive should not be used for copper or copper containing alloys. RoVer has the ability to remove cupric ion from solution by the formation of an ethylenediaminetetraaceto complex; therefore, for copper or copper alloys, the corrosive properties would increase with the use of this additive.

The nonionic additive, Jaguar J 2S-1, was effective in preventing corrosion of stainless steel and aluminum 2024; however, copper, brass, and cold rolled steel showed corrosion effects. The great amount of corrosion observed for the latter was associated with the gel-like properties of the additive which seemed to cause precipitation of the ions in solution.

The use of polymer 1212 A as an additive to prevent corrosion is not suggested unless more studies are made with varied concentrations of the polymer in solution. The gel-like properties of the polymer seem to pull ions out of solution at the expense of the corrosion of the metal.

The kerosene-hydrazine mixture seems highly suited as an additive to prevent corrosion; however, it is necessary that the organic materials be freshly distilled before use and that a closed system be employed. The ability of hydrazine to act as a scavenger of oxygen is well known (refs. 2 to 6), but if an excess of oxygen is available, the solution becomes highly contaminated and the pH and k values may fluctuate from desired values. The system proved to be very effective for all metallic systems (little or no ionic impurities were noted in solution) except cadmium and molybdenum. The highly basic nature of the additive is probably affecting these two materials.

The LC-15 additive, in the concentrations employed in these studies, was not very effective in preventing corrosion. Further work should be done on this material for it was suspected that the reagent (as received from the purchasing company) was somewhat contaminated.

In conclusion, if the water exhibits slight contamination from atmospheric carbon dioxide or oxygen, it is suggested that a pure hydrazine-kerosene mixture (approximately 1 ml of each reagent in 175 ml of water - in a closed system) or other organic additives be introduced into the system. The possible additives include chloroform, cyclohexylamine, diethyleneimide oxide, and similar amines and hydrocarbons. The amines will be effective in removing the carbon dioxide, and the hydrocarbons will put an effective coating on the metal to prevent further oxidation and hence corrosion.

## APPENDIX A

### THE COMBINATION OF THERMAL AND ULTRASONIC DATA TO CALCULATE GRUNEISEN RATIOS AND VARIOUS THERMODYNAMIC FUNCTIONS

Sister Rosalie Urzendowski, Ph.D.\*

and

Arthur H. Guenther, Ph.D.

Kirtland Air Force Base  
Albuquerque, New Mexico 87117

#### ABSTRACT

Thermal expansion, specific heat, and ultrasonic data are presented for several metals, alloys, ceramics, and polymers, in order to define the magnitude of energy changes which occur when the materials are heated or cooled. Thermal Gruneisen ratios were computed as a function of temperature and numerous ultrasonic and thermodynamic equations were derived from the thermal data combined with measured compressibility data. Attempts to relate the volume coefficient of expansion,  $\beta$ , to heat capacity at constant volume,  $C_V$ , and to the elastic properties of polymers are discussed. Correlations are made between the measured thermal Gruneisen coefficients and those obtained from the change of atomic vibrational frequency with the change of volume as defined ultrasonically.

#### INTRODUCTION

\*A knowledge of the Gruneisen parameter,  $\gamma$ , is a prerequisite to any evaluation of temperature dependence in numerous thermodynamic properties. In addition, the proper formulation for this parameter lends much to the accuracy of any theoretical analysis which may depend upon it.

Barker<sup>1</sup>, Wada<sup>2</sup>, and others<sup>3,4,5</sup>, have demonstrated the importance of the Gruneisen parameter in measuring the anharmonicity of crystals and of interchain binding forces of polymeric solids through its relationship to the variation of lattice vibrational frequencies with volume as well as the thermal expansion. Barron<sup>6</sup>, Slater<sup>7</sup>, Blackman<sup>8</sup>, and others<sup>9,10</sup>, have illustrated the dependence of lattice frequencies on strain and thus the relationship of  $\gamma$  to ultrasonic measurements. Partington<sup>11</sup> has shown that the temperature independence of the Gruneisen parameter is associated with the proportionality

\*University of Albuquerque, Albuquerque, New Mexico 87140  
AF Contract 29601-73-C-0110

NOTE: This paper was presented at the 1973 International Symposium on Thermal Expansion of Solids, held at Lake of the Ozards, Missouri, November 7-9, 1973.

constant,  $\beta/C_v$ , where  $\beta$  is the volume coefficient of expansion and  $C_v$  is the specific heat at constant volume.

Recent advances in solid state technology have made it necessary to define more accurately the parameters involved in the equation of state for solids. For example, a complete thermodynamic description of the solid is necessary to evaluate the Gruneisen parameter  $\gamma$  which occurs in a useful equation of state formulation which is in the form of a power expansion in the compressibility as defined by

$$P - P_0 + au^1 + bu^2 + cu^3 + \dots + \gamma \frac{\rho}{\rho_0} \cdot E \quad (1)$$

where  $P$  is the pressure,  $u = \rho/\rho_0 - 1$ , the compression,  $a$ ,  $b$ , and  $c$  are constants,  $E$  the thermal energy of the solid, and  $\rho$  the density at pressure,  $P$ . Zero subscripts denote normal pressure values.

The evaluation of the Gruneisen parameter by means of the specific heat and the linear coefficient of thermal expansion measurements, coupled with ultrasonic sound velocity data was the main objective of this study. This relation can be defined as

$$\gamma_g = \frac{\beta \cdot B^T}{C_v \cdot \rho} = \frac{\beta \cdot B^S}{C_p \cdot \rho} = \frac{\beta[\rho(c_l^2 - 4/3 c_t^2)]}{C_p \cdot \rho} \quad (2)$$

where  $\gamma_g$  is the Gruneisen ratio,  $\beta$  is the volume coefficient of thermal expansion,  $\rho$  is the density,  $C_v$  and  $C_p$  are the heat capacity at constant volume and constant pressure, respectively,  $B^T$  and  $B^S$  represent the isothermal and adiabatic bulk moduli, and  $c_l$  and  $c_t$  are the longitudinal and transverse ultrasonic sound velocities, respectively, for isotropic media.

The temperature independent ratio follows from the proportionality of the volume coefficient of expansion to the specific heat at low temperatures. This temperature independent ratio,  $\gamma_j$ , is defined by

$$\gamma_j = - \frac{d \ln v_j}{d \ln v} = - \frac{v}{v_j} \left( \frac{\partial v_j}{\partial v} \right)_T \quad (3)$$

where each frequency,  $v_j$ , is assumed to be the same for all frequencies and is strictly a volume dependent function.

The temperature dependent formulation of the Gruneisen law arises from the formal theory of thermal expansion in the quasi-harmonic approximation and its relationship to the Debye frequency,  $v_m$ . Under these conditions, the  $\gamma_g$  defined by equation (2) is regarded as a temperature dependent integrated value which often departs from constancy as a result of the temperature dependence of the corresponding frequencies.

The pressure dependency of  $\gamma_g$  (Equation 2) may be determined if the individual parameters were obtained dynamically as a function of pressure and volume. At the present time such measurements are difficult to obtain due to pressure calibration difficulties as well as the occurrence of material failure, however, the pressure dependency may be estimated by the proper application of thermodynamic variables for specific ultrasonic and thermal data.

In this study, thermal and ultrasonic measurements made at various temperatures were used to calculate the temperature dependence of the Gruneisen ratio according to equation (2). Atomic and molecular frequencies were estimated from specific heat thermal expansion and sound velocity data in order to study the variation of frequency with volume and to determine the characteristic temperature,  $\theta$ . The thermal or ultrasonic data were obtained at high pressures, however, the high pressure derivative ( $\partial\gamma/\partial P$ ), was estimated by applying proper thermodynamic relationships.

#### THEORY

The equation of state of a solid as a function of temperature, pressure and volume, may be derived from the Helmholtz free energy  $A$ , where  $A$  is defined by the thermodynamic identity,

$$A = E - TS \quad (4)$$

where  $E$  is the internal energy and  $S$  the entropy. The variation of free energy with pressure ( $\Delta F = F_p - F_0$ ) at constant temperature, increases with pressure since it is equal to the work of compression forces ( $\Delta F = - \int p dV = dA$ ) or

$$p = - \left( \frac{\partial A}{\partial V} \right)_T \quad (5)$$

Thus, equation (4) may now be written as

$$A = E_0(V) + A^*(V,T) \quad (6)$$

where  $E_0(V)$  is the internal energy at  $0^\circ\text{K}$  and  $A^*(V,T)$  is the contribution of the lattice vibrations to the free energy. The individual terms of the equation are very difficult to calculate from first principles for it presumes a knowledge of the vibrational spectrum of the lattice and its variation with volume. The simple assumption that all vibrational frequencies are changed in the same manner by a change in volume led to the Mie-Gruneisen equation of state<sup>11</sup>

$$p = - \frac{dE_0}{dV} + \frac{\gamma}{V} E^*(V,T) \quad (7)$$

where the Gruneisen ratio describes the volume variation of the vibrational frequencies as defined by equation (3) and  $E^*(V,T)$  is the thermal energy. Differentiation of equation (7) led to equation (2) which expresses  $\gamma$  in terms of measurable thermodynamic quantities. If one assumes a Debye model to describe the thermal energy, a special case of the Gruneisen equation exists as defined by

$$p = - \frac{dE_D}{dV} + \frac{\gamma}{V} E_D \quad (8)$$

where  $E_D$  is the appropriate Debye integral and  $\gamma$  is given in terms of the Debye characteristic temperature,  $\theta_D$ , by

$$\gamma = - \frac{d \ln \theta_D}{d \ln V} \quad (9)$$

According to the Debye theory, the maximum frequency of oscillations of atoms in an isotropic solid,  $\nu_m$ , can be expressed in terms of the corresponding rate of propagation of elastic oscillations by

$$\nu_D = \left\{ \frac{9N}{4\pi v} \right\}^{\frac{1}{3}} \left\{ \frac{1}{c_l^3} + \frac{2}{c_t^3} \right\}^{-\frac{1}{3}} \quad (10)$$

where  $N$  is Avogadro's number,  $v$  is the volume per mole, and  $c_l$  and  $c_t$  are the rates of propagation of longitudinal and transversal oscillations.

Employing the relationship  $\gamma \equiv \theta(v)/T$ , equation (9) can be used to define the entropy per mole,  $S(V,T)$  as a function of  $\gamma$  so that

$$\left( \frac{\partial S}{\partial V} \right)_T = \frac{\gamma T}{V} \left( \frac{\partial S}{\partial T} \right)_V = \frac{\gamma C_V}{V} \quad (11)$$

or

$$\left( \frac{\partial S}{\partial V} \right) \equiv \frac{B}{X} \quad (12)$$

which again leads to the Gruneisen ratio as defined by equation (2) and makes some of the information available through equation (8) unnecessary.

Equation (9) therefore provides a relationship between the Debye characteristic temperature and ultrasonic and thermal measurements. This should provide enough information to determine the physical properties of the solid except those associated with a change of state.

If the material is isotropic, and no phase changes occur over the pressure range of interest, the pressure derivative,  $(\partial\gamma/\partial P)$ , may be estimated. This is done by estimating the pressure derivative of each term of equation (2) so that

$$\left(\frac{\partial\gamma}{\partial P}\right)_T = -\frac{\beta B^S}{\rho^2 c_p} \left(\frac{\partial\rho}{\partial P}\right)_T - \frac{\beta B^S}{\rho c_p^2} \left(\frac{\partial c_p}{\partial P}\right)_T + \frac{B^S}{\rho c_p} \left(\frac{\partial\beta}{\partial P}\right)_T + \frac{\beta}{\rho c_p} \left(\frac{\partial B^S}{\partial P}\right)_T \quad (13)$$

Thurston<sup>12</sup> has shown that the pressure derivatives of  $\beta$  and  $C_p$  at constant temperature are related to the mechanical properties of an isotropic solid by

$$\left(\frac{\partial\beta}{\partial P}\right)_T = -\left(\frac{\partial x^T}{\partial T}\right) = \frac{1}{(B^T)^2} \left(\frac{\partial B^T}{\partial T}\right)_P \quad (14)$$

$$\left(\frac{\partial C_p}{\partial P}\right)_T = -\frac{T}{\rho} \left[ \left(\frac{\partial\beta}{\partial T}\right)_P + \beta^2 \right] = -T \left(\frac{\partial^2 v}{\partial T^2}\right) \quad (15)$$

where the superscript T refers to the isothermal moduli and T is the absolute temperature. If one has the means of measuring the temperature dependence of the bulk modulus and the expansion coefficient, equations (14) and (15) allow an estimation of the pressure derivatives of  $\beta$  and  $C_p$ .

Since  $\rho = 1/v$ , where  $v$  is the specific volume, the quantity,  $(\partial\rho/\partial P)_T$ , follows from

$$\left(\frac{\partial\rho}{\partial P}\right)_T = -\frac{1}{v^2} \left(\frac{\partial v}{\partial P}\right)_T \quad (16)$$

and from the definition of the isothermal compressibility

$$\chi^T = -\frac{1}{v} \left(\frac{\partial v}{\partial P}\right)_T = \frac{1}{B^T} \quad (17)$$

so that equation (16) can be defined as

$$\left(\frac{\partial\rho}{\partial P}\right)_T = \frac{\rho}{B^T} \quad (18)$$

The isothermal bulk modulus,  $B_0^T$ , can be obtained from

$$B_0^T = B_0^S / (1 + \beta\gamma T) \quad (19)$$

and the pressure derivative  $(\partial B^S/\partial P)_{0,T}$  can be determined ultrasonically.

Since the adiabatic bulk modulus may be expressed in terms of the longitudinal and transverse sound velocities, Asay et al.<sup>13</sup>,

and Lamberson<sup>14</sup>, have shown that the differentiation of the equation at constant temperature and zero pressure yields

$$\left(\frac{\partial B^S}{\partial P}\right)_{0,T} = 2\rho_0 [c_L c_L' - 4/3 c_t c_t']_{P=0} + (1 + \beta\gamma T) \quad (20)$$

where  $(\partial B^S/\partial P)_{0,T}$  is the pressure derivative of the adiabatic bulk modulus, and  $c_L$  and  $c_t$  are the pressure derivatives of the longitudinal and transverse velocities, respectively.

The above derivation leads to

$$\left(\frac{\partial \gamma}{\partial P}\right)_{0,T} = \gamma_0 \left[ -\frac{1}{B_0^T} - \frac{1}{c_P} \left(\frac{\partial c_P}{\partial P}\right)_{0,T} + \frac{1}{\beta} \left(\frac{\partial \beta}{\partial P}\right)_{0,T} + \frac{1}{B_0^S} \left(\frac{\partial B^S}{\partial P}\right)_{0,T} \right] \quad (21)$$

where the zero subscripts refer to atmospheric pressure.

Anderson<sup>15</sup> has shown that ultrasonic data taken at relatively low pressures may be used to estimate the pressure-volume isotherm to pressures of the order of the bulk modulus. His assumption that the bulk modulus has a linear pressure dependence resulted in the Murnaghan and logarithmic equation of state<sup>16</sup> defined by

$$\ln \left(\frac{V_0}{V}\right) = \frac{1}{B_0} \ln \left\{ B_0' \frac{P}{B_0} + 1 \right\} \quad (22)$$

From the similarity of definitions for the adiabatic and isothermal bulk moduli (Equation 19) the use of  $B_0^S$  and  $B_0^{S'}$  in equation (22) results in an adiabat while  $B_0^T$  and  $B_0^{T'}$  results in the isotherm. Furthermore, Dugdale and MacDonald<sup>17</sup> have shown that the derivative  $B_{0,S}'$  may be estimated from

$$B_{0,S}' = 2\gamma + 1 \quad (23)$$

which is applicable for all pressures lower than  $B_0$ .

Since ultrasonic data yield adiabatic bulk moduli and shock wave measurements define the isothermal quantities, the proper conversions are made by

$$B_{0,T}^{S'} = B_{0,S}^{S'} - \left(\frac{\partial B^S}{\partial T}\right)_P \cdot \frac{\gamma}{\beta S} \quad (24)$$

where  $(\partial B^S/\partial T)_P$  is the temperature derivative of the adiabatic bulk modulus.

Equation (21) for  $\gamma'$  can be put in a form more suitable in using experimental data by referring to the definition of the temperature derivative of  $\gamma$ .

$$\left(\frac{\partial \gamma}{\partial T}\right)_P = \frac{\partial \gamma}{\partial \rho} \left(\frac{\partial \rho}{\partial T}\right)_P + \frac{\partial \gamma}{\partial B^S} \left(\frac{\partial B^S}{\partial T}\right)_P + \frac{\partial \gamma}{\partial B} \left(\frac{\partial B}{\partial T}\right)_P + \frac{\partial \gamma}{\partial c_p} \left(\frac{\partial c_p}{\partial T}\right)_P \quad (25)$$

Equation (21) may now be expressed through a more convenient estimation by

$$\left(\frac{\partial \gamma}{\partial P}\right)_T = \frac{\gamma}{B^S} \left[\left(\frac{\partial B^S}{\partial P}\right)_T + \left(\frac{1 + \beta \gamma T}{\beta B^S}\right) \left(\frac{\partial B^S}{\partial T}\right)_P - \gamma - T \left(\frac{\partial \gamma}{\partial T}\right)_P\right] \quad (26)$$

where all the quantities are determined experimentally except  $(\partial B^S / \partial P)_T$ .

#### EXPERIMENTAL TECHNIQUES

The heat capacity data were obtained with appropriately calibrated differential scanning calorimeters. Both the DuPont DSC and the Perkin Elmer DSC-1B were used for the measurements. The heat capacity values are accurate to approximately  $\pm 2.0$  percent. For the polymeric materials transitional regions were eliminated by extrapolating before and after said transitions.

Linear thermal expansions between  $-100^\circ$  and  $200^\circ\text{C}$  were made on machined samples (0.25 in  $\times$  0.25 in) by means of a DuPont 940 Thermomechanical Analyzer. Details of the experimental procedure were previously described<sup>13,18</sup>. After proper application of chromel alumel thermocouple corrections, individual temperature determinations agreed to within  $0.2^\circ\text{C}$  and to within 2.0 to  $4.0^\circ\text{C}$  of values reported in the literature. The total probable error of the expansion measurements calculated is the square root of the summation of all errors associated with each component of the instrument was  $\pm 2.5$  percent.

Ultrasonic sound velocity measurements of longitudinal and shear waves at approximately 1 and 3 Mc/sec were made at this laboratory by Asay, et al.<sup>13,14,19</sup>, and were used to calculate the adiabatic bulk modulus and related ultrasonic data. For most of the velocity-temperature data a quadratic function was found to fit the data to an accuracy of approximately 1 percent.

The materials studied included metals, alloys, and polymeric materials. The pure metallic specimens (purity greater than 99.9 percent) of aluminum, copper, nickel and lead were obtained from Electronics Space Products, Inc. The gold was a standard block specimen with a density of  $18.94\text{g/cm}^3$ .

The two aluminum alloys were 1060 Al (measured bulk density of  $2.703 \pm 0.002\text{ g/cm}^3$ ) and 6061-T6 Al (bulk density of  $2.704$

$\pm 0.003 \text{ g/cm}^3$ ). The 1060 alloy was essentially pure aluminum (99.6 percent Al) whereas the 6061 alloy contained approximately 98 percent aluminum with minor amounts of magnesium, chromium, silicon and copper.

The carbon phenolic resin was furnished by the Stanford Research Institute (SRI) who in turn purchased the materials from Haver Industries, Inc. Detailed specification data have been reported previously<sup>14</sup>. The specimen density was  $1.430 \pm 0.005 \text{ g/cm}^3$ .

The Nylon 6 polymer was obtained from the Cadillac Plastic Corp. The polymer density was  $1.14 \text{ g/cm}^3$  and the repeating unit was  $[(\text{CH}_2)_5\text{-CO-NH-}]_x$ .

The Delrin Acetal sample (density  $1.43 \text{ g/cm}^3$ ) was a highly crystalline form of polymerized formaldehyde. The material is said to contain the oxymethylene  $(-\text{OCH}_2)_n$  structural repeating unit.

Maraset epoxy was a crystal clear epoxy purchased from the Marblett Corporation. The measured material density was  $1.21 \text{ g/cm}^3$ .

The phenolic resin (density  $1.18 \text{ g/cm}^3$ ) was a block phenolic cast from Monsanto SC 1008 resin by the AVCO Corporation. The polymer contained no added filler.

#### RESULTS AND DISCUSSION

Specific heat data in the form of linear equations are presented in Table 1. For the polymeric materials the data represent values extrapolated from nontransitional regions. The tables also include the Debye temperatures obtained from ultrasonic measurements as defined by equation (10). The reported characteristic temperatures (Table 1) for the pure metals (copper, gold, nickel, and lead) agree well with previously reported values for high purity materials obtained from low temperature specific heat data. Kneip, et al.<sup>20</sup> have shown that slight deviations in reported  $\theta_D$  values are associated with the degree of sample purity. His value for 99.99 percent copper was 342 K which is in excellent agreement with our value of 341 K.

The  $\theta_D$  versus temperature diagrams (Figure 1) indicate that the value of  $\theta_D$  obtained from ultrasonic methods agrees well with low temperature specific heat data. The straight lines of Figure 1 define a value of  $\theta_D$  constant for the measured temperature interval. This suggests that there is a tendency for the vibrations to center about one particular frequency and this frequency is a fair representation of the specific heat in this region.

The scatter of the  $\theta$ 's so obtained for the various materials is a sensitive indication of the validity of the Debye theory to corroborate the experimental results. The Debye theory predicts a constant value of  $\theta$  but from the nature of vibrations present in crystalline materials,  $\theta$  values for real substances do show a slight temperature dependence. More information concerning the

Table I. Specific heat and Debye temperatures for the materials studied.

$$C_p = aT + b \text{ cal/g}^\circ\text{K}$$

Sample	$a \times 10^4$	b	$\theta, ^\circ\text{K}$	Temp. Range, $^\circ\text{K}$
Aluminum	1.34	0.1738	415.0	253 - 403
Aluminum 1060	1.16	0.1656	415.0	273 - 483
Aluminum 6061	1.61	0.1647	416.0	273 - 483
Carbon Phenolic	7.02	-0.0045	162.8	273 - 323
Copper	0.47	0.0743	331.0	73 - 423
Delrin Acetal	17.60	-0.0283	105.8	243 - 353
Epoxy, Maraset	11.60	-0.0484	53.0	273 - 323
Gold	0.12	0.0269	161.0	273 - 483
Lead	21.99	0.0240	94.3	253 - 383
Nickel	1.71	0.0526	448.0	233 - 373
Nylon 6	10.00	0.0984	69.0	173 - 453
Phenolic Resin	13.99	-0.0566	65.0	273 - 323

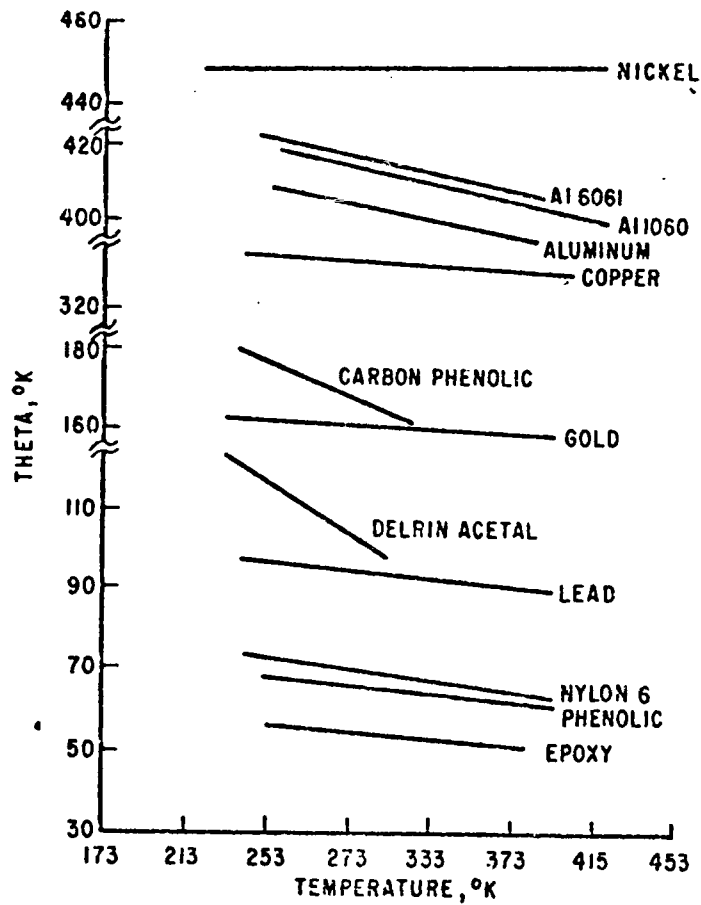


Figure 1. The temperature dependence of the Debye temperature,  $\theta_D$ , for the materials studied.

vibrational characteristics of polymers is necessary before the observed  $\theta$  values can be fully understood. The values presented here were calculated from the defined molecular weight of each repeating unit. In general, the  $\theta$  values represent the vibrational frequencies of the materials which were determined from the material elastic properties. Jacobsen<sup>21</sup> has shown that the temperature variation of  $\theta$  is more sensitive to changes in the elastic coefficients  $C_{44}$  and  $C_{11} - C_{12}$  for transversely isotropic materials than in  $C_{11}$  and  $C_{12}$ , the elastic coefficients for isotropic materials, however, no further attempts at discussion of  $\theta$  values will be included in this paper.

Volume coefficient of expansion data for the materials studied are presented in Table 2. Since for a cubic structure,

Table II. Volume coefficient of expansion data for the materials studied.

$$\beta = aT + b/^\circ K$$

Sample	$a \times 10^8$	$b \times 10^5$	Temp. Range, $^\circ K$
Aluminum rod	5.82	5.20	253 - 403
Aluminum 1060	9.00	3.81	273 - 483
Aluminum 6061	9.18	3.79	273 - 483
Carbon Phenolic	5.98	1.75	273 - 323
Copper	2.86	3.99	173 - 423
Delrin Acetal	66.35	1.53	243 - 353
Epoxy Maraset	122.82	-11.48	273 - 323
Gold	1.22	3.66	273 - 483
Lead	7.20	6.64	253 - 383
Nickel	3.59	2.71	233 - 373
Nylon 6	122.35	-8.50	173 - 453
Phenolic Resin	138.55	-9.81	273 - 323

the linear coefficient of expansion,  $\alpha_x = \alpha_y = \alpha_z$ , the volume coefficient was obtained as  $3\alpha$ . For the anisotropic materials  $\beta$  was calculated from

$$\beta = \alpha_{||} + 2\alpha_{\perp} \quad (27)$$

where  $\alpha_{||}$  and  $\alpha_{\perp}$  represent the linear coefficient of expansion parallel and perpendicular to the chain alignment of the polymer, assuming transverse isotropy.

The  $\beta/C_p$  versus temperature graphs (Figure 2) illustrate the validity of the Gruneisen law. For the polymeric materials, the presence of a transition near room temperature greatly affects the interpretation of the  $\beta/C_p$  ratio. Figure 3 for Maraset Epoxy and Nylon 6 illustrates the effect if the ratio was calculated without extrapolation through transitional regions. Maraset Epoxy has a pronounced glass transitional temperature peak at

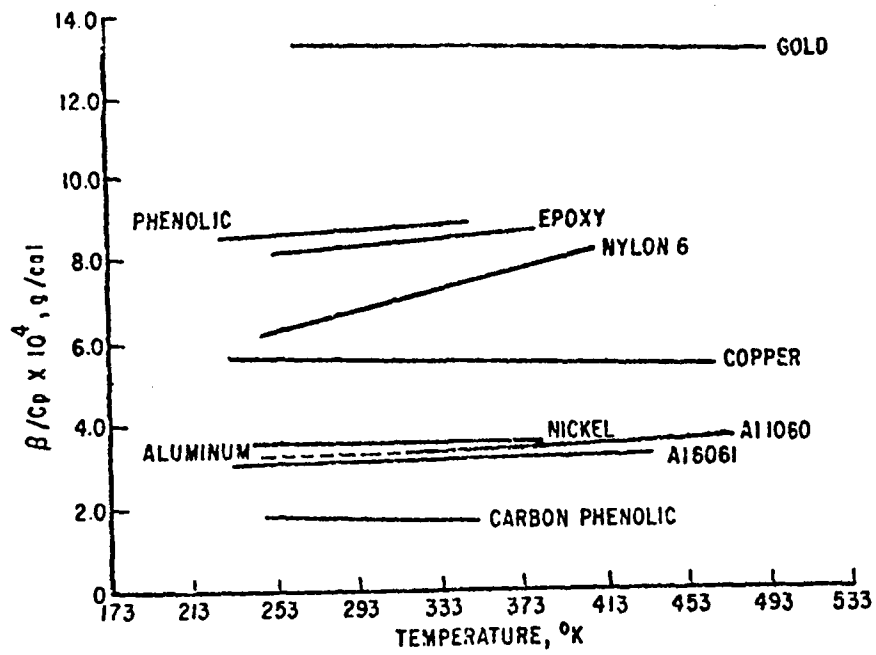


Figure 2. The temperature dependence of the  $B/C_p$  ratio for the materials studied.

40°C. As previously illustrated<sup>13</sup>, the deviation from linearity of the specific heat and elongation curves begins at approximately -20 to +20°C, therefore, the proper extrapolation of the data is necessary to define the proper  $\beta/C_p$  ratio measured.

Previous differential thermal studies on the polyamide (Nylon 6)<sup>13</sup> indicated that the polymer exhibited well-defined fusion and second order transitional regions. A minor transition at -20°C was said to represent the onset of segmental motion while the pronounced glass transitional temperature occurred at 50°C. The  $\beta/C_p$  ratio of the original polymer (Figure 3) illustrates these transitions while Figure 2 defines the ratio for the extrapolated values.

Previous differential thermal studies on delrin acetal<sup>13</sup>, phenolic resin<sup>18</sup>, and carbon phenolic<sup>13</sup> showed similar transitionally induced deviations from linearity. For delrin acetal the melt endothermal peak at 180°C was preceded by a break at 75°C which was attributed to the onset of rotational vibrations. A secondary transition on the expansion plot at -20°C was said to be due to the motion of the (-O-CH<sub>2</sub>-O-) group. For the thermally unstable phenolic resin a broad endothermal decomposition peak with an onset temperature as low as -20°C was observed. For carbon phenolic, the linear expansivity versus temperature data showed a slight decrease in expansion from 30 to 80°C. This decrease was less pronounced in the z-direction ( $\alpha_{||}$  perpendicular to the layers) than in either of the two other orthogonal directions described by  $\alpha_{\perp}$  (parallel to the layers). Proper extrapolations of linear expansivity data are less significant for this polymer, however, improper extrapolations could result in a 3 to 6 percent change in the volume coefficient of expansion value reported.

The thermodynamic data necessary to estimate the Gruneisen ratio as a function of pressure are given in Tables 3 through 5. All values listed in this table have been experimentally determined except the pressure derivative of the adiabatic bulk modulus,  $(\partial B^S/\partial P)_T$ , which was estimated from the Dugdale-MacDonald, formula  $B_{0,S}^S$  (Equation 23). The  $B_{0,T}^S$  value was derived from equation (24).

The specific heat and volume coefficient of expansion data were taken from Tables 1 and 2. The ultrasonically determined longitudinal and transverse sound velocities were used to derive the adiabatic and isothermal bulk moduli for all materials<sup>13,14,19</sup> except copper and nickel. The sound velocity data for these metals were obtained from room temperature extrapolations presented by Grover<sup>22</sup>, McQueen and Marsh<sup>23</sup>, and handbook data. The conversion of the heat capacity data at constant pressure to that of constant volume was effected from the relationship  $C_p/C_v = B^S/B^T$ . The proper density variations were calculated from the corresponding volume variations by means of  $V_T = V_0(1 + \beta T)$ . The corresponding temperature derivatives of the initially measured

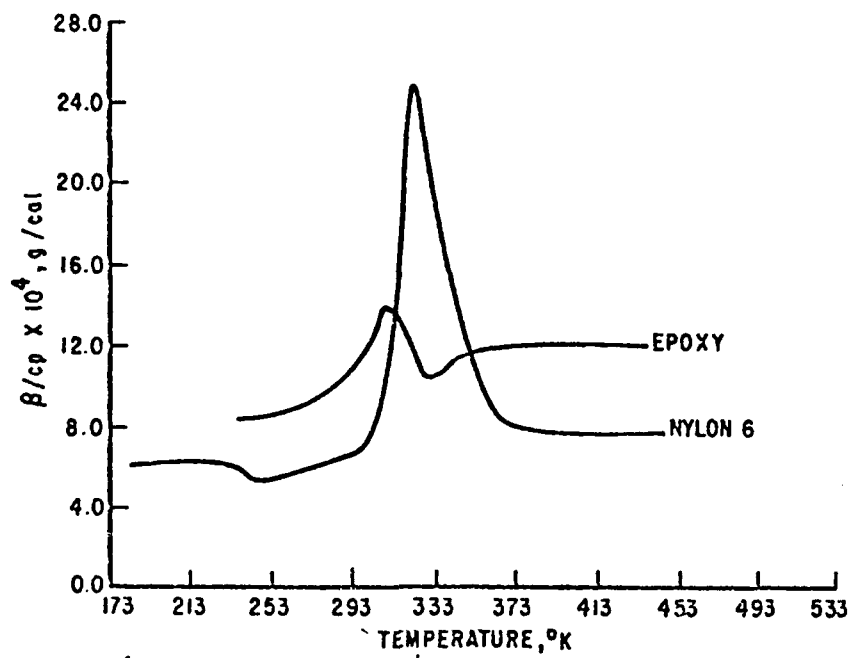


Figure 3. The temperature dependence of the  $\beta/c_p$  ratio for Nylon 6 and Maraset Epoxy (along transitional regions).

Table 3: Experimental thermodynamic data to estimate the pressure derivative of the Grüneisen ratio.

FUNCTION	Aluminum	AL 1060	AL 6061	Copper
$\rho_0$	2.70	2.70	2.70	8.87
$(\rho'_0)_p \times 10^4, \text{ g/cm}^3 \text{ } ^\circ\text{K}$	-2.00	-2.20	-2.23	-4.31
$(\rho'_0)_T \times 10^{12}, \text{ g/dyne cm}$	3.82	3.80	3.76	6.75
$\beta_0 \times 10^5 / ^\circ\text{K}$	6.91	6.45	6.48	4.90
$(\beta'_0)_p \times 10^8 / ^\circ\text{K}^2$	5.82	9.00	9.18	2.86
$(\beta'_0)_T \times 10^{15}, \text{ cm}^2 / ^\circ\text{K dyne}$	-0.69	-0.79	-0.68	-0.13
$C_{p0} \times 10^2 \text{ cal/g } ^\circ\text{K}$	21.38	20.16	21.24	8.68
$(C'_p)_0)_p \times 10^4 \text{ cal/g } ^\circ\text{K}^2$	1.34	1.16	1.61	0.51
$(C'_p)_0)_T \times 10^6 \text{ cm}^3 / \text{g } ^\circ\text{K}$	-6.83	-10.30	-10.40	-1.02
$B^S_0 \times 10^{-11}, \text{ dyne/cm}^2$	7.38	7.40	7.49	13.73
$B^T_0 \times 10^{-11}, \text{ dyne/cm}^2$	7.07	7.09	7.19	13.55
$(B^S_0)_p \times 10^{-8}, \text{ dyne/cm}^2 \text{ } ^\circ\text{K}$	-2.19	-2.18	-1.79	-0.82
$B^S_0)_T$	5.22	5.18	5.06	5.12
$B^S_0)_S$	5.40	5.36	5.20	5.16
$B^S_0)_T$	2.11	2.09	2.03	2.06
$\gamma_0$	-0.41	10.44	8.22	-0.02
$(\gamma'_0)_p \times 10^4 / ^\circ\text{K}$	1.93	1.63	1.53	0.93
$(\gamma'_0)_T \times 10^5, \text{ cm}^2 / \text{dyne}$				

Table 4: Experimental thermodynamic data employed to calculate the pressure derivative of the Grüneisen ratio.

FUNCTION	Gold	Nickel	Lead	C	P
$\rho_0$	18.94	8.88	11.39	1.43	
$(\rho'_0)_p \times 10^4 \text{ g/cm}^3 \text{ K}$	8.13	3.45	10.57	0.53	
$(\rho'_0)_T \times 10^{12} \text{ g/dyne cm}$	11.78	1.23	2.00	15.10	
$\gamma_0 \times 10^5 / \text{K}$	4.06	3.79	8.75	3.47	
$(\gamma'_0)_p \times 10^3 / \text{K}^2$	1.22	3.60	7.21	7.20	
$(\gamma'_0)_T \times 10^{15} \text{ cm}^2 / \text{K dyne}$	-0.19	-0.13	-3.54	1.74	
$C_{pe} \times 10^2 \text{ cal/g}^\circ \text{K}$	3.04	10.59	3.00	20.40	
$(C_{p'_0})_p \times 10^4 \text{ cal/g}^\circ \text{K}^2$	0.12	1.71	0.22	6.30	
$(C_{p'_0})_T \times 10^6 \text{ cm}^3 \text{ g}^\circ \text{K}$	-0.21	-1.23	-2.00	15.10	
$g^S_0 \times 10^{-11} \text{ dyne/cm}^2$	16.64	17.55	4.77	1.59	
$g^T_0 \times 10^{-11} \text{ dyne/cm}^2$	16.08	17.49	4.41	1.39	
$(g^S_0)_p \times 10^{-6} \text{ dyne/cm}^2 \text{ K}$	-3.05	-2.73	-6.49	0.48	
$g^S_{1,C,S}$	6.60	4.46	6.84	1.70	
$g^S_{0,T}$	6.75	4.52	8.00	1.73	
$\gamma_0$	2.80	1.73	2.92	0.46	
$(\gamma'_0)_p \times 10^3 / \text{K}$	-0.64	-1.52	-3.39	-0.53	
$(\gamma'_0)_T \times 10^6 / \text{K}$	1.89	0.65	8.00	0.32	

Table 5: Experimental thermodynamic data to estimate the pressure derivative of the Grüneisen ratio.

FUNCTION	Epoxy	Phenolic	Nylon 6	Del. Ac.
$\rho_0$ g/cm <sup>3</sup>	1.21	1.18	1.14	1.43
$(\rho'_0)_p \times 10^4$ g/cm <sup>3</sup> /°K	-3.44	-4.16	-4.03	-3.38
$(\rho'_0)_T \times 10^{12}$ g/dyne cm	23.92	19.97	19.00	22.34
$B_0 \times 10^7$ /°K	2.46	3.08	2.67	2.00
$(B'_0)_p \times 10^7$ /°K <sup>2</sup>	12.28	13.86	12.20	6.60
$(B'_0)_T \times 10^{15}$ cm <sup>2</sup> /°K dyne	56.90	161.16	-60.33	-43.39
$CP_0 \times 10^2$ cal/g°K	29.20	35.83	39.16	23.26
$(C'_p)_p \times 10^4$ cal/g°K <sup>2</sup>	11.60	1.40	10.00	17.60
$(C'_p)_T \times 10^6$ cm <sup>3</sup> /g°K	300.49	368.00	-18.35	-143.42
$B^S_0 \times 10^{-11}$ dyne/cm <sup>2</sup>	0.54	0.65	0.65	0.68
$B^T_0 \times 10^{-11}$ dyne/cm <sup>2</sup>	0.49	0.59	0.65	0.66
$(B^S_0)_p \times 10^{-8}$ dyne/cm <sup>2</sup> /°K	-1.32	-6.36	-0.60	-2.08
$B^S_0$	2.80	3.26	2.86	2.76
$B^S_0$	3.44	6.50	3.11	3.81
$\gamma_0$	0.90	1.13	0.93	0.97
$(\gamma'_0)_p \times 10^3$ /°K	-1.08	-10.27	1.15	-7.99
$(\gamma'_0)_T \times 10^9$ cm <sup>2</sup> /dyne	9.05	37.53	3.53	17.45

thermodynamic quantities:  $(\rho_0)_p, (B_0)_p, (C_{pp})_p, (B_0^S)_p$  and  $(\gamma_0)_p$ , were obtained from the appropriate linear least square polynomial expressions. Figure 4 illustrates the variation of the Gruneisen ratio with temperature.

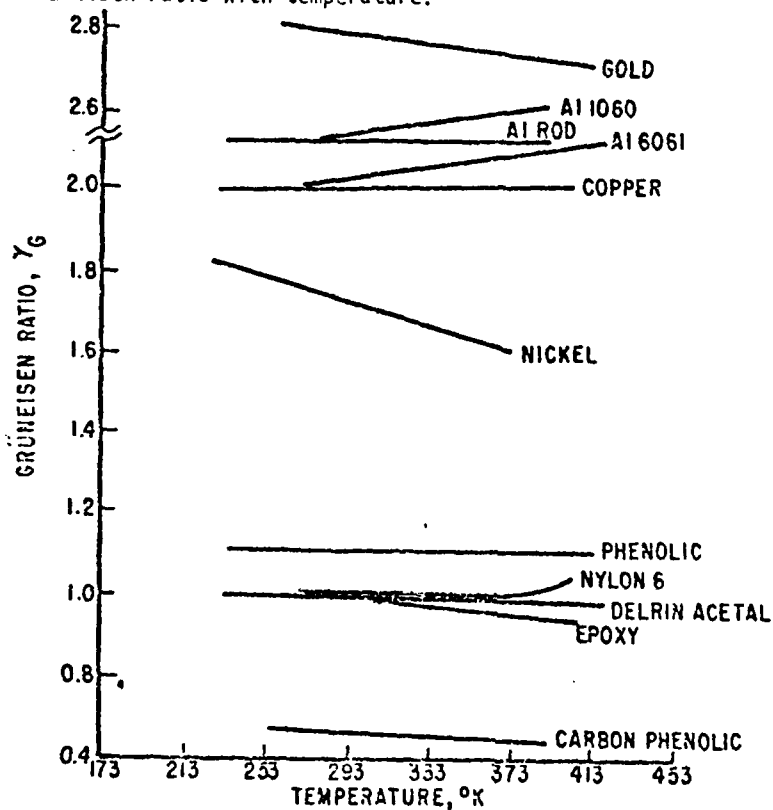


Figure 4. The temperature dependence of the Gruneisen ratio for the materials studied.

Since Lamberson<sup>14</sup> has shown that carbon phenolic is transversely isotropic, at standard conditions, the five independent elastic coefficients were used to calculate the isothermal and adiabatic bulk moduli of Table 2. The  $\gamma_0$  value for this material was calculated from the Gruneisen tensor which was represented as a diagonal matrix. For details of the calculations see references 14 and 24. Lamberson's value for  $\gamma_0$ <sup>14</sup> was 0.352 at 30°C. The  $\gamma_0$  tensor value reported by Benson, et al.<sup>19</sup>, for carbon phenolic was 0.554 at 20°C. The smaller value reported by Lamberson resulted from the extrapolation of  $\gamma$  values through minor transitional regions. Our value of  $\gamma_0 = 0.46$  (Table 4) is due to a

more refined extrapolation of the linear expansivity data in the parallel and perpendicular directions.

The pressure derivatives of the volume coefficient of expansion,  $(\beta_0)_T$ , of the specific heat,  $(C_p)_T$ , and of the density,  $(\rho_0)_T$ , were obtained from equations (14), (15) and (18) as previously defined. The proper correction for comparing shock wave and ultrasonic data was made by equation (24) to yield the desired  $(\beta_0)_T$ . Equation (26) was used to derive the pressure derivative of the Gruneisen ratio,  $(\gamma_0)_T$ .

The basic thermal and density data agree well with similar data presented by various authors<sup>25-29</sup>. Initial ultrasonic data for copper and gold agreed to within 1.2 percent of the values reported by Schmunk<sup>30</sup> and Goens<sup>31</sup> and to within 5.5 percent of earlier results presented by Bridgeman<sup>32</sup>.

Values for  $(\partial B_0/\partial P)_T$  reported for copper and gold by Daniels and Smith<sup>27</sup> were 5.47 to 5.59 for copper and 6.43 for gold. Differences between the value for copper and our value were probably due to the ultrasonic velocity data compiled from other sources to fit our sample. The value for gold agrees well with our value of 6.60. Vaidya and Kenedy<sup>23</sup> report a value of 6.51 for the pressure derivative of copper.

Asay, et al.<sup>13</sup>, have illustrated the applicability of using the Murnaghan equation and the Dugdale and MacDonald relation to estimate the high pressure equation of state of the two aluminum alloys reported here. Proper comparisons were made with some dynamically determined high pressure points by Lundergan and Herman<sup>33</sup> and a least squares compilation by Walsh, et al.<sup>34</sup>. The results showed agreement between the estimated curve and the actual data to approximately 450 kbars.

The  $B_{0,S}$  value for lead estimated by Anderson was 6.30 while our value was 6.84. Anderson's value was based on a Gruneisen ratio of 2.65 as opposed to our value of 2.92. For the lead sample used in this study no shear velocity data was available due to voids originating from the recasting of the metal. Differences in the  $B_{0,S}$  value may again be due to the use of inaccurate ultrasonic velocity data<sup>35-36</sup>. This may also account for the slightly lower  $\gamma_0$  value for nickel observed in this study.

Lamberson<sup>14</sup> has compared high pressure ultrasonic measurements for the carbon phenolic sample studied with data from shock wave experiments obtained from various sources<sup>37-38</sup>. For this material it was observed that pressure points from the ultrasonic and low pressure gas gun studies, as well as the high pressure data, showed considerable spread, however, similarities between the three methods were observed. The application of the Dugdale and MacDonald estimation would be valid to approximately 7 to 8 kbars, beyond this region a relaxation and yielding process in the carbon phenolic was observed.

Previous high pressure measurements made on teflon<sup>32</sup> and polystyrene<sup>30</sup> suggest that the Murnaghan equation was reliable to approximately 10 kbars. Discontinuities in volume were attributed to transitional regions, and estimations resulting through use of the Dugdale and MacDonald relation were not too

reliable. The unreliability of the latter was probably due to the improper compilation of initial basic data to calculate the Gruneisen ratio. Since estimated values were obtained from average single temperature measurements of  $\gamma_0$ , it is assumed that proper extrapolations through or along transitional regions would better define the equation of state of plastics. Further comparisons with dynamic high pressure data is necessary before definite conclusions can be presented.

Because of the pronounced transitions occurring between 40 to 80°C for the nylon, epoxy, acetal and phenolic polymers it is assumed that the  $B_{\delta,s}$  and  $B_{\delta,T}$  data of Table 5 are accurate to approximately 10 kbars.

The accuracy of the  $(\gamma_0)_T$  values presented in Tables 3 through 5 is based on the degree of accuracy obtained in estimating the  $B_{\delta,s}$  ratio, since the latter is the only one not measured directly.

#### CONCLUSION

The detailed experimental thermal and ultrasonic measurements presented for metals, alloys and polymeric materials has made it possible to define the equation of state for these materials. The use of the Dugdale and MacDonald relation is justified within limited pressure regions provided the initial Gruneisen values are obtained from reliable thermal and ultrasonic measurements. For polymeric materials it is necessary to account for observed transitional regions in making the proper extrapolations.

## REFERENCES

1. R.E. Barker, Jr., *J. Appl. Phys.* **38**, 4234 (1967).
2. Y. Wada, "Conferences in Relaxation Phenomena in Polymeric Systems", sponsored by Institute of Phys. and Chem. Res. of Tokyo, Tokyo, Japan, September, 1966.
3. A. Schauer, *Canadian Jour. Phys.*, **43**, 523 (1965).
4. R.E. Barker, *J. Appl. Phys.*, **34**, 107 (1963).
5. A. Schauer, *Can. J. of Phys.*, **42**, 1857 (1964).
6. T.H.K. Barron, *Phil. Mag.* **46**, 720 (1955).
7. J.C. Slater, *Introduction to Chemical Physics* (McGraw-Hill, New York, 1939).
8. M. Blackman *Handbook of Physics*, **7**, 325 (1957), *Proc. Phys. Soc. Land. B*, **70**, 827 (1957), **74**, 17 (1959).
9. W.C. Overton, Jr., *Jour. Chem. Phys.*, **37**, 116 (1963).
10. J.R. Neighbors and G.A. Alers, *Phys. Rev.*, **111**, 707 (1958).
11. J.R. Partington, *An Advanced Treatise on Physical Chemistry*, Vol. III, *The Properties of Solids* (Longmans).
12. R.N. Thurston, *Proceedings of the IEEE* **53**, 1320 (1965).
13. J.R. Asay, S.R. Urzendowski and A.H. Guenther, *Ultrasonic and Thermal Studies of Selected Plastics, Laminated Materials, and Metals*, Tech. Rept. 67-91, Air Force Weapons Lab, Kirtland, New Mexico, January, 1968.
14. D.L. Lamberson, Ph.D. Dissertation, Air Force Institute of Technology, Wright-Patterson AFB, Ohio, 1969.
15. O.J. Anderson, *J. Phys. Chem. Solids*, **27**, 547 (1966).
16. F.D. Murnaghan, *Proc. Natl. Acad. Sci.*, **30**, 244 (1944).
17. J.S. Dugdale and D.K.C. MacDonald, *Phys. Rev.*, **89**, 832 (1953).
18. S.R. Urzendowski and A.H. Guenther, *Thermal Properties and Gruneisen Parameters for Several Polymers, Concretes and Composite Materials*, Tech Rept. 72-37, Air Force Weapons Lab, Kirtland, New Mexico, September 1972.
19. D.A. Benson, R.N. Junck, and J.A. Klosterbauer, *Temperature and Pressure - Dependent Elastic Properties of Selected Isotropic and Composite Materials from Ultrasonic Measurements*, Tech. Rept. 70-169, Air Force Weapons Lab, Kirtland, New Mexico, March 1971.
20. G.D. Kneip, Jr., J.O. Betterton, Jr., and J.O. Scarbrough, *Phys. Rev.*, **130**, 1687 (1963).
21. E.H. Jacobsen, *Phys. Rev.* **97**, 654 (1955).
22. R. Grover, *J. Phys. Chem. Solids*, **31**, 2347 (1970).
23. R.G. McQueen and S.P. Marsh, *J. Appl. Phys.* **31**, 1253 (1960).
24. S.W. Key, *J. Appl. Phys.*, **38**, 2923 (1967).
25. F.C. Nix and D. MacNair, *Phys. Rev.*, **61**, 74 (1941).
26. P.F. Meads, W.R. Forsythe, and W.F. Geauque, *J. Am. Chem. Soc.*, **63**, 1902 (1941).
27. R.A. Miller and D.E. Schuele, *J. Phys. Chem. Solids*, **30**, 589 (1969).
28. W.B. Daniels and C.S. Smith, *Phys. Rev.*, **111**, 713 (1959).

29. S.N. Vaidya and G.C. Kenedy, *J. Phys. Chem. Solids*, 31, 2329 (1970).
30. R.E. Schmunk, M.S. Thesis, Case Institute of Technology.
31. E. Goens, *Ann. Physik* 38, 456 (1940).
32. P.W. Bridgeman, The Physics of High Pressures (G. Bell and Sons, London, 1952).
33. C.D. Lundergan and W.J. Herrmann, *J. Appl. Phys.*, 34, 2046 (1963).
34. J.M. Walsh, M.H. Rice, R.C. McQueen, and F.L. Yeager, *Phys. Rev.*, 108, 196 (1957).
35. D.J. Pastine and D. Piacesi, *J. Phys. Chem. Solids*, 27, 1973 (1966).
36. D.S. Hughes and J.L. Kelly, *Phys. Rev.*, 92, 1145 (1953).
37. N.A. Louie, W.W. Kinney, and D.D. Reid, Jr. Dynamic Properties of Materials, AFWL-TR-68-101, Air Force Weapons Lab, Kirtland AFB, New Mexico, 1968.
38. G.P. Croswell, Jr. and H.P. Ward, Hugoniot Data on Several Materials, AFWL, TR-68-82, Air Force Weapons Lab, Kirtland AFB, New Mexico, 1968.

## APPENDIX B

### THE USE OF THERMAL AND ULTRASONIC DATA TO CALCULATE THE PRESSURE DEPENDENCE OF THE GRUNEISEN PARAMETER

S.R. Urzendowski and A.H. Guenther

Air Force Weapons Laboratory

Kirtland Air Force Base, New Mexico

#### INTRODUCTION

A knowledge of the Gruneisen parameter is a prerequisite to any practical or theoretical evaluation of the pressure or temperature dependence of thermodynamic properties in equation of state studies. As demonstrated by Gruneisen (1) and others (2,3,4), the Gruneisen ratio may be determined from mechanical properties (such as the bulk modulus and sound velocities), and from thermal properties such as volume coefficient of expansion and specific heat data. This relation is defined by

$$\gamma_g = \frac{\beta \cdot B^T}{C_v \cdot \rho} = \frac{\beta \cdot B^S}{C_p \cdot \rho} = \frac{\beta [c_l^2 - 4/3 c_t^2]}{C_p \cdot \rho} \quad (1)$$

where  $\gamma_g$  is the Gruneisen ratio,  $\beta$  is the volume coefficient of thermal expansion,  $\rho$  is the density,  $C_v$  and  $C_p$  are the heat capacity at constant volume and constant pressure, respectively,  $B^T$  and  $B^S$  represent the isothermal and adiabatic bulk moduli, and  $c_l$  and  $c_t$  are the longitudinal and transverse ultrasonic sound velocities, respectively, for isotropic media.

In this study we are interested in the variation of the thermodynamic and elastic property data of Equation (1) as a function of temperature and pressure. Although the temperature dependence of the Gruneisen ratio can be determined from the temperature dependence of the thermo-mechanical properties, this information is generally not available for polymeric materials, alloys, or nonisotropic metals. Difficulties in obtaining temperature derivatives of these materials are associated with

NOTE: This paper was presented at the American Chemical Society Symposium on Analytical Calorimetry held at Los Angeles, California, April 1974.

material property failure as well as the necessity of multiple thermal expansion and ultrasonic sound velocity measurements to account for contributions along the three coordinate axes of the materials.

It is known that the shock technique has been the most widely applicable technique for the determination of pressure-volume data for equation of state studies. Since the reliability of shock measurements decreases below 100 kbar, most equation of state data has been obtained above 100 kbar. It is necessary to complement the shock data between 1 atm to a pressure of approximately 100 kbar.

Swenson (5) has discussed the difficulties involved in the static determination of equation of state data for certain solids. Due to strong interatomic binding forces, valence and ionic solids (such as diamond and the silver halides) are relatively incompressible. For more complex metals (such as iron or beryllium), very great pressures are necessary to produce significant changes in the cohesive energies or the high temperature thermal properties of these substances. Although molecular solids are the most appropriate for pressure volume studies, further complications arise from material property failure.

In this work, thermal and ultrasonic measurements made at various temperatures were used to calculate the temperature dependence of the Gruneisen ratio according to Equation (1). Although ultrasonic data were obtained for some of the materials at high pressures, the high pressure derivative  $(\partial\gamma/\partial P)$  was estimated by applying proper thermodynamic relationships.

#### DERIVATIONS

The equation of state of solid materials under shock-loaded conditions (6,7) may be expressed as

$$P = au^1 + bu^2 + cu^3 + \dots + \gamma\partial E/\rho_0 \quad (2)$$

where  $u$  is the compressibility,  $u = (\rho/\rho_0)^{-1}$ ,  $a$ ,  $b$ , and  $c$  are constants,  $E$  is the internal energy,  $\gamma$  is the Gruneisen ratio,  $\gamma = (1/\rho)(\partial P/\partial E)_V$ , and  $\rho$  is the density.

The constant  $a$  may be expressed in terms of the bulk modulus,  $B$ , in the Maclaurin expansion as

$$a = (\partial P/\partial u)_0 = \rho_0(c_l^2 - 4/3 c_t^2) = B \quad (3)$$

where  $c_l$  and  $c_t$  are longitudinal and transverse velocities, respectively.

PRESSURE DEPENDENCE OF THE GRUNEISEN PARAMETER

As derived previously (8,9) the temperature derivative of the Gruneisen ratio,  $(\partial\gamma/\partial T)_0$ , was obtained by differentiating each term of Equation (1) to give

$$\begin{aligned} \left(\frac{\partial\gamma}{\partial T}\right)_0 &= \frac{\partial\gamma}{\partial\rho} \left(\frac{\partial\rho}{\partial T}\right)_p + \frac{\partial\gamma}{\partial BS} \left(\frac{\partial BS}{\partial T}\right)_p + \frac{\partial\gamma}{\partial\beta} \left(\frac{\partial\beta}{\partial T}\right)_p + \frac{\partial\gamma}{\partial C_p} \left(\frac{\partial C_p}{\partial T}\right)_p \\ &= \gamma_0 \left\{ \frac{1}{\beta} \left[ \left(\frac{\partial\beta}{\partial T}\right)_p + \beta^2 \right] + \frac{1}{BS} \left(\frac{\partial BS}{\partial T}\right)_p - \frac{1}{C_p} \left(\frac{\partial C_p}{\partial T}\right)_p \right\} \end{aligned} \quad (4)$$

where the zero subscript represents 0°K and atmospheric pressure.

The temperature derivative for the specific heat,  $(\partial C_p/\partial T)$ , for the thermal expansion,  $(\partial\beta/\partial T)$ , and for the density,  $(\partial\rho/\partial T)$ , was obtained from linear least square curves of the respective data. The proper specific heat data at constant volume,  $C_v$ , was obtained from the following conversion

$$C_p - C_v = TV\beta^2/x^T \quad (5)$$

where  $x^T$  is the isothermal compressibility.

Although the experimental measurements yield adiabatic bulk moduli, the data were converted to the isothermal counterparts by

$$B^T = B^S/1 + \beta\gamma T \quad (6)$$

where  $T$  is the absolute temperature.

The temperature derivative of the bulk modulus was obtained from the differentiation of Equation (6) to give

$$\left(\frac{\partial B^T}{\partial T}\right)_p = \frac{(\partial B^S/\partial T)_p}{1 + \beta\gamma T} - \frac{B_p^S \beta \gamma}{(1 + \beta\gamma T)^2} - \frac{B_p^S \gamma T (\partial\beta/\partial T)_p}{(1 + \beta\gamma T)^2} - \frac{B_p^S \partial T (\partial\gamma/\partial T)_p}{(1 + \beta\gamma T)^2} \quad (7)$$

and all of the quantities appearing on the right can be determined from thermal and ultrasonic data.

The pressure derivative,  $(\partial\gamma/\partial P)$ , may be obtained by differentiating Equation (1) with respect to pressure, so that

$$\begin{aligned} \left(\frac{\partial\gamma}{\partial P}\right)_T &= \frac{\partial\gamma}{\partial\rho} \left(\frac{\partial\rho}{\partial P}\right)_T + \frac{\partial\gamma}{\partial C_p} \left(\frac{\partial C_p}{\partial P}\right)_T + \frac{\partial\gamma}{\partial\beta} \left(\frac{\partial\beta}{\partial P}\right)_T + \frac{\partial\gamma}{\partial BS} \left(\frac{\partial BS}{\partial P}\right)_T \\ &= -\frac{\beta B^S}{\rho^2 C_p} \left(\frac{\partial\rho}{\partial P}\right)_T - \frac{\beta B^S}{\rho C_p^2} \left(\frac{\partial C_p}{\partial P}\right)_T + \frac{B^S}{\rho C_p} \left(\frac{\partial\beta}{\partial P}\right)_T + \frac{\beta}{\rho C_p} \left(\frac{\partial BS}{\partial P}\right)_T \end{aligned} \quad (8)$$

Thurston (10) has shown that the pressure derivatives of  $\beta$  and  $C_p$  at constant temperature are related to the mechanical properties of an isotropic solid by

$$\left(\frac{\partial \beta}{\partial P}\right)_T = - \left(\frac{\partial \chi^T}{\partial T}\right)_P = \frac{1}{(\beta^T)^2} \left(\frac{\partial \beta^T}{\partial T}\right)_P = \beta^T \quad (9)$$

$$\left(\frac{\partial C_p}{\partial P}\right)_T = - \frac{T}{\rho} \left[ \left(\frac{\partial \beta}{\partial T}\right)_P + \beta^2 \right] = - T \left(\frac{\partial^2 v}{\partial T^2}\right) = C_p^T \quad (10)$$

where the superscript T refers to the isothermal moduli and T is the absolute temperature. If one has the means of measuring the temperature dependence of the bulk modulus and the expansion coefficient, Equations (9) and (10) allow an estimation of the pressure derivatives of  $\beta$  and  $C_p$ .

The quantity  $(\partial \rho / \partial P)_T$ , follows from the relationship of density to volume and from the definition of the isothermal compressibility so that

$$(\partial \rho / \partial P)_T = \rho / \beta^T \quad (11)$$

where  $\rho$  is the density.

Since the adiabatic bulk modulus may be expressed in terms of the longitudinal and transverse sound velocities, Asay et al. (8), and Lamberson (11), have shown that the differentiation of Equation (1) at constant temperature and zero pressure yields

$$\left(\frac{\partial \beta^S}{\partial P}\right)_{0,T} = 2\rho_0 [c_l c_l' - 4/3 c_t c_t']_{P=0} + (1 + \beta \gamma T) = \beta^S \quad (12)$$

where  $(\partial \beta^S / \partial P)_{0,T}$  is the pressure derivative of the adiabatic bulk modulus.

Anderson (12) has shown that the conversion to the isothermal pressure derivative results from

$$\begin{aligned} \left(\frac{\partial \beta^T}{\partial P}\right)_{0,T} &= \beta_{0,T}^S + \beta \gamma T \left(\frac{\beta_0^T}{\beta_0^S}\right) \left[ 1 - \frac{2}{\beta \beta_0^T} \left(\frac{\partial \beta_0^T}{\partial T}\right)_P - 2\beta \delta_{0,T}' \right] \\ &+ \left[ \beta \gamma T \left(\frac{\beta_0^T}{\beta_0^S}\right) \right]^2 \left[ \beta_{0,T}^S - 1 - \frac{1}{\beta^2} \left(\frac{\partial \beta}{\partial T}\right)_P \right] = \beta^T \quad (13) \end{aligned}$$

PRESSURE DEPENDENCE OF THE GRUNEISEN PARAMETER

where the temperature derivative of  $B_0^T$  was obtained from Equation (7).

The above derivation leads to

$$\left(\frac{\partial \gamma}{\partial P}\right)_{0,T} = \gamma_0 \left[ -\frac{1}{B_0^I} - \frac{1}{C_p} \left(\frac{\partial C_p}{\partial P}\right)_{0,T} + \frac{1}{B} \left(\frac{\partial \beta}{\partial P}\right)_{0,T} + \frac{1}{B_0^S} \left(\frac{\partial B^S}{\partial P}\right)_{0,T} \right] \quad (14)$$

where the zero subscripts refer to atmospheric pressure and  $(\partial \gamma / \partial P)_{0,T}$  is  $\gamma'$ .

Anderson (12) has shown that ultrasonic data taken at relatively low pressures may be used to estimate the pressure-volume isotherm to pressures of the order of the bulk modulus. His assumption that the bulk modulus has a linear pressure dependence resulted in the Murnaghan or logarithmic equation of state (13) defined by

$$\ln \left(\frac{V_0}{V}\right) = -\frac{1}{B_0^I} \ln \left\{ B_0^I \frac{P}{B_0} + 1 \right\} \quad (15)$$

From the similarity of definitions for the adiabatic and isothermal bulk moduli (Equation 6) the use of  $B_0^S$  and  $B_0^{S'}$  in Equation (15) results in an adiabat while  $B_0^I$  and  $B_0^{I'}$  results in the isotherm. Furthermore, Dugdale and MacDonald (14) have shown that the derivative  $B_{0,S}^I$  may be estimated from

$$B_{0,S}^I = 2\gamma + 1 \quad (16)$$

which is applicable for all pressures lower than  $B_0$ .

Since ultrasonic data yield adiabatic bulk moduli and shock wave measurements define the isothermal quantities, the proper conversions are made by

$$B_{0,T}^{S'} = B_{0,S}^{S'} - \left(\frac{\partial B^S}{\partial T}\right)_P \cdot \frac{T\gamma}{B^S} \quad (17)$$

which utilizes the pressure and temperature derivative of the adiabatic bulk modulus.

Equation (14) may be expressed by a more convenient estimation by

$$\left(\frac{\partial \gamma}{\partial P}\right)_{0,T} = \frac{\gamma}{B^S} \left[ \left(\frac{\partial B^S}{\partial P}\right)_T + \left(\frac{1 + \beta \gamma T}{\beta B^S}\right) \left(\frac{\partial B^S}{\partial T}\right)_P - 1 - \gamma - T \left(\frac{\partial \gamma}{\partial T}\right)_P \right] \quad (18)$$

where all the quantities are determined experimentally except perhaps  $(\partial B^S/\partial P)_T$ .

#### EXPERIMENTAL TECHNIQUE

Thermal Expansion. A DuPont 940 Thermomechanical Analyzer was used to measure linear thermal expansions between -100 to 200°C. Details of the experimental procedure were previously described (8,9,15). After proper application of chromel alumel thermocouple corrections, individual temperature determinations agreed to within 0.2°C and to within 2.0 to 4.0°C of values reported in the literature. The total probable error of the expansion measurements was ±2.5 percent. This was calculated as the square root of the summation of all errors associated with each component of the instrument.

Heat Capacity. The heat capacity data were obtained with appropriately calibrated differential scanning calorimeters. Both the DuPont DSC and the Perkin Elmer DSC-1B were used for the measurements. The heat capacity values are accurate to approximately ±2.0 percent. For the polymeric materials, transitional regions were eliminated by extrapolating before and after said transitions.

Ultrasonic Sound Velocities. Sound velocity measurements of longitudinal and shear waves at approximately 1 and 3 Mc/sec were made at this laboratory by Asay, et al., (8), and Lamberson (11) and were used to calculate the adiabatic bulk moduli and related ultrasonic data. For most of the velocity-temperature data, a quadratic function was found to fit the data to an accuracy of approximately 1 percent.

Materials Studied. The materials studied included high purity metals, alloys and polymeric materials. Tungsten rod (99.9995 percent pure) was obtained from Alfa Inorganics. The sample density was 19.265 g/cm<sup>3</sup>.

The steel sample No. 314 contained the following constituents: 51.2 percent iron, 0.3 percent carbon, 2.0 percent manganese, 0.4 percent phosphorous, 1.5 to 3.0 percent silicon, 23 to 26 percent chromium and 19 to 22 percent nickel. The measured sample density was 7.62 g/cm<sup>3</sup>.

Aluminum 2024 was chosen because of its availability, its good machining properties and also because a vast amount of shock wave data is available for comparative purposes. The alloy

PRESSURE DEPENDENCE OF THE GRUNEISEN PARAMETER

(density 2.785 g/cm<sup>3</sup>) contained 93.4 percent aluminum, 4.5 percent copper, 1.5 percent magnesium and 0.6 percent manganese. Before heat treatment, the porous sample had a density of 2.65 g/cm<sup>3</sup>.

The solid polymeric materials studied were teflon, density 2.186 g/cm<sup>3</sup> (E.I. DuPont de Nemours Co.), polystyrene, density 1.046 g/cm<sup>3</sup> (Cadco Corporation), and an epoxy resin, density 1.242 g/cm<sup>3</sup> (Shell Chemical Co.).

RESULTS AND DISCUSSION

Specific heat data in the form of linear equations are presented in Table I. For the polymeric materials the data represent values extrapolated from nontransitional regions, however, for Teflon-1 and Epoxy-1 the data were obtained along transitional regions. The data tabulated for Epoxy-2 represents data extrapolated at higher temperatures.

Table I  
Specific Heat and Debye Temperatures  
for the Materials Studied

$$C_p = a + bT, \text{ cal/g}^\circ\text{K}$$

Material	a	b x 10 <sup>3</sup>	$\theta, ^\circ\text{K}$	Temp. Range, $^\circ\text{K}$
Epoxy	-0.0922	1.166	54.2	243 - 353
Epoxy-1	-0.0732	1.099	56.1	263 - 423
Epoxy-2	0.0026	0.887	49.2	343 - 388
Polystyrene	-0.0846	1.270	70.4	233 - 353
Teflon	0.1544	0.250	52.7	243 - 313
Teflon-1	0.1481	0.304	52.7	253 - 413
Tungsten	0.0284	0.012	321.1	233 - 383
Steel No. 314	0.0281	0.258	454.0	253 - 373
Al 2024	0.1788	0.126	408.5	243 - 373

The Debye characteristic temperatures ( $\theta$ ), of Table I were obtained from the ultrasonic calculations as defined previously (8,9,15). The  $\theta$  values agree well with previously reported values calculated from low temperature specific heat data. Kok, et al. (16) and Phillips (17) report Debye temperatures for aluminum of  $\theta = 423 \pm 5$  at 0 $^\circ\text{K}$  and  $\theta = 390$  at 298 K.

For teflon, Wunderlich (18) fitted low temperature specific heat data to a Tarasov-type model and obtained a  $\theta$  value of 47.8 K which agrees with our value obtained at 298 K.

For polystyrene  $\theta = 70.4$  at 273 K agrees well with the temperature of 68 K reported by Reese (19) and Choy, et al. (20).

In general, the  $\theta$  values reported here represent the vibrational frequencies of the materials as determined ultrasonically, however, more information concerning the vibrational characteristics of the polymers is necessary before the observed  $\theta$  values can be fully understood. The values presented here were calculated from the defined molecular weight of each repeating unit.

Volume coefficient of expansion versus temperature data are presented in Table II. Since the steel and the aluminum alloys were expected to exhibit some anisotropy, expansivity measurements were made parallel and perpendicular to the stratification layers. Expansivity data in the "c" direction, parallel to the axis ( $\alpha_{11}$ ) was 0.8 percent higher than that observed in the perpendicular direction ( $\alpha_{\perp}$ ) for the temperature range studied. Since this increase was within the experimental limitations of the instrument, the volume coefficient of expansion data of Table II was taken as  $3\alpha_{11}$ .

Table II  
Volume Coefficient of Expansion  
Data for the Materials Studied

$$\beta = a + bT, /^{\circ}\text{K}$$

Material	$a \times 10^5$	$b \times 10^7$	Temp. Range, $^{\circ}\text{K}$
Epoxy	5.65	5.49	243 - 353
Epoxy-1	-128.40	53.30	263 - 423
Epoxy-2	-125.65	43.17	343 - 383
Polystyrene	10.46	3.92	233 - 353
Teflon	-72.59	35.87	243 - 413
Teflon-1	-65.33	34.17	253 - 413
Tungsten	0.45	0.31	233 - 383
Steel No. 314	-5.40	2.99	253 - 373
Al 2024	-1.44	2.79	243 - 373

The adiabatic bulk moduli as a function of temperature are given in Table III. The ultrasonic longitudinal and transverse velocities used to calculate the moduli were measured at this laboratory for all the materials listed except tungsten. For this material the elastic data of Featherston and Neighbours (21) were used to calculate the bulk moduli.

The temperature variation of the Gruneisen ratio is given in Table IV. This parameter was calculated from the previously defined thermodynamic relationship of Equation 1.

PRESSURE DEPENDENCE OF THE GRUNEISEN PARAMETER

Table III

Adiabatic Bulk Moduli For The  
Materials Studied

$$B^S = a + bT, \text{ dyne/cm}^2$$

MATERIAL	a x 10 <sup>-11</sup>	b x 10 <sup>-8</sup>	Temp. Range, °K
Epoxy	0.98	-1.47	243 - 353
Epoxy-1	87.32	-1.12	263 - 423
Epoxy-2	2.02	-4.52	343 - 388
Polystyrene	0.58	-0.70	233 - 353
Teflon	0.81	-1.50	243 - 313
Teflon-1	0.79	-1.44	243 - 413
Tungsten	32.02	-3.14	233 - 383
Steel No. 314	16.45	-3.37	253 - 373
Al 2024	8.33	-2.34	243 - 373

Table IV

Gruneisen Parameters For  
The Materials Studied

$$\gamma = a + bT$$

MATERIAL	a	b x 10 <sup>3</sup>	Temp. Range, °K
Epoxy	2.21	-4.35	243 - 353
Epoxy-1	-1.73	9.89	263 - 423
Epoxy-2	1.07	-1.00	243 - 388
Polystyrene	1.50	-2.84	233 - 353
Teflon	0.13	1.49	243 - 413
Teflon-1	0.34	0.86	243 - 413
Tungsten	0.51	2.91	233 - 383
Steel No. 314	-1.11	9.11	253 - 373
Al 2024	0.11	6.61	243 - 373

Table V

Experimental Thermodynamic Data  
Used to Calculate the Pressure Derivatives  
of the Gruneisen Ratio

FUNCTION*	UNITS	EPOXY	EPOXY-1	EPOXY-2
$\rho_0$	g/cm <sup>3</sup>	1.25	1.25	1.20
$(\partial\rho_0/\partial P)_T \times 10^{11}$	g/dyne cm	2.29	2.35	2.76
$B_0 \times 10^4$	/°K	2.04	2.04	2.46
$(\partial B_0/\partial P)_T \times 10^{14}$	cm <sup>2</sup> /°K dyne	-5.23	-4.51	-19.43
$C_{p0} \times 10^2$	cal/g°K	22.27	22.27	30.58
$(\partial C_{p0}/\partial P)_T \times 10^5$	cm <sup>3</sup> /g°K	-20.40	-47.15	-68.16
$B_0^S \times 10^{-10}$	dyne/cm <sup>2</sup>	5.77	5.59	20.21
$B_0^T \times 10^{-10}$	dyne/cm <sup>2</sup>	5.44	5.28	20.13
$B_{0,s}^{S'}$	.	3.03	2.98	2.48
$B_{0,T}^{S'}$		3.73	3.51	2.94
$B_{0,T}^{T'}$		3.53	3.33	2.80
$\gamma_0$		1.01	0.99	0.74
$(\partial\gamma_0/\partial P)_T \times 10^{11}$	/°K cm <sup>2</sup> /dyne	-17.99	-20.35	-2.97

\*Zero subscript denotes T = 273 K

The data necessary to calculate the Gruneisen ratio as a function of pressure are given in Tables V, VI, and VII, (Zero subscripts denote values obtained at 273°K). The pressure derivative of the density, the volume coefficient of expansion and the heat capacity,  $(\partial\rho/\partial P)_T$ ,  $(\partial B/\partial P)_T$  and  $(\partial C_p/\partial P)_T$ , respectively.

PRESSURE DEPENDENCE OF THE GRUNEISEN PARAMETER

Table VI  
Experimental Thermodynamic Data  
Used to Calculate the Pressure Derivatives  
of the Gruneisen Ratio

FUNCTION*	UNITS	POLYSTYRENE	TEFLON	TEFLON-T
$\rho_0$	$\text{g/cm}^3$	1.05	2.19	2.19
$(\partial\rho_0/\partial P)_T \times 10^{11}$	$\text{g/dyne cm}$	2.84	5.99	5.78
$\beta_0 \times 10^4$	$/^{\circ}\text{K}$	2.36	2.97	3.18
$(\partial\beta_0/\partial P)_T \times 10^{14}$	$\text{cm}^2/^{\circ}\text{K dyne}$	-1.92	12.38	-19.42
$C_{p0} \times 10^2$	$\text{cal/g}^{\circ}\text{K}$	26.23	22.27	23.42
$(\partial C_{p0}/\partial P)_T \times 10^5$	$\text{cm}^3/\text{g}^{\circ}\text{K}$	-58.87	-9.57	-9.44
$B_0^S \times 10^{-10}$	$\text{dyne/cm}^2$	3.88	4.06	4.00
$B_0^T \times 10^{-10}$	$\text{dyne/cm}^2$	3.68	3.87	3.79
$B_{0,S}^S$		2.59	2.18	2.18
$B_{0,T}^S$		2.99	2.75	2.77
$B_{0,T}^T$		2.84	2.65	2.63
$\gamma_0$		0.80	0.59	0.59
$(\partial\gamma_0/\partial P)_T \times 10^{11}$	$/^{\circ}\text{K cm}^2/\text{dyne}$	-12.42	-17.81	-16.25

\*Zero subscript denotes  $T = 273 \text{ K}$

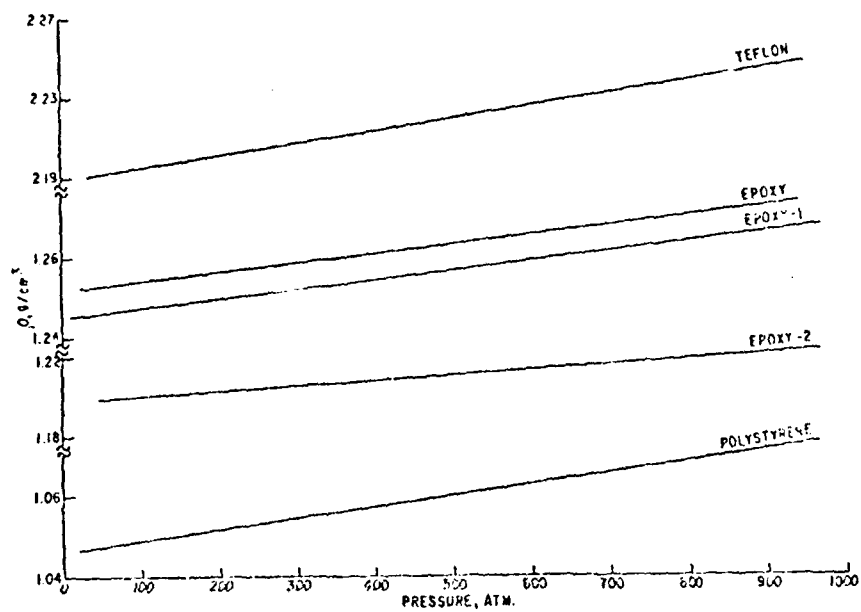


Fig. 1. Density as a function of pressure.

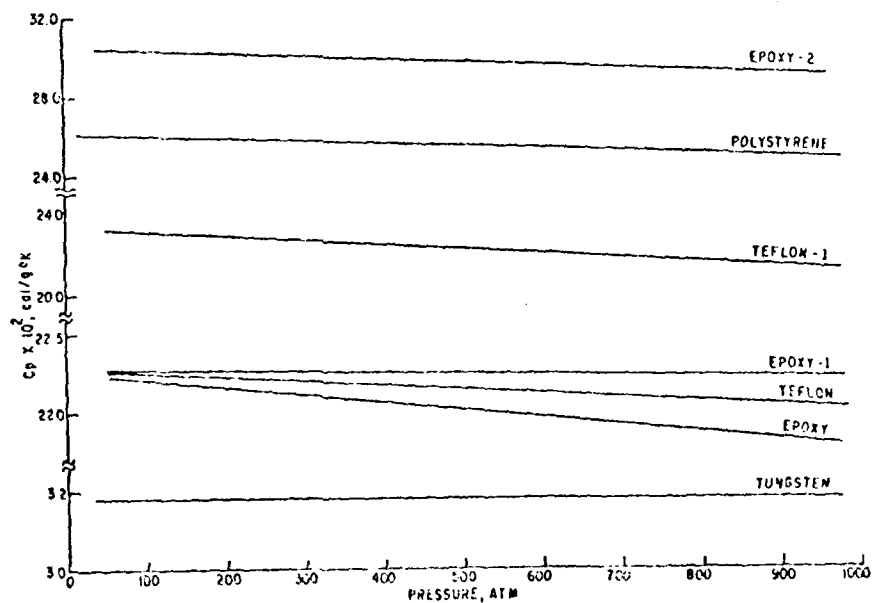


Fig. 2. The specific heat as a function of pressure.

#### PRESSURE DEPENDENCE OF THE GRUNEISEN PARAMETER

were obtained by the proper substitution of experimental data into Equations 9 through 11. The pressure derivative of the bulk modulus,  $(\partial B^S/\partial P)_T = B_{0,T}^S$ , was estimated from the Dugdale MacDonald formula,  $B_{0,T}^S$  as defined by Equation 16. The proper conversion to the adiabatic derivative,  $B_{0,T}^S$ , was made by Equation 17. The function  $B_{0,T}^S$  defines the corresponding isothermal pressure derivative. The pressure derivative of the Gruneisen ratio was obtained by the proper substitution of data into Equations (8) and/or (18) where all quantities were determined experimentally except  $(\partial B^S/\partial P)_T$ .

For polystyrene, the ultrasonic data of Lamberson (11) were used to calculate the adiabatic bulk moduli data of Tables III and VI. The variation of sound velocities with pressure were also experimentally determined for this material to the 10 kbar region. Both Lamberson (11) and Asay, et al. (8) have shown that for polystyrene the validity of the Murnaghan equation was apparent by the linearity of the bulk modulus to the 10 kbar region with a pressure derivative of 8.89. This study indicates that the Dugdale MacDonald relation estimated as 2.59 was valid only to a pressure of 950 atmospheres. There was a significant difference between the actual derivative and that estimated through the Dugdale MacDonald relation, however, for this plastic the compressibility data of Bridgman (22), and the dynamic data of Wagner, et al. (23) and Hauver, et al. (24) were not in complete agreement from the 3 to the 20 kbar region. This is probably due to the transition which occurs within this region.

Ku (25) compared the specific volume of teflon at 30°C with the calculated values obtained by a 12-parameter polynomial, and by the Murnaghan, Birch and Tait equations. The accepted value at 1000 atm was 0.4367 cm<sup>3</sup>/g or a density of 2.289 g/cm<sup>3</sup>. This value compares well with the value of 2.251 g/cm<sup>3</sup> at 0°C and a pressure of 100 atm obtained in this study (Table VI and Figure 1).

The bulk modulus reported by Ku (25) for teflon for the 1 to 5000 atm region was  $2.97 \times 10^{10}$  dyne/cm<sup>2</sup>. The values obtained in this study for the actual and extrapolated teflon samples were  $4.28 \times 10^{10}$  dyne/cm<sup>2</sup> and  $4.34 \times 10^{10}$  dyne/cm<sup>2</sup>, respectively.

The bulk moduli versus pressure data for teflon agree well with data for teflon extrapolated through its room temperature transition as presented by Weir (26) and Ku (25). For the actual data (Teflon-1) Ku has shown a more pronounced drop in the bulk modulus with a transitional shift appearing in the  $3 \times 10^3$  atm region.

The  $C_p$  versus pressure data (Figure 2) and the volume coefficient of expansion versus pressure data (Figure 3) are in

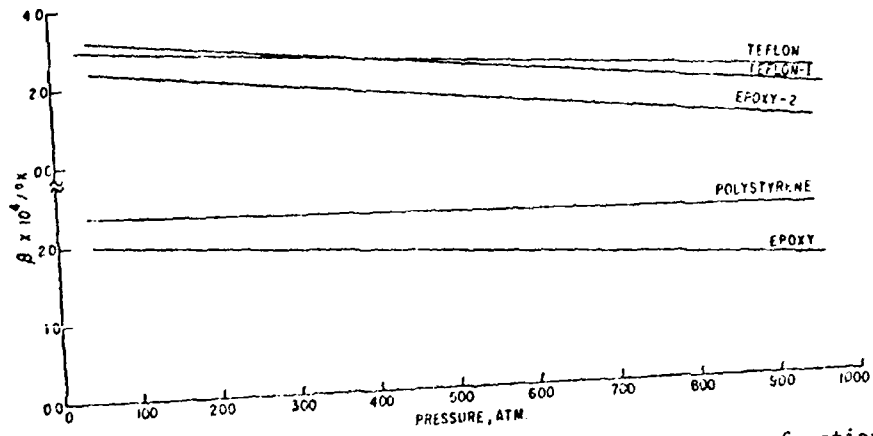


Fig. 3. The volume coefficient of thermal expansion as a function of pressure.

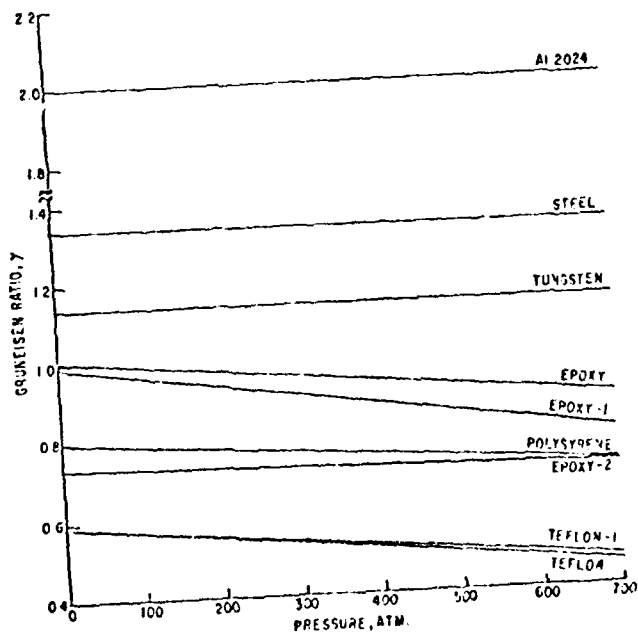


Fig. 4. The Gruneisen ratio as a function of pressure.

PRESSURE DEPENDENCE OF THE GRUNEISEN PARAMETER

agreement with previously reported data obtained from thermodynamic measurements (2,8,15,18, and 25). Since some of the metallic materials exhibited only slight changes for the pressure ranges reported, they were not included on some of the graphs.

The Gruneisen ratio as a function of pressure is given in Figure 4. Previously reported data for teflon and polystyrene (25,28,29) list a 1.54 percent decrease in polystyrene and a 30.4 percent decrease for teflon. Our studies indicate a 15.7 percent decrease in  $\gamma$  for polystyrene and a 3.06 percent decrease in teflon for similar temperature and pressure ranges. Differences in reported initial  $\gamma$  values are due to extrapolations through transition temperatures.

For Al 2024 the ultrasonic sound velocity data to calculate the bulk moduli (Table III) were compiled from single valued data presented by Kohn (29) and McQueen, et al. (30). The Hugoniot curves, the Mie-Gruneisen equation of state, and the Dugdale - MacDonald relation were employed by McQueen et al., to calculate the complete thermodynamic description of the alloy. The relation between shock and particle velocity was applied in order to obtain the ultrasonic data. In terms of the expansion of the shock velocity,  $\mu_s$ , to quadratic terms in the particle velocity,  $\mu_p$ ,

$$\mu_s = a + b\mu_p^2 \quad (19)$$

Ruoff (31) and Pastine (32) give the coefficients a, b, and c as

$$a = \mu_s (P = 0) = \sqrt{B_0^S/\rho} \quad (20)$$

$$b = 1/4 (1 + B_{0,s}^{\prime S}) \quad (21)$$

$$c = b/6a (2 - b + B_{0,s}^{\prime S}/2b + \gamma) \quad (22)$$

where the terms have been defined previously

For Al 2024, McQueen, et al. (30) reported a value for b of 1.54 for a sample with a density similar to the one reported in this paper. Substitution of this value into Equation (21) gave a shock velocity value of  $B_{0,s}^{\prime S} = 5.161$  and  $\gamma = 2.08$ . This value agrees to within 2.3 percent of our value ( $B_{0,s}^{\prime S} = 5.28$ , Table VII) which was estimated by the Dugdale-MacDonald relationship. The  $\gamma = 2.14$  of Tables IV and VII, calculated by the thermodynamic equation agrees to within 2 to 3 percent. Values for  $\gamma$  previously obtained for two similar alloys, Al 1060 and Al 6061 (3), were 2.05 and 2.13, respectively. It is thus clearly seen that the accuracy with which  $\gamma$  is obtained will determine the accuracy of the estimated pressure derivative.

Table VII  
 Experimental Thermodynamic Data  
 Used to Calculate the Pressure Derivative  
 of the Gruneisen Ratio

FUNCTION*	UNITS	TUNGSTEN	STEEL # 314	AL 2024
$\rho_0$	g/cm <sup>3</sup>	19.27	7.62	2.79
$(\partial\rho_0/\partial P)_T \times 10^4$	g/dyne cm	6.20	4.91	3.77
$\beta_0 \times 10^5$	/°K	1.30	2.78	6.92
$(\partial\beta_0/\partial P)_T \times 10^{17}$	cm <sup>2</sup> /°K dyne	-0.67	-12.48	-121.56
$C_{p0} \times 10^2$	cal/g°K	3.18	10.10	21.31
$(\partial C_{p0}/\partial P)_T \times 10^7$	cm <sup>3</sup> /g°K	-3.43	-92.77	275.01
$B_0^S \times 10^{-11}$	dyne/cm <sup>2</sup>	31.15	15.52	7.69
$B_0^T \times 10^{-11}$	dyne/cm <sup>2</sup>	31.06	15.36	7.38
$B_{0,S}^S$		3.61	3.68	5.28
$B_{0,T}^S$		3.65	3.76	5.46
$B_{0,T}^T$		3.63	3.72	5.25
$\gamma_0$		1.30	1.34	2.14
$(\partial\gamma_0/\partial P)_T \times 10^{12}$	cm <sup>2</sup> /dyne	-3.02	-7.73	-6.60

\*Zero subscript denotes T = 273 K

#### PRESSURE DEPENDENCE OF THE GRUNEISEN PARAMETER

As previously stated, the elastic constants of Featherston and Neighbours (21) were used to calculate the bulk moduli data (Table III) for tungsten. Since the elastic wave propagation was directly along a principle direction, the elastic constants were said to be accurate to  $\pm 0.5$  percent. The value of  $B = 3.08 \times 10^{12}$  dyne/cm<sup>2</sup> calculated from Bridgman's dynamic compressibility data agrees well with the calculated difference between the room temperature adiabatic and isothermal value of this study.

No ultrasonic data illustrating the change of elastic constants with pressure were available for tungsten, however, the  $(\partial B/\partial P)$  value derived from Bridgman's dynamic data was 3.67. This value is in good agreement with the Dugdale-MacDonald estimation of  $B_{0,S}^{\gamma} = 3.61$  (Table VII) of this study. The corresponding  $(\partial \gamma/\partial P)_T$  is listed in Table VII and  $\gamma$  versus pressure is shown in Figure 4. Since no significant change with pressure was noted, the  $(\partial \gamma/\partial P)$  value should apply to the 10,000 kg/cm<sup>2</sup> pressure range limit given by Bridgman (22).

For the oxidation resistant steel studied, the ultrasonic transverse and longitudinal velocity data of Kohn (29) and McQueen, et al. (30) were used to determine the bulk moduli given in Tables III and VII. The  $B_{0,S}^{\gamma}$  value estimated from the shock velocity data of Kohn was 4.94.<sup>5</sup> The room temperature value of this study ( $B_{0,S}^{\gamma} = 4.54$ , Table VII) agreed to within 8 percent of the value obtained from the shock data. Values for  $B_{0,S}^{\gamma}$  of Tables V, VI and VII were calculated for  $T = 273$  K.

In order to understand the specific heat and thermal expansion data for the epoxy polymer, the differential thermogram of the sample (Figure 5) was compared with Maraset epoxy previously studied (9 and 33). The thermograms show distinct differences with a pronounced transition at 46°C for the Maraset epoxy and a much broader transition approaching 125°C for the Shell epoxy. Both thermograms show decomposition beyond 200°C, however, an exothermal double peak was noted for the Shell epoxy as opposed to the broad endothermal peak observed for the Maraset sample. The double peak may be associated with substituents which were added to stabilize the material. A comparison of the thermal expansion data (9 and 33) also showed a slight increase in stability for the Shell epoxy as noted by the shift of the 46°C transition to slightly higher temperatures. Since the transition is evident, three sets of data were derived for this polymer. Table V, column 1 (labeled Epoxy) illustrates the data obtained as extrapolated through transitional regions. Column 2 (labeled Epoxy-1) defines the actual polymeric thermal and ultrasonic measurements along the transitions and Epoxy-2 defines the high temperature region.

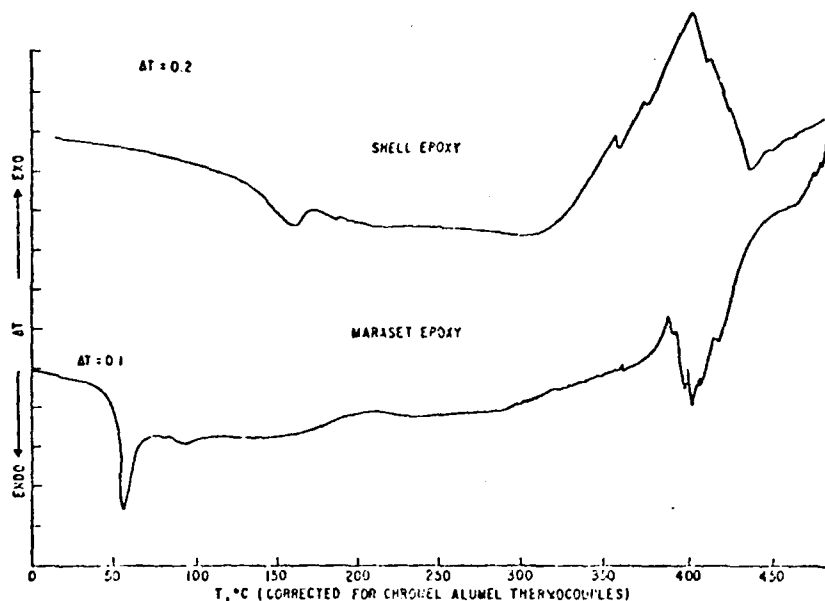


Fig. 5. Differential thermograms for Maraset and Shell epoxies.

The ultrasonic transverse and longitudinal velocities used to calculate the adiabatic bulk moduli (Table III) were obtained at this laboratory by Benson, et al. (34). No dynamic shock wave data are available, however, Benson did fit ultrasonic pressure data to the Birch equation and found that at 1 kbar pressure, the adiabatic bulk modulus was  $6.2 \times 10^{10}$  dyne/cm<sup>2</sup>. The value calculated from this study is  $5.95 \times 10^{10}$  dyne/cm<sup>2</sup>, therefore, the bulk modulus pressure derivative is applicable to approximately 1 kbar. The  $\gamma$  versus pressure data are illustrated in Figure 4.

#### CONCLUSIONS

In this paper a relationship between the adiabatic and isothermal pressure derivatives were presented which involves only the temperature dependent thermodynamic properties of the volume coefficient of expansion, the heat capacity, volume or density, and the bulk moduli. The pressure derivatives were estimated by a Dugdale-MacDonald relation so that the variation of the Gruneisen ratio with pressure could be determined. Although the pressure derivatives of the polymers are accurate only for small pressure ranges, the data will be useful to propose theoretical models for these materials. Moreover, in high pressure experiments, the constants of the equation of state are affected by imperfections in the solid, therefore, it is possible that the ultrasonic measurements are more reliable.

PRESSURE DEPENDENCE OF THE GRUNEISEN PARAMETER

REFERENCES

1. E. Gruneisen, *Handbuch der Phys.*, 10, 1 (1926).
2. S.R. Urzendowski and A.H. Guenther, *Thermal Analysis*, Vol. 1, p. 493, Edited by R.F. Schwenker, Jr. and P.D. Garn, Academic Press, New York, 1969.
3. C. Kittel, *Introduction to Solid State Physics*, John Wiley & Sons, Inc., New York, 1968, page 182.
4. R.E. Barker, Jr., *J. Appl. Phys.*, 38, 4234 (1967).
5. C.A. Swenson, *The Physics and Chemistry of High Pressures*, Editor, A.R. Ubbelohde, Society of Chemical Industry, London, England, 1963, p. 39.
6. A.H. Guenther, *Symposium on Dynamic Behavior of Materials*, Special Technical Publication No. 336, Am. Soc. for Testing Materials (1962).
7. J.C. Slater, *Introduction to Chemical Physics*, McGraw-Hill, New York, 1963.
8. J.R. Asay, S.R. Urzendowski, and A.H. Guenther, Air Force Weapons Laboratory, Tech Rept. No. 67-91, Kirtland Air Force Base, New Mexico, 1968.
9. S.R. Urzendowski and A.H. Guenther, Air Force Weapons Laboratory Tech. Rept. 71-6, Kirtland Air Force Base, New Mexico, 1971.
10. R.N. Thurston, *Proceedings of the IEEE* 53, 1320 (1950).
11. D.L. Lamberson, *Dissertation*, Air Force Institute of Technology, Wright-Patterson AFB, Ohio.
12. O.L. Anderson, *J. Phys. Chem. Solids* 27, 547 (1966).
13. F.D. Murnaghan, *Proc. Nat'l. Acad. Sci.*, 30, 244 (1944).
14. J.S. Dugdale and D.K.C. MacDonald, *Phys. Rev.*, 89, 832 (1953).
15. S.R. Urzendowski, D.A. Benson and A.H. Guenther, *Thermal Analysis*, Vol. 3, 365 (1971), Editor H.G. Wiedemann, Birkhauser Verlag, Basel und Stuttgart, Davos, Switzerland.
16. J.A. Kok, *Physics*, 24, 1045 (1958).
17. H.E. Phillips, *Phys. Rev.*, 118, 664 (1960).